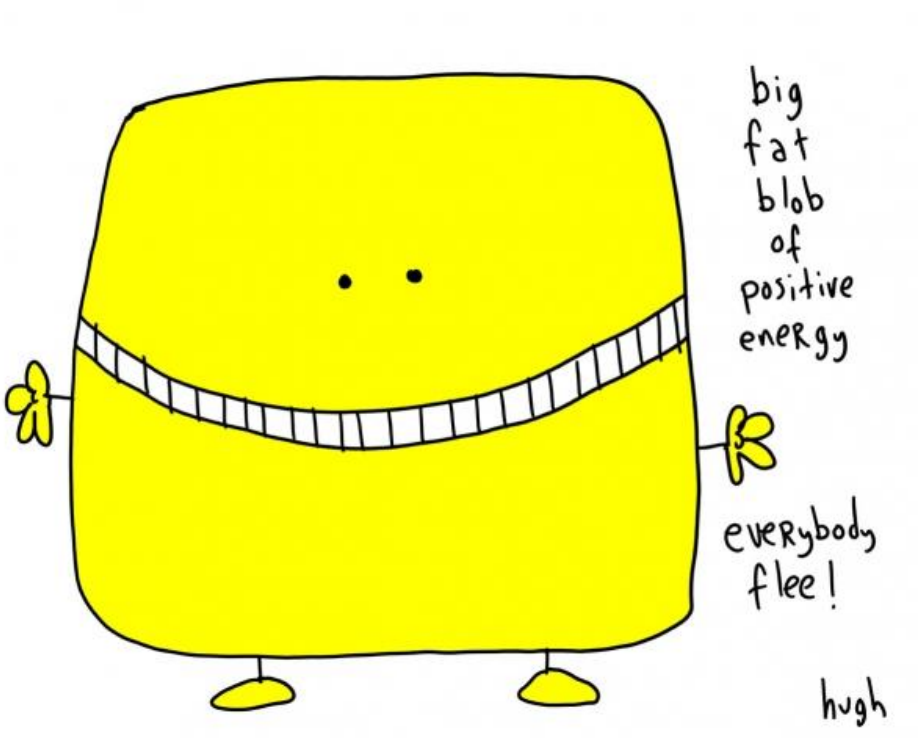

- A Comic by Hugh Macleod.
www.gapingvoid.com

University of Alberta

Suspension of Mixtures of Solids in Stirred Tanks:
Problem Definition and Model Identification

by

Inci Ayranci

A thesis submitted to the Faculty of Graduate Studies and Research
in partial fulfillment of the requirements for the degree of

Doctor of Philosophy

in

Chemical Engineering

Department of Chemical and Materials Engineering

Spring 2012
Edmonton, Alberta

Dedicated to my mom, Dr. Guler Ayranci, my dad, Dr. Erol Ayranci,

my brother, Dr. Cagri Ayranci, and my brother, soon to be Dr. Korhan Ayranci

Abstract

Solids suspension in stirred tanks has many applications in industry. The contributions of this thesis are particularly interesting for applications in mineral processing and nuclear waste clean up. The main issue in design of mixing tanks for such applications is the gap between industry and research. These applications involve mixtures of solids at high solids loadings; however, research has been limited to unimodal slurries at low solids loadings. This limitation is a result of the complexity of solids suspension. The fundamental understanding of solids suspension has not been fully established, and the effect of numerous parameters is not fully understood. The objective of this thesis is to contribute to the fundamental understanding of solids suspension, and provide a bridge between research and industry with improved design methods.

To provide this bridge, first a thorough experimental study was conducted and the behaviour of mixtures of solids at high solids loadings was investigated. The effect of the ratio of the particle size, particle density and solids loadings of the two solid phases in binary mixtures was analyzed. The total solids loading of the mixtures was increased up to that of industrial cases. The findings were discussed and the validity of general design heuristics was tested. Based on these findings additional data was collected and a deeper analysis was done to obtain a model for predicting mixture just suspended speed. The analysis showed that the current design heuristic that is used in industry is incapable of predicting physics behind solids suspension. A new model, based on the power required to suspend each solids fraction, showed accurate predictions up to high solids loadings. This

study also revealed necessary improvements to the Zwietering correlation for predicting unimodal slurry just suspended speed.

While these studies targeted solving an industrial problem, another study was carried out to enhance the fundamental understanding of solids suspension. Solids suspension mechanisms in stirred tanks were investigated. An analogy between slurry pipeline flow and river sediment transport suggested that similar mechanisms apply in all three geometries. In this study the active solid suspension mechanisms in a stirred tank were defined, and the effect of geometry on the dominant solid suspension mechanism was investigated.

Acknowledgements

When you write the acknowledgements of a thesis, you understand that "the time" has really come. The time to let the thesis go, to defend, to finish a chapter in your life and start a new one… I had a great experience along my PhD journey. I am very lucky to be surrounded by many wonderful people to give me the support I needed, to make me smile and to never make me feel alone. They took the time to support me along this journey, so now I would like to take the time and space, and show them my appreciation.

First of all I would like to thank my supervisor, Dr. Suzanne Kresta. Dr. Kresta, you have been an excellent supervisor to me. I learned something from you with each conversation we had. I always felt that you were watching out for me, not only for the course of my studies, but also for my future career. You always showed me ways to improve myself. Your energy and motivation always have and will inspire me. It was an invaluable experience to do research with you. I also enjoyed teaching with you very much. I don't know how, but you realized how much I like teaching early in my program and had me involved more in it. I learned an incredible amount from you. In addition to the student-supervisor relationship I think we built a friendship. I enjoy our conversations with lots of laughter very much. Thank you very much for your guidance, patience, friendship and everything else you did for me to improve myself as a researcher, a future academic, and a person. I can only hope to be as good a supervisor as you are to my students in the future.

I would also like to thank Dr. Jos Derksen. I enjoyed our discussions all of which made me look at the subject from a different perspective and from a bigger picture, and made me think deeper. I appreciate your patience with all my questions over the course of my studies.

I would like to thank Dr. Sean Sanders for his support, help, and for all the discussions we had. You always encouraged me, and I learned a lot from you not only as a student in your class, but also as a researcher.

Dr. Semagina, even though we could not include our research in this thesis it was a great experience and I appreciate your help and support. Research we did helped me combine two research areas, and it is invaluable to my future career.

Next set of thanks go to my lovely family. My mother, Güler, and my father, Erol, you were there with me all along this journey. Our almost daily conversations over two different time zones always made me happy. I always felt your love and support with me and I want to thank you for that. My brother, Korhan, thank you very much for all your support along the way. My brother, Çağrı, I don't know how to thank you. You were involved in my PhD the most in the family, starting from day one as I arrived Edmonton. I appreciate everything you taught me, all your support, all the laughs we had together, and simply for everything you did for me. Thank you very very much for everything. I would also like to thank my sister-in-law, Stephanie. You were always there to support, help, cheer me up and to detect the times that needed celebration and make us enjoy them. I appreciate that very much. My beautiful niece Talya, you made it to the last quarter of my PhD, but you for sure had a very happy effect. Thank you for all the smiles you brought to my life. My grandmother, Anneannecigim, and my grandfather, Dedem, I thank you both for believing in me and encouraging me all the time. Dedem, I know you are watching me and you are proud of your granddaughter.

Next comes mixing group members. Imran, you have been an incredible friend and support since the first day. You are one of the key people who made me enjoy this process the most with all the laughs, fun conversations and turbulence and fluid mechanics talks you brought to my life ☺ The way you see life changed my persepective in a great way. Thank you for all these. Marcio, you have always been a great friend. You calmed me down every time things went a little off with your calm-wise-self. I enjoyed our conversations, discussions and your always sincere friendship a lot. I thank you for these, and also for conducting the PIV experiments. I would also like to thank Alena, Shad, Oscar, Patrick,

Navid, Theo, Shaun and Jeng Yi for all the happy conversations. Theo, thank you for conducting some of the experiments.

I would like to thank Dr. Arthur W. Etchells III for very valuable discussions and contributions to my thesis. Richard Kehn and Bernie Gigas from Lightnin, I thank you for all the great discussions and for your financial support.

Dr. Nobes thank you for making your experimental setup for PIV measurements available to us. Adam Madej, thank you for helping us in the use of the setup.

Kartik, Ramya, Hector, Hua, Qi, Vivek, and Yan thank you for your friendship and support, and for all the fun things we did together.

There are numerous friends who know me since I was a kid, who know that this was my dream and supported me all along from thousands of miles away: Gökçe, Dilek, Burak, Gülçin, Yalçın, Damla, Koray, Şafak, Murat and Elif. People say friendships lose strength as you move away from each other. These wonderful people showed me this was completely wrong. I thank you all from the depth of my heart.

Jason, Julie and Elle, thank you all for your friendship, support and for all the great food you made me.

I also thank Dr. Zeki Aktas for supporting me getting into this journey, and following up from miles away.

I also would like to extend my thanks to everyone in the Department of Chemical and Materials Engineering for making me smile and helping things go smooth, and everyone in Machine Shop for all the fun conversations. Special thanks go to Dave Parlin and James McKinnon for building my setup. I like running experiments a lot, and a setup that works perfectly helped me enjoy my experiments. Finally, I greatly appreciate the financial support from Lightnin and NSERC.

Table of Contents

List of Tables

List of Figures

List of Symbols

Roman characters

a	the exponent on concentration as given in Equation 3-14
A	constant in equation 4-15, 4-16, and 4-17
b	the constant in Equation 3-14
C	off-bottom clearance of the impeller (m)
c_s	Smagorinsky model constant
D	impeller diameter (m)
d_A	diameter of particle A (m)
d_B	diameter of particle B (m)
d_p	particle diameter (m)
d^+	dimensionless particle diameter (-)
F_B	buoyancy force (N)
F_D	drag force on the sphere (N)
F_G	gravity force (N)
F_L	lift force (N)
F_M	Magnus force (N)
F_S	Saffman force (N)
F_T	turbulence force (N)
g	acceleration due to gravity (m/s^2)
H	liquid height (m)
h	height of the calibration plate from the tank bottom (mm)
i	the distance of the horizontal plane from the bottom of the tank for LES data(mm)
k	the slope in Equation 3-13
L	integral length scale (m)
M	momentum (kg m/s^2)
M_{js}	momentum at just suspended conditions (kg m/s^2)
$M_{js,1}$	M_{js} for particle one (kg m/s^2)
$M_{js,2}$	M_{js} for particle two (kg m/s^2)
$M_{js,mix}$	M_{js} for mixture (kg m/s^2)

Mo	momentum number (-)
m_A	mass of particle A (kg)
m_B	mass of particle B (kg)
m_L	mass of liquid (kg)
m_s	mass of solid (kg)
N	impeller rotational speed (rpm)
N_{expt}	impeller speed for the PIV experiments (rpm)
N_{js}	just suspended speed (rps)
$N_{js,\ 1}$	N_{js} for particle 1 (rps)
$N_{js,\ 2}$	N_{js} for particle 2 (rps)
N_p	power number (-)
$N_{p,A310}$	power number of the A310 impeller
$N_{p,\ max}$	power number for P_{js}, max
$N_{js,\ mix}$	mixture N_{js} (rps)
$N_{js,\ modified}$	N_{js} calculated by the modified Zwietering correlation (rps)
$N_{p,PBT}$	power number of the PBT
n	the intercept in Equation 3-13and clearance index in equation 4-13
P_{js}	power consumption at just suspended speed conditions (J/s)
$P_{js,\ 1}$	P_{js} for particle 1 (J/s)
$P_{js,\ 2}$	P_{js} for particle 2 (J/s)
$P_{js,\ max}$	maximum P_{js} in Table 1 (J/s)
$P_{js,\ mix}$	P_{js} for mixture (J/s)
R	radial position in the tank (mm)
R^2	fraction of variance
r	radius (m)
S	Zwietering's N_{js} constant
S_{max}	Zwietering's N_{js} constant for $P_{js,\ max}$
T	tank diameter (m)
U	velocity in Equation 3 (m/s)
U^*	shear velocity (m/s)
$V_{measured}$	measured velocity (m/s)

V_L	volume of liquid (m^3)
V_r	mean radial velocity (m/s)
V_s	volume of solids (m^3)
V_{scaled}	scaled mean radial or axial rms velocity (m/s)
V_t	terminal settling velocity (m/s)
V_{tip}	tip velocity (m/s)
V_z	velocity in the axial direction
v_z'	axial rms velocity (m/s)
W	blade width (m)
W_b	baffle width (m)
X	solids loading (mass of solid/mass of liquid*100) or Zwietering's mass ratio percent in Chapter 3
X_v	volume percent (volume of solid/total volume of slurry*100%)
X_w	weight percent (mass of solid/total mass of slurry*100%)
x	the length scale (m)
x_n	velocity at the n^{th} off-bottom clearance
x_{mean}	the mean velocity over all six clearances
x_L	wt% of the liquid phase
x_s	wt% of the solids
y	distance from the solid surface (m)
y^+	dimensionless distance from the solid surface (-)
Z	Baldi's N_{js} constant

Greek characters

ν	kinematic viscosity of water (m^2/s)
μ_L	dynamic viscosity of the liquid (kg/m.s)
ρ	density (kg/m^3)
ρ_L	liquid density (kg/m^3)
ρ_S	solid density (kg/m^3)
ρ_{sl}	slurry density (kg/m^3)
$\rho_{sl,1}$	unimodal slurry density for particle 1 (kg/m^3)

$\rho_{sl,2}$	unimodal slurry density for particle 2 (kg/m^3)
$\rho_{sl,mix}$	mixture slurry density (kg/m^3)
$\Delta\rho$	change in density (kg/m^3)
σ	variance on S in Chapter 2, and normalized standard deviation in Chapter 4 (Equation 4-12)
$\Delta\sigma$	difference between the normalized standard deviations of the scaled and measured velocities (Equation 13)
$\Delta\sigma_r$	$\Delta\sigma$ for mean radial velocities
$\Delta\sigma_z$	$\Delta\sigma$ for axial rms velocities
η	Kolmogoroff length scale
η_{est}	estimated Kolmogoroff length scale
ε	rate of dissipation of turbulent kinetic energy per unit mass (m^2/s^3)
δ	viscous sub-layer thickness (m)

Abbreviations

Ar	Archimedes number
A310	axial impeller provided by Lightnin
B	bronze
BNE	Brazil nut effect
DNS	direct numerical simulations
HE-3	high efficiency
IM single	single Imtermig impeller
IM dual	dual Imtermig impellers
LES	large eddy simulations
LG	large glass beads
min	minimum
max	maximum
Ni	nickel
PBT	pitched blade turbine impeller
PBT6D	down pumping 6-bladed pitched blade turbine impeller

PBT6U	up pumping 6-bladed pitched blade turbine impeller
PIV	particle image velocimetry
R	ion exchange resin
Re	Reynolds number
RBNE	reverse Brazil nut effect
RT	Rushton turbine
rms	root mean square
SG	small glass beads or specific gravity
S	sand
UF	urea formaldehyde
wt%	weight percent

Chapter 1 : Introduction

Solid-liquid mixing is at the heart of many process industries, particularly mineral processing and nuclear waste clean-up. It is a power intensive operation because mineral processing is done in very large tanks with large impellers, and the main design parameter is the impeller speed: power consumption increases with the fifth power of diameter and the cube of the impeller speed. An accurate design method is needed, but is difficult to obtain because there is limited fundamental knowledge about solids suspension. With this thesis we aim to contribute to the fundamental understanding of solids suspension and find practical solutions to some industrial problems.

Complete off-bottom suspension is the most common operating condition for solid-liquid mixing, unless there are some other specific process requirements. At complete off-bottom suspension all of the surface area of the solids is in contact with the liquid; therefore, it is efficient for mass transfer. The impeller speed at complete off-bottom condition is called the just suspended speed, N_{js}. N_{js} is defined as the impeller speed at which there are no particles remaining stationary at the bottom of the tank for more than 1 or 2 seconds (Zwietering, 1958). While it is clear that determining N_{js} accurately is important, there are serious problems related to measurement and prediction of N_{js}. Several measurement methods have been used, but three of these methods stand out: visual observation of the tank bottom, visual observation of cloud height of the slurry volume and hydrostatic pressure increase on the bottom due to solids suspension. The definition of N_{js} requires observation of the particle motion which introduces uncertainty and limits the experimental methods significantly. Only the pressure method allows automation of the N_{js} measurement.

Visual observation of the tank bottom, which is the most common technique, was first used by Zwietering (1958). A mirror is placed underneath the transparent tank bottom and the particle motion at the bottom of the tank is

visually observed. The advantage of this technique is that the observer can fix the time that the bottom of the tank is observed, and can easily reach repeatable results. It is also an advantage that the observer has direct visual access to the solids behaviour at the bottom of the vessel. There are however, some disadvantages mainly arising from the definition of N_{js}. First, the repeatability between observers may vary up to 20% because every observer may have a slightly different calibration for timing, or observing the vessel bottom. Second, different particles have different visibility and the visibility of the particles affects the repeatability of the measurement. Third, designing a vessel with a clear bottom is not practical for industrial applications, so it is difficult to validate the scalability of the results. In any case, this method still seems to give the most reliable results, and it is used for N_{js} measurements in this thesis.

The second method was found by Einenkel and Mersmann (1977). It is based on the cloud height of the solids volume. As reviewed by Kasat and Pandit (2005), in this method N_{js} is defined as the impeller speed at which the cloud height is approximately 90% of the total liquid height. The visual observation is performed from the side of the tank regardless of the particle motion at the bottom of the tank. While this is an easy way of observing N_{js}, it is not very reliable. Solids suspension occurs at the bottom of the vessel; therefore, the measurement has to be related to the bottom of the vessel. Comparison between the Zwietering method and the cloud height method shows that most of the particles may be distributed throughout the tank while there are still many particles remaining motionless at the bottom. In the case of a mixture of solids with varying densities and particle sizes it is very likely that the less dense particles are distributed in the entire tank while the dense particles are almost stationary. This method is flawed and does not provide accurate N_{js} measurements.

The last method was reported recently by Micale et al. (2002) and was confirmed by Selima et al. (2008). This method is based on the pressure increase at the bottom of the tank as the solids are suspended. A force balance is done before and after the suspension of solids. The force balance is correlated to the

pressure increase and the mass of solids that are suspended is found. This is a very promising method considering the fact that it eliminates possible differences between the visual observers. It should however be noted that the critical speed for solids suspension for this method is defined as the sufficient speed (N_{ss}), which is the impeller speed at which 98% of all the solids are suspended. This is close to N_{js}, but it is not exactly the same definition. This also shows that in order to find a more efficient experimental method to determine N_{js} the definition of N_{js} needs to be modified. In this work, the definition given by Zwietering was accepted as the most widely used definition and therefore visual observation was selected for the experiments.

While measurement is the most reliable way to determine N_{js}, it is not always practical for industrial cases. Predicting N_{js} through empirical correlations is the common sense in industry. The first correlation was proposed by Zwietering (1958). This correlation was further investigated, or parts of it were improved by many authors; however, the original Zwitering correlation remains the most commonly used form:

$$N_{js} = S\left(\frac{g\left(\rho_S - \rho_L\right)}{\rho_L}\right)^{0.45} \frac{X^{0.13}\, d_p^{0.2}\, \nu^{0.1}}{D^{0.85}} \qquad 1\text{-}1$$

This correlation is analyzed in detail in the following chapters of this thesis. A quick overview of the limitations and flaws is given here. The correlation is limited to low solids loadings (<10 wt%), low viscosities, limited geometries, and unimodal slurries (i.e. particles with same density and narrow particle size distribution). With all these drawbacks, the correlation fails to predict N_{js} accurately in many practical cases. Improvements to the correlation have not been very successful because solids suspension is very complex, and without a clearer fundamental understanding it is difficult to suggest pioneering solutions.

At this point it is crucial to identify the most problematic parameters. The geometry has a strong effect on N_{js}. It is not only the effect of impeller diameter

as given explicitly in the correlation, but also the effect of tank diameter, off-bottom clearance, number of baffles, shape of the baffles, type of the impeller, shape of the tank bottom and more that impact N_{js} significantly. In addition to the effect of geometry, the interaction between other parameters such as the particle diameter, particle density and solids loading requires investigation. A better predictive model can be obtained only after building a better understanding of all these effects and the interactions between them.

While research in the area of solids suspension is struggling to find pragmatic and useful answers within these limitations, industrial applications include much more complicated problems. The nuclear waste and mineral processing industries employ mixed slurries with solids with varying densities and particle sizes at high solids loadings – as high as 60-80 wt%. Predicting the mixture N_{js} accurately is critical for these processes; however, there is no knowledge of the behaviour of mixed slurries, the particle-particle interactions, and there is no real model to do accurate predictions. For mixtures, N_{js} is predicted using a design heuristic. This thesis aims to improve design methods for mixtures of solids and to begin to develop a more fundamental understanding of solids suspension.

1.1. Thesis Structure

The objectives of this thesis are to establish a fundamental understanding for the solids suspension mechanisms and the effect of geometry on the mechanisms, and to establish an understanding of the behaviour of mixtures of solids, the effect of particle-particle interactions on N_{js}, and also to develop a model to predict mixture N_{js}. Figure 1-1 shows the parameters that were defined as the most pressing effects on solids suspension. These parameters were all investigated in the thesis. The thesis is based on three journal papers. Chapters 3, and 4 have been submitted to a scientific journal and are under review, and Chapter 2 is already published (Ayranci and Kresta, 2011).

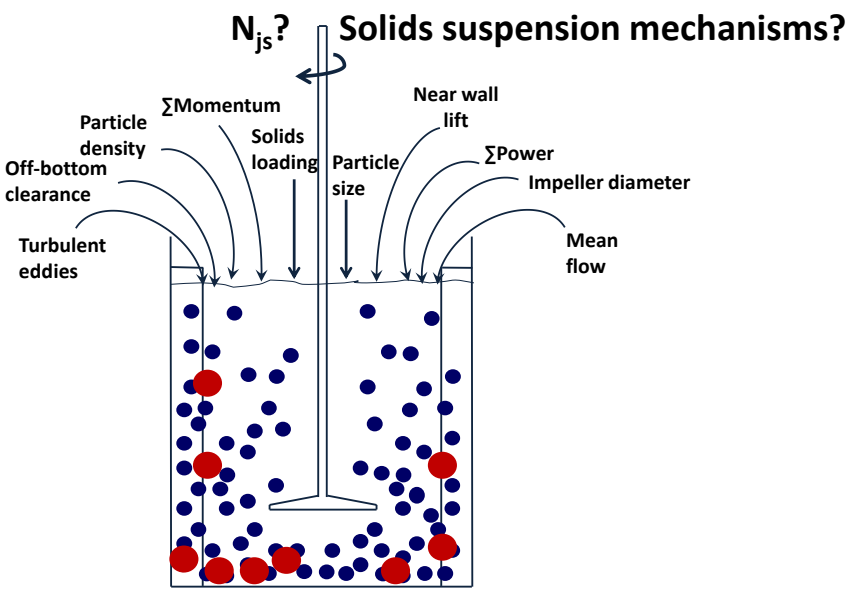

Figure 1-1: Visual abstract of the solids suspension problem

Chapter 2 investigates the complete off-bottom suspension behaviour of mixtures of solids. The key points of this chapter are the fact that the slurries are composed of two solid phases and the solids loadings are increased up to 56 wt%. Investigation of these key points is a first in the stirred tank literature. The effect of the increasing solids loadings, and the ratio of particle density and particle size of the two solid phases on the N_{js} of the binary mixtures and the particle-particle interactions was analyzed. At low solids loadings (below 12 wt%) the effect of concentration on mixture N_{js} is not very significant; however, further increasing solids loadings of the less dense particles can result in a significant drop *or* an increase in mixture N_{js} based on the physical properties of the two solid phases. This chapter also provides an understanding and basis for Chapter 3.

Chapter 3 proposes and tests two new models to predict the mixture N_{js}. The analysis starts with the current design heuristic used in industry and highlights the shortcomings of this heuristic. The two new models proposed are the power and the momentum models. Both of these models are compared to the current design heuristic. The current design heuristic fails to predict the physics behind solids suspension. The momentum model tends to over-predict. The power model, however, predicts mixture N_{js} accurately for a variety of geometries and

up to high solids loadings. The effect of off-bottom clearance and solids concentration is investigated and a more accurate form of the correlation to predict unimodal slurry N_{js} is presented. The off-bottom clearance cannot be represented by a simple model since it is a function of type of the particles, type of the impeller and solids concentration. Accounting for the effect of concentration is also quite challenging. Three possible exponents were found: one for the entire data set with some scatter in data, and two for two groups of particles. Overall, this chapter answers part of a quite challenging problem in industry by providing a model to predict mixture N_{js} at high solids loadings.

Chapter 4 explores the solids suspension mechanisms and the effect of geometry on the dominant solids suspension mechanism in stirred tanks. In this chapter solids suspension is explored starting from a simple case of flow over a flat plate. This is followed with a literature review of the solids suspension mechanisms proposed in two other research areas: slurry pipeline flow and river sediment transport. The results are combined with an analysis of stirred tanks, giving two possible solids suspension mechanisms in a stirred tank: turbulent eddies and mean flow. The analysis leads to the conclusion that to understand solids suspension the focus should be on the flow near the bottom of the tank. A hypothesis is proposed that at complete off-bottom suspension a critical flow condition exists close to the bottom of the tank which is independent of clearance for fixed solids, tank geometry, and constant circulation pattern. The critical flow condition can be dominated by mean flow or turbulent eddies. Based on this hypothesis the effect of geometry, mainly the impeller diameter, on the dominant solids suspension mechanism was investigated for two Lightnin A310 impellers.

Chapter 5 gives a general discussion of the results and general conclusions, as well as recommendations for future work.

1.2. References

Ayranci, I., Kresta, S.M., 2011. Design rules for suspending concentrated mixtures of solids in stirred tanks. Chem. Eng. Res. and Des., 89, 1961-1971.

Einenkel, W.D. and A. Mersmann, 1977. Required rpm for suspending in agitators [Erforderliche drehzahl zum suspendieren in ruerhwerken], Verfahrenstechnik, 11(2), 90-94.

Kasat, G.R. and A.B. Pandit, 2005. Review on mixing characteristics in solid-liquid and solid-liquid-gas reactor vessels. Can. J. Chem. Eng. 83, 618-643.

Selima, Y.S., Y.S. Fangary, N.A. Mahmoud, 2008. Determination of minimum speed required for solids suspension in stirred vessels using pressure measurements, Can. J. Chem. Eng., 86(4), 661-666.

Zwietering, Th.N. 1958. Suspending of solid particles in liquid by agitators. Chem. Eng. Sci. 8, 244-253.

Chapter 2 : Design Rules for Suspending Concentrated Mixtures of Solids in Stirred Tanks*

2.1. Introduction

Solid-liquid mixing in stirred tanks has a wide variety of applications in industry, including suspension of solids, solid-catalyzed reactions, solids dissolution, crystallization and precipitation. In these operations, especially in solid-catalyzed reactions and solids dissolution, the key process objective is to make all the surface area of the solids available for mass transfer. The impeller speed should be chosen to just satisfy this objective, because solid-liquid mixing operations are power intensive and the power consumption increases with the impeller speed cubed. The just suspended speed (N_{js}) provides complete off-bottom suspension conditions where no particles remain stationary on the bottom of the tank for more than 1 or 2 seconds (Zwietering, 1958). Zwietering found an empirical correlation for N_{js} that includes solid and liquid properties, impeller diameter and also a constant (S) that is a function of impeller and tank geometry:

$$N_{js} = S\left(\frac{g\,(\rho_S - \rho_L)}{\rho_L}\right)^{0.45} \frac{X^{0.13}\, d_p^{0.2}\, \nu^{0.1}}{D^{0.85}} \qquad 2\text{-}1$$

Many other studies have followed this work. The major studies substantially agree with Zwietering (Nienow, 1968; Chapman et al., 1983; Myers et al., 1994; Armenante et al., 1998), and a compilation of reported S values is given in Table 2-1. In the last column the power consumption at just suspended conditions is compared for a wide range of geometries, given a fixed particle size, density, and concentration, and a fixed fluid density and viscosity. The power at just suspended conditions, P_{js}, is normalized with the maximum power, $P_{js,\,max}$ for the varying combinations of impeller type and diameter, off-bottom clearance, N_{js}, power number, and S.

---

* *A version of this chapter has been published in Chemical Engineering Research and Design: Ayranci, I. and S.M. Kresta, Chem. Eng. Res. and Des.,2011, 89, 1961-1971.*

$$P_{js} = \rho_{sl}\, N_p\, N_{js}^3\, D^5 \qquad 2\text{-}2$$

$$\frac{P_{js}}{P_{js,max}} = \frac{N_p}{N_{p,max}} \left[\frac{S}{S_{max}}\right]^3 \left[\frac{D}{D_{max}}\right]^{2.45} \qquad 2\text{-}3$$

Comparing the various geometries to find the most efficient configuration shows some general trends, and some specific deviations. The maximum power consumption recorded is for the Rushton turbine at its highest reported clearance, C=T/3. When the impeller is changed from radial to axial, the power consumption drops by 70% or more from the base case, and reducing the clearance reduces the power consumption for any impeller.

Table 2-1: Zwietering N_{js} constant, S, for different impellers and geometries

Impeller[a]	**D/T**	**C/T**	**S**	**Source**[b]	**P_{js}/P_{max}** [c]
A310 (N_p=0.3)	0.417	0.250	6.90	2	0.060
	0.500	0.250	7.10	2	0.101
	0.520	0.170	6.39	1	0.081
	0.520	0.250	7.03	1	0.108
	0.520	0.330	7.71	1	0.143
45º PBT (N_p=1.3)	0.333	0.167	4.87	3	0.052
	0.333	0.250	5.58	3	0.079
	0.333	0.333	6.39	3	0.118
	0.500	0.167	2.72	3	0.025
	0.500	0.250	2.77	3	0.026
	0.500	0.333	3.40	3	0.048
	0.714	0.125	4.50	2	0.268
	0.714	0.250	5.40	2	0.463
HE-3 (N_p=0.35)	0.350	0.170	7.07	1	0.049
	0.350	0.250	7.39	1	0.056
	0.350	0.330	8.17	1	0.075
	0.390	0.170	6.6	1	0.052
	0.390	0.250	6.88	1	0.059
	0.390	0.330	7.82	1	0.086
	0.440	0.170	6.49	1	0.066
	0.440	0.250	6.64	1	0.071
	0.440	0.330	7.23	1	0.091
	0.470	0.170	6.26	1	0.070
	0.470	0.250	6.25	1	0.069
	0.470	0.330	6.81	1	0.090
	0.520	0.170	6.89	1	0.119

HE-3 (N_p=0.35)	0.520	0.250	6.88	1	0.118
	0.520	0.330	7.72	1	0.167
PBTD6 (N_p=1.7)	0.380	0.170	4.24	1	0.062
	0.380	0.250	3.99	1	0.052
	0.380	0.330	4.78	1	0.089
	0.520	0.170	5.39	1	0.277
	0.520	0.250	5.72	1	0.331
	0.520	0.330	6.52	1	0.490
PBTU6 (N_p=1.7)	0.520	0.170	5.14	1	0.240
	0.520	0.250	5.19	1	0.247
	0.520	0.330	5.30	1	0.263
RT[d]	0.250	0.143	8.70	4	0.489
	0.250	0.167	9.20	4	0.646
	0.250	0.200	9.90	4	0.805
	0.330	0.170	5.42	1	0.272
	0.330	0.250	6.96	1	0.574
	0.330	0.330	8.37	1	1.000
	0.333	0.143	5.80	4	0.293
	0.333	0.167	6.10	4	0.389
	0.333	0.200	6.60	4	0.503
	0.500	0.143	3.20	4	0.136
	0.500	0.167	3.40	4	0.189
	0.500	0.170	4.34	1	0.386
	0.500	0.200	3.60	4	0.229
	0.500	0.250	4.44	1	0.413
	0.500	0.330	4.69	1	0.487
IM single (N_p=0.61)	0.600	0.170	6.78	1	0.281
	0.600	0.250	6.85	1	0.289
	0.600	0.330	7.55	1	0.387
IM dual (N_p=0.61)	0.600	0.170	7.44	1	0.370
	0.600	0.250	8.30	1	0.515
	0.600	0.330	8.72	1	0.597

a All impellers listed have standard blade height.

b 1: Ibrahim and Nienow (1996) averaged S
2: Paul et al. (2004)
3: Machado et al. (2009)
4: Armenante and Nagamine (1998)

c P_{max} is the highest power requirement within the impellers listed

d N_p for RT varies with Reynolds number

Zwietering did not explicitly include the effect of clearance on N_{js} in his work. He included it in the S values. Later studies showed that N_{js} has a strong dependence on clearance (Nienow, 1968; Baldi et al., 1978; Ibrahim and Nienow, 1996; Armenante et al., 1998; Sharma and Shaikh, 2003) and that other geometrical properties such as the shape of the tank bottom, the impeller type (Ibrahim and Nienow, 1996) and the baffle off-bottom clearance (Myers and Fasano, 1992) also have a significant effect.

Baldi et al. (1978) recognized the importance of off-bottom clearance and proposed a correlation for N_{js} in terms of the parameter Z:

$$N_{js} = \left(\frac{g\,(\rho_S - \rho_L)}{\rho_L}\right)^{1/2} \frac{d_p^{1/6}}{N_p^{1/3}} \left(\frac{T}{D}\right) \frac{1}{D^{2/3}\,Z} \qquad 2\text{-}4$$

For the specific case of C/D=1 and (0.645×10^{-3} kg/m.s < μ_L < 3.17×10^{-3} kg/m.s), Baldi found the following expression for Z:

$$Z \propto \left(\frac{\mu_L\,T}{\rho_L D^3 N_{js}}\right)^{-0.2} X^{-0.15} \qquad 2\text{-}5$$

From this expression N_{js} can be defined as:

$$N_{js} \propto \left(\frac{g\,(\rho_L - \rho_S)}{\rho_L}\right)^{0.42} \frac{X^{0.125} d_p^{0.14} \nu^{0.17}}{D^{0.89}} \qquad 2\text{-}6$$

which is almost identical to Equation 2-1. The effect of C/D could not be reduced to a single term for Baldi's data. Both of these correlations can be used for N_{js} calculations, but a ±20% deviation from experiments should be expected. Kasat and Pandit (2005) provide a more extensive review of the literature on the suspension of unimodal solids in stirred tanks.

Baldi et al. (1978) investigated N_{js} for bi-modal slurries with the same density and showed that there is no significant difference in N_{js} between the bi-modal and unimodal slurries if a weight averaged diameter is used for the bi-modal slurry. It should be noted that Baldi et al. (1978) worked with very dilute systems where particle-particle interactions are insignificant. Montante and

Magelli (2007) studied the distribution of solids with dilute slurries of binary mixtures with particles that have the same size, but different densities. This work showed that the two solid phases act independently when the slurries are limited to low solids loadings.

While all of the correlations and most of the experimental data available in the literature are limited to unimodal slurries and low solids loadings, many industrial applications involve a solid phase which is a mixture of solids with varying densities and sizes. The current design approach for mixtures of particles is to set the impeller speed based on the particles that are hardest to suspend. These particles are the ones which have the highest N_{js} value compared to the other particles in the mixture. The accuracy and reliability of this approach has not been tested.

For high solids loadings, or dense phase suspensions, it is known that the Zweitering correlation is not reliable, but the limitations of the simple exponential term have not been defined. Particle-particle interactions increase as the solids loading is increased and particles both draft behind the other particles and collide with them. Particle-particle collisions cause a change in the momentum transfer between the particles and can have a strong effect on solids suspension at the bottom of the tank.

Several mechanisms of solids suspension have been proposed. It is generally accepted that solids are suspended from the tank bottom due to the action of lift and drag forces and turbulent eddies on the solid particles (Paul et al., 2004). The particles that are suspended in the tank circulate and then settle to the bottom of the tank, where they may come to rest for no more than 1 to 2 seconds before they are resuspended. Baldi et al. (1978) proposed that the particles take on fluctuating velocities as a result of turbulent eddies which are somewhat larger than the particles (Kuboi et al., 1972), and further that the particles are suspended mainly due to the action of these eddies. Molerus and Latzel (1987 a, b) investigated the off-bottom lifting mechanism for fine and coarse particles in more detail. They used an Archimedes number defined as:

$$Ar = \frac{d_p^3\, g}{\nu^2}\ \frac{(\rho_S - \rho_L)}{\rho_L} \qquad 2\text{-}7$$

to describe the ranges over which different suspension mechanmisms were dominant. Molerus and Latzel (1987 a, b) carried out experiments in three geometrically similar vessels and showed that for Ar < 40 the particles are completely submerged in the viscous sublayer. Under these conditions, the velocity gradient in the near wall region generates a lift force, moving the small particles away from the wall. For Ar > 40, the particles are protruding into the buffer layer and turbulent outer layer where the velocity gradient is much smaller, so the viscous sublayer lift is no longer an important effect. A third mechanism based on solid-solid interactions in a dense bed of mixed solids is proposed for very high concentrations of solids. This effect is known as the Brazil Nut Effect (BNE) (Hong et al., 2001). In mixtures of solids, the larger solids have a tendency to rise to the top when the bed is shaken, or sheared. Hong et al. (2001) found that the limiting condition for the Brazil Nut Effect is:

$$\frac{d_A}{d_B} = \sqrt{\frac{m_A}{m_B}} \qquad 2\text{-}8$$

where A is the species with the larger diameter. Below this critical diameter ratio, the Brazil Nut Effect can be reversed, with the larger particles segregated on the bottom of the mixture. Liao et al. (2010) recently extended this work to the case of a wetted solids mixture, and concluded that when low viscosity liquids, such as water, are added, the BNE persists, regardless of the quantity of liquid, but for higher viscosity liquids, the solids segregation effect could be dramatically reduced, leading to a homogeneous mixture. Although the BNE could cause severe segregation of solids in stirred tanks, it has not previously been considered for this application.

The experimental design is based on mixtures of particles with varying density, mass, and particle size. The first objective is to test the applicability and limitations of design based on the particle with the highest N_{js}. The second

objective is to consider differences in behaviour between mixtures of particles as the solids loading increases.

2.2. Experimental Procedure

Five test particles were selected: two large, one medium, and two small; two dense (SG=9), two moderately dense (SG=2.5), and one nearly neutrally buoyant (SG=1). The objective is to combine different pairs of particles to isolate the effects of relative density and particle size, and to explore the N_{js} behaviour at high solids loadings.

A cylindrical tank with an inner diameter of 0.24 m and four equally spaced baffles (W_b=T/10), shown in Figure 2-1a, was used for all experiments. The liquid height was equal to the tank diameter (H=T). Two impellers, both with a diameter of D=T/3, were used: a Lightnin A310, and a four bladed down pumping 45° PBT with an actual blade width, W=D/5. The A310 is a purely axial impeller whereas the PBT is a mixed flow impeller. The shaft had a diameter of 0.127 m≅D/6 in order to minimize shaft wobble at high impeller speeds. The off-bottom clearance, C/T, was varied from 0.125 to 0.36. Tap water was used as the liquid phase.

The cylindrical tank was placed inside a square tank which was filled with water to minimize optical distortion. These two tanks were bolted to a steel platform to maximize the stability of the system at high impeller speeds, as shown in Figure 2-1b. An opening in the middle of the platform made the tank bottom visible from below and a 45° mirror was placed under the tank, as shown in Figure 2-1c, to assist with observations. The motor was attached to a motorized traverse in order to adjust the off-bottom clearance of the impeller.

Figure 2-2 shows SEM pictures of the nickel (Ni), bronze (B), glass beads with two particle sizes (SG and LG), and ion exchange resin (R) particles. The particle sizes and densities are given in Table 2-2. The particles were selected to give high, middle and low densities. The particle sizes were chosen to allow mixtures of approximately the same particle size, with close or dissimilar

densities, in addition to cases where the less dense particle is larger or smaller than the more dense particle. The mixtures along with the ranges of solids loadings are given in Table 2-3.

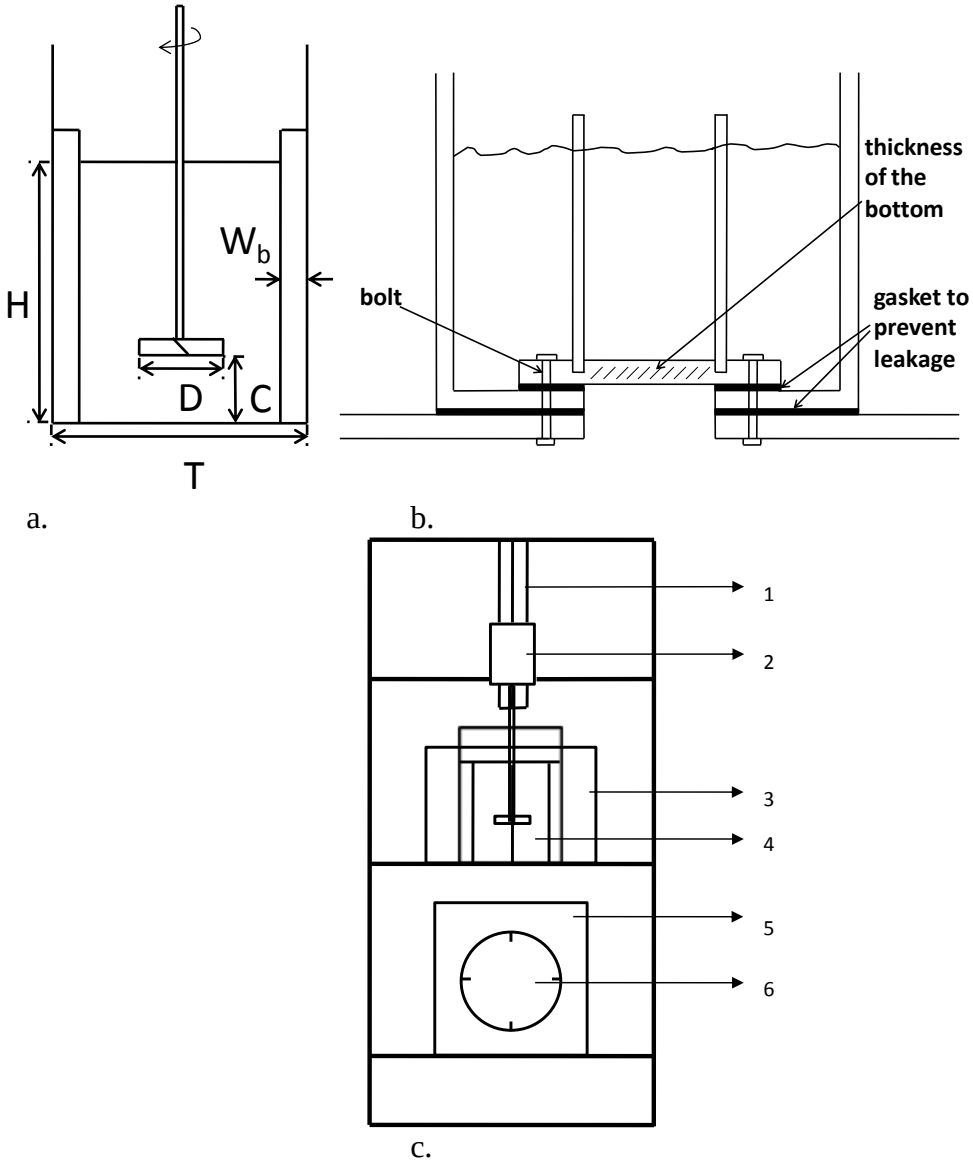

Figure 2-1: a. Cross-section of cylindrical tank b. cross-section of cylindrical and square tank together bolted on a platform c. front view of experimental setup: 1. slide, 2. motor, 3. square tank, 4. cylindrical tank, 5. mirror, 6. reflection of the tank bottom from the mirror.

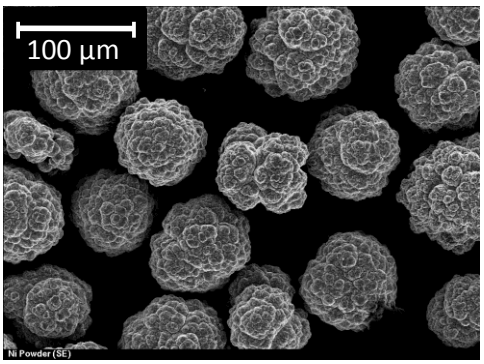

a. nickel

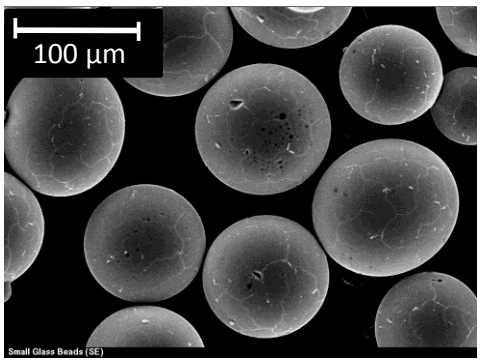

b. small glass beads

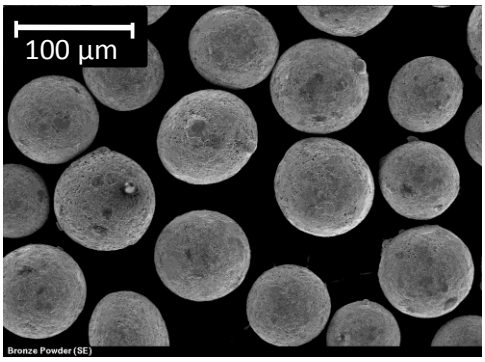

c. bronze powder

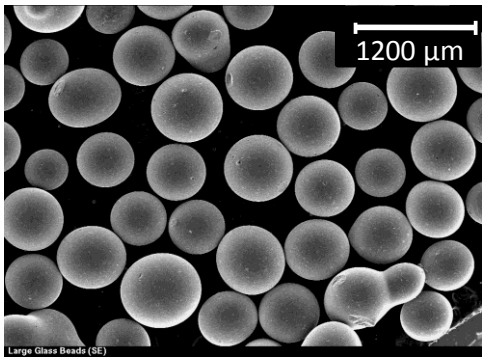

d. large glass beads

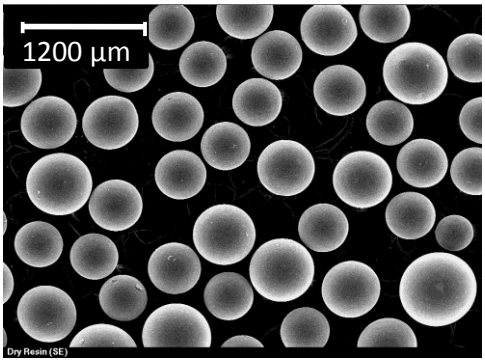

e. ion exchange resin (dry)

Figure 2-2: SEM images of the particles

Table 2-2: Particle specifications

Size (μm)	Type	Density (kg/m^3)	Ar	Shape
61-104	Nickel (Ni)	8900	47.6	Non-uniform
74-125	Small glass beads (SG)	2500	14.7	Spherical
150-297	Bronze (B)	8855	820.5	Spherical
595-841	Large glass beads (LG)	2500	5378.7	Spherical
677	Ion exchange resin (R)	1370	1126.3	Spherical

Table 2-3: Particle combinations and total solids loadings ranges

Less dense particle (wt%)	Denser particle (wt%)	Total solids loading (wt%)	Total solids loading (vol%)	Density ratio	Particle size ratio
SG (1.5 – 55)	B (1.5 – 1.0)	3-56	0.6-33	1:3.5	~1:2
LG (1.5 – 26)	B (1.5 – 1.3)	3-27.3	0.8-12	1:3.5	~3:1
R (1.5 – 35)	B (1.5)	3-36.5	1.3-28	1:6.5	~3:1
R (1.5 – 25)	LG (1.5 -1.4)	3-26.4	1.7-20	1:1.8	~1:1
SG (1.5 – 35)	Ni (1.5 – 1.2)	3-36.5	0.17-18	1:3.6	~1:1

In each set of experiments, the particles were weighed and poured into the tank with the water. The clearance of the impeller was adjusted, and then the impeller was started. The impeller speed was gradually increased and at every increment the system was left for 1 to 2 minutes to reach steady state. The particle behaviour at the bottom of the tank was observed over the entire tank bottom, but the location of last particle suspension was consistently from behind the baffle. The speed was increased until no particles remained stationary at the bottom of

the tank for more than 1 or 2 seconds (Zwietering, 1958) over an observation period of approximately 30 seconds. Then the motor was turned off, the clearance adjusted, and a new measurement started. When the solids loading was increased the total liquid height was kept constant by siphoning the excess water from the tank. When the experiments were finished, the slurry was siphoned out, filtered, and left on the lab bench to air dry.

The experimental accuracy was evaluated in two ways: first by comparing the results to the Zwietering correlation using literature values for S at low solids loadings (Ibrahim and Nienow, 1996), and second by comparing results between two observers. The comparison with the Zwietering correlation for the A310 impeller is shown in Figure 2-3a and b. Figure 2-3a shows the results for small glass beads at three solids loadings: 1, 3 and 6 wt%, with the deviation between the experiments and correlation always within 9%. Figure 2-3b shows the results for all five of the solids tested at 1.5 wt%, with densities decreasing from nickel to ion exchange resin (Ni > B > SG = LG > R). As expected, the denser particles (B and Ni) have much higher N_{js} values than the less dense ones (SG and R). The N_{js} results for large glass (LG) are higher than for small glass (SG) because the particle size of the LG is approximately six times larger than the SG. The experimental results are consistently somewhat higher than the Zwietering results, but are well within the expected variability based on the literature data.

The difference in measurements made by two observers depended on the solids mixture. For the unimodal slurry experiments, bronze slurries and small glass beads slurries were tested. The results for bronze slurries agreed to within 15%. For the small glass slurries the deviation is bigger, sometimes up to 38%. The small glass beads are very small and the colour contrast is weak, so it is difficult to see the particles.

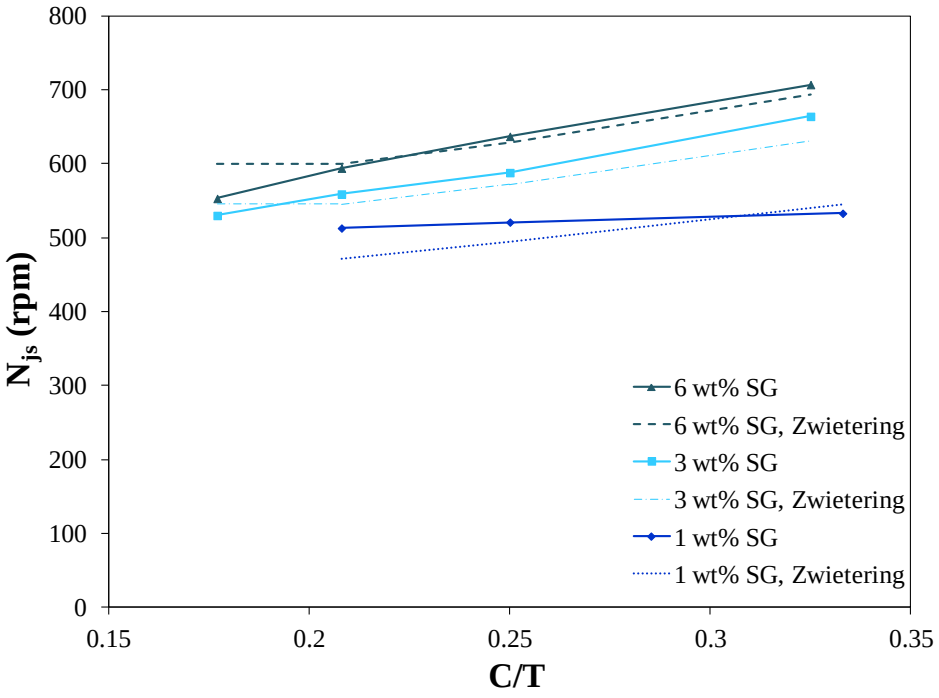

a.

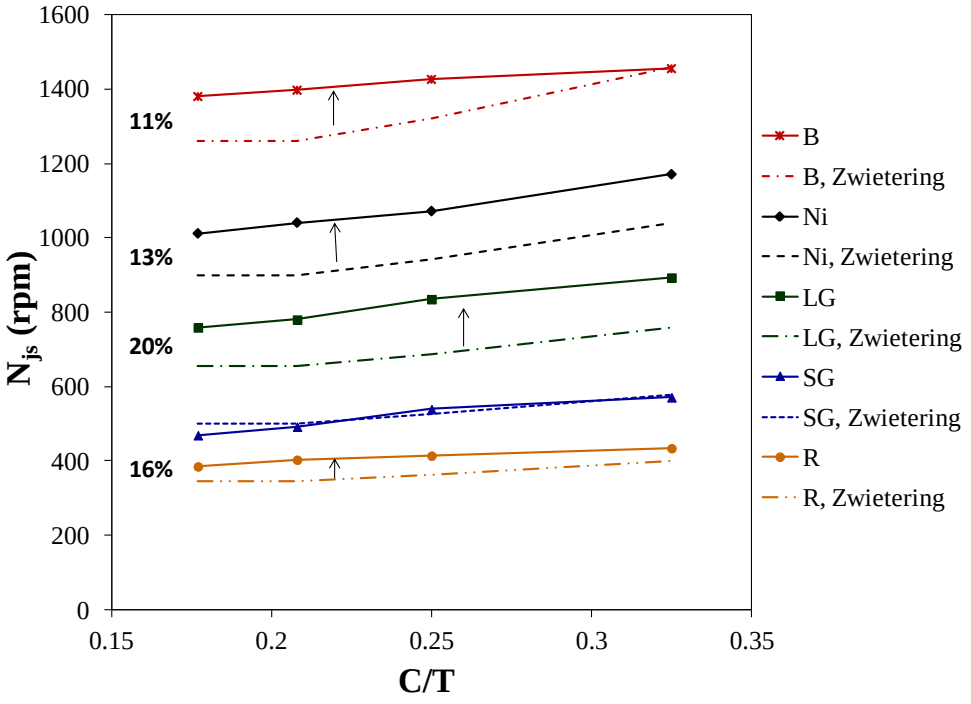

b.

Figure 2-3: Comparison between the Zwietering correlation for a D=T/3 A310 impeller (dashed lines) and experimental results a. small glass beads with varying solids loadings (weight %) b. All five particle classes at a fixed solids loading of 1.5 wt%. The maximum percent difference between the Zwietering correlation and the data is shown for each data set.

The colour contrast between bronze and water in a unimodal bronze slurry, and between bronze and small glass beads in a mixture is very significant. In the mixtures, small glass beads were typically suspended before the bronze and as a consequence, the results between the observers agreed to within 7%. Some of the results were repeated by the same observer over a period of 24 hours. The smallest increment for the impeller speed was 3 rpm in all the experiments. The repeated results were almost the same within the 3 rpm difference. In summary, the accuracy of the measured N_{js} ranges from 7% to 38% between observers, depending on the particle(s) in the slurry, with the unimodal small glass beads being twice as difficult to measure as any other mixture.

The main objective of this work was to study the behaviour of N_{js} for binary mixtures of solids at high solids loadings. Five different binary mixtures of particles were used in the experiments, as given in Table 2-3. There are two particle properties that can be changed: particle density and particle size. Since particle sizes are almost the same for R with LG and SG with Ni, these mixtures represent solely the effect of density ratio on N_{js}. The effect of particle size can be seen in results for mixtures of SG with B and LG with B since SG and LG have the same density, but different particle sizes. In mixtures of R with B both the particle size ratio and the density ratio are different than the other mixtures which allows one to investigate the effect of both of the properties at once, using the information obtained from other combinations. The experiments were performed from low solids loadings up to high solids loadings, in many cases reaching the point where significant particle-particle interaction effects were observed.

2.3. Results and Discussion

The results cover a range of solids loadings from 1.5 wt % to up to 56 wt %, depending on the particle combination. They are presented in several parts:

- The base case is a mixture of SG with B, where a networking effect reduces N_{js} as the loading is increased from 1.5 wt % to 55 wt % SG.

The base case clearly illustrates the complexities which can arise in this problem.

- The effect of inverting the diameter ratio (LG with B, and R with B).
- The effect of varying the density ratio in mixtures of particles of a similar size: first LG with R, where the densities are similar, then SG with Ni, where the densities are quite different
- A review of the data considering the validity of design based on the largest N_{js} in the mixture.
- Consideration of possible mechanisms of suspension in mixed slurries
- A comparison of power consumption and S values at high solids loadings, particularly with respect to the effect of off-bottom clearance.

All of the legends give the weight percentages of the particles in the mixture, with the less dense particle identified first. The symbols in the figures are consistent throughout the paper, varying with wt %. The N_{js} of the unimodal slurry of the more dense phase is always higher than the less dense phase, and this line is shown with starred symbols.

2.3.1. Base case: SG+B (density ratio 1:3.5, diameter ratio 1:2)

In Figure 2-4a and b, the effect of solids loading on mixtures of SG with B is compared with the results for unimodal slurries of SG and B at 1.5 wt% solids loading. In these figures, all of the mixture results collapse around the results for 1.5 wt% B. This suggests that the N_{js} of the mixture is dominated by the bronze particles, and the design rule is correct.

Figure 2-5a and b continue the experiments shown in Figure 2-4a and b to higher loadings of SG. When the SG loading is increased from 12 to 26 wt%, N_{js} drops by 13-15 % for the A310 impeller and 8-13 % for the PBT impeller. N_{js} continues to drop, but more slowly, as the loading of SG is further increased. At the highest loading of SG, which is 55 wt%, the drop in N_{js} is 12-22% for the A310 impeller and 8-21% for the PBT impeller relative to 12 wt% SG. It is

concluded that at high solids loadings particle-particle interactions can have a significant effect on N_{js}.

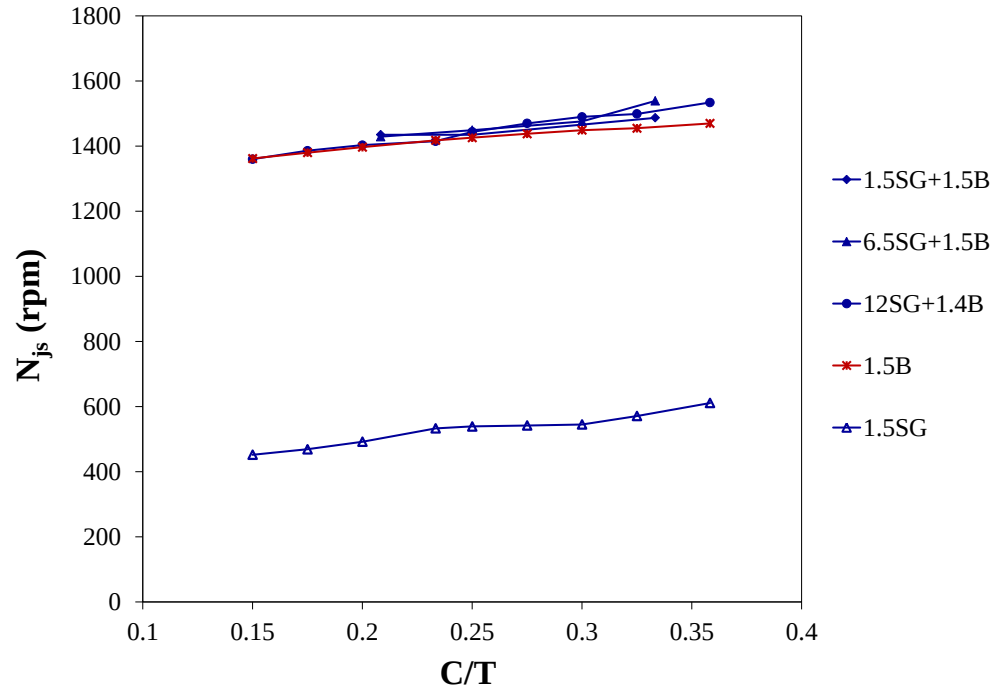

a.

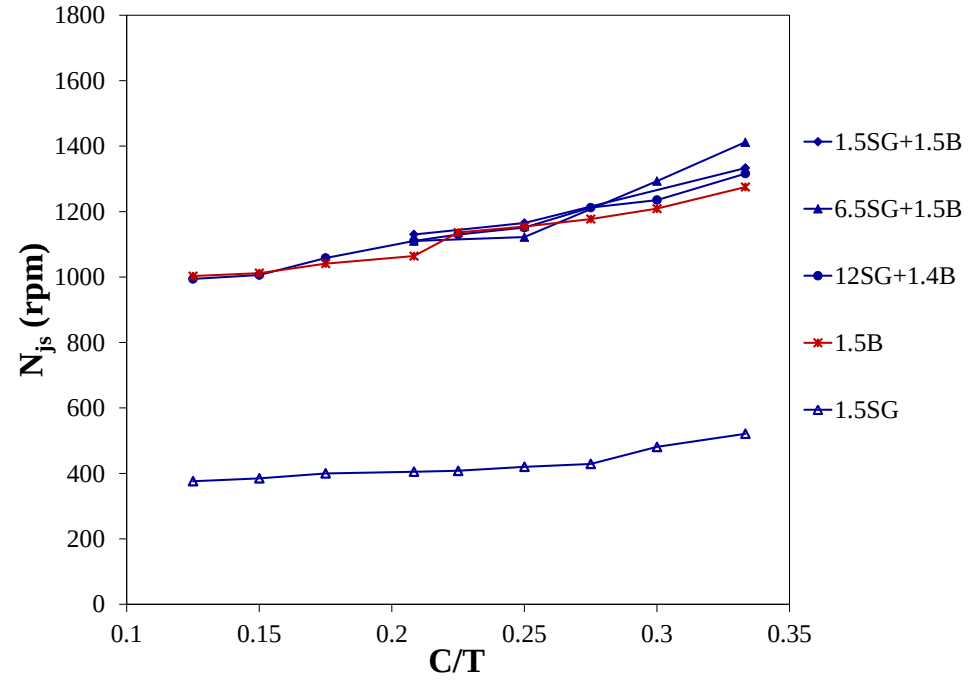

b.

Figure 2-4: Effect of density on N_{js} of mixtures of SG with B for low solids loadings a. A310 b. PBT

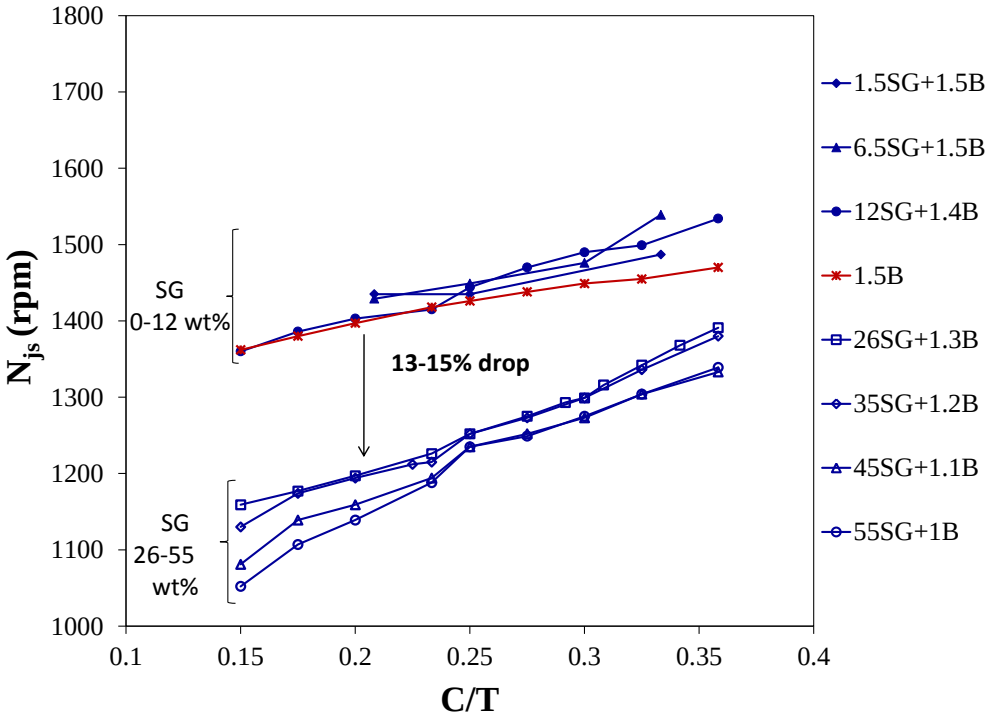

a.

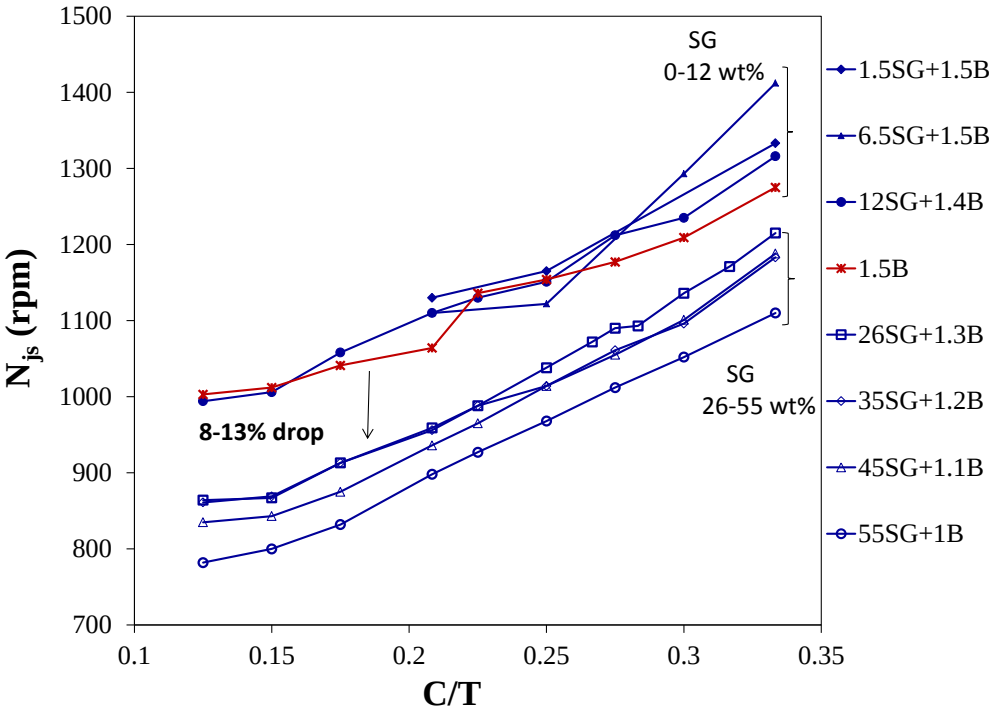

b.

Figure 2-5: At high solids loadings of small glass particles (SG) with bronze (B) where $d_{p,SG} < d_{p,B}$, N_{js} decreases with increasing solids loadings. a. A310 b. PBT

During the SG+B experiments, all of the SG particles were suspended with B particles remaining at the bottom of the tank until the complete off-bottom suspension condition was satisfied. Since the SG particles are suspended first, further increases in the impeller speed also increase the speed of the small particles. As the SG loading was increased, the bronze particles were obscured from view at the bottom of the tank and only the glass beads approached the bottom. Based on this observation a networking mechanism is proposed. The suspended bronze particles circulate in the tank and try to settle back down to the bottom, but they cannot reach the tank bottom because there are many small glass beads in the way, forming a network of fast moving particles. Since the bronze particles are approximately twice as large as the small glass beads, the bronze cannot pass through the network and remains suspended in the tank. As a result, less energy is needed to suspend B in a mixture containing very high loadings of SG than for lower loadings. The networking mechanism does not indicate network of particles based on surface charges, or a pseudohomogeneous fluid assumption, because the small glass particles are too large to observe this effect. It seems that in a mixture of small less dense particles and large denser particles, the small particles start supporting the large ones, leading to a drop in N_{js}.

2.3.2. Inverting the diameter ratio from the base case LG+B (density ratio 1:3.5, diameter ratio 3:1) and R+B (density ratio 1:6.5 and diameter ratio 3:1)

To test the proposed networking mechanism, the high solids loadings experiments were repeated with large glass beads instead of small glass beads. As seen in Figure 2-6a and b N_{js} increases steadily for LG solids loadings up to 12 wt%. When the loading of LG is increased from 12 to 26 wt%, N_{js} increases beyond the maximum motor speed for the A310 impeller. The same increase in the LG loading for the PBT impeller resulted in a 12-15% increase in N_{js}. In the mixture of LG with B, the LG particles, which are approximately three times larger than the B particles, are suspended first. These particles collide with the B particles but the collisions do not result in suspension of the B particles. Instead,

experimental observations showed that the LG particles push the B particles towards the periphery of the tank and form a network above them. Once the B particles are suspended, they circulate in the tank and settle back down to the bottom. Since the B particles are much smaller than the LG particles, they easily slip through the gaps between the LG particles. While the SG forms a network supporting the B, the LG forms a network preventing suspension of B.

The mixtures of R with B showed very similar results to the mixtures of LG with B, as shown in Figure 2-7. As the loading of R increases, the N_{js} of the mixture increases steadily. These results clearly show that the particle size of the less dense particles has an effect on the behaviour of the mixture at high solids loadings. Note also that the density of the resin is approximately one half that of the glass, but for both particles, the behaviour of the mixture is similar.

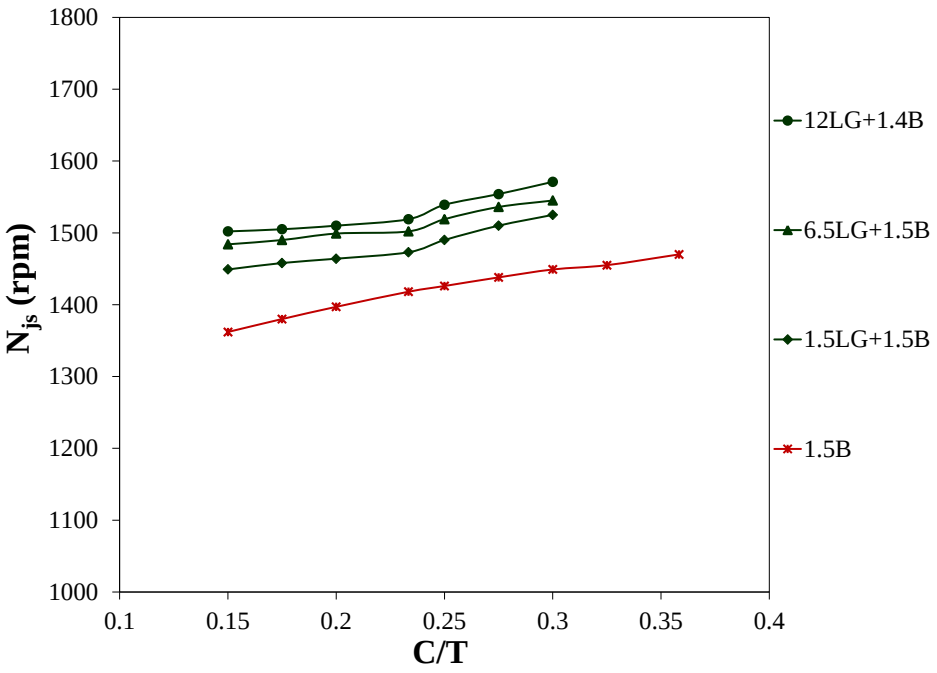

a.

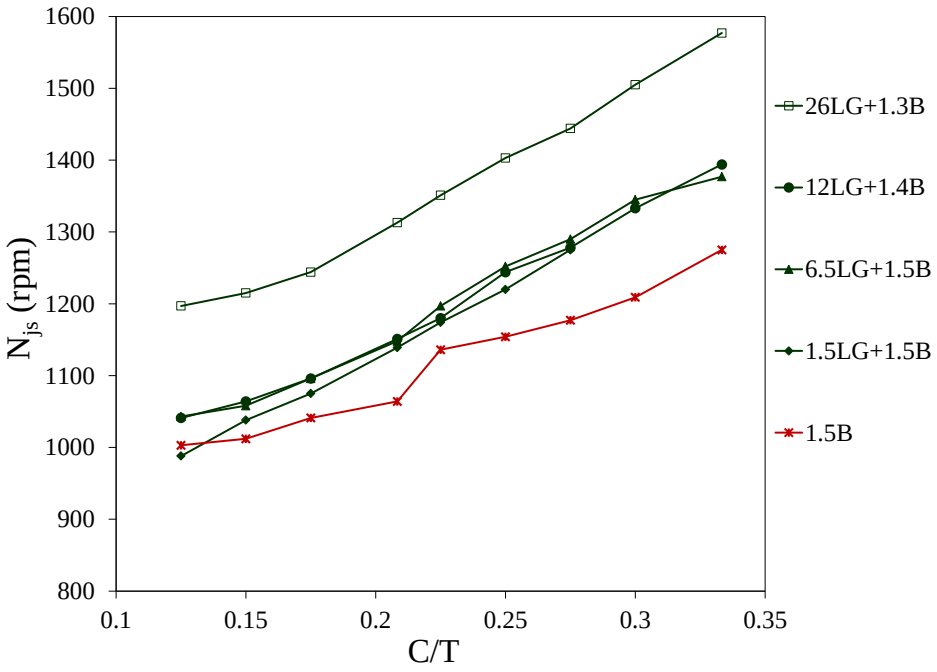

b.

Figure 2-6: At high solids loadings of particles which are larger than the bronze particles, N_{js} increases. The mixture large glass beads with bronze a. A310 b. PBT

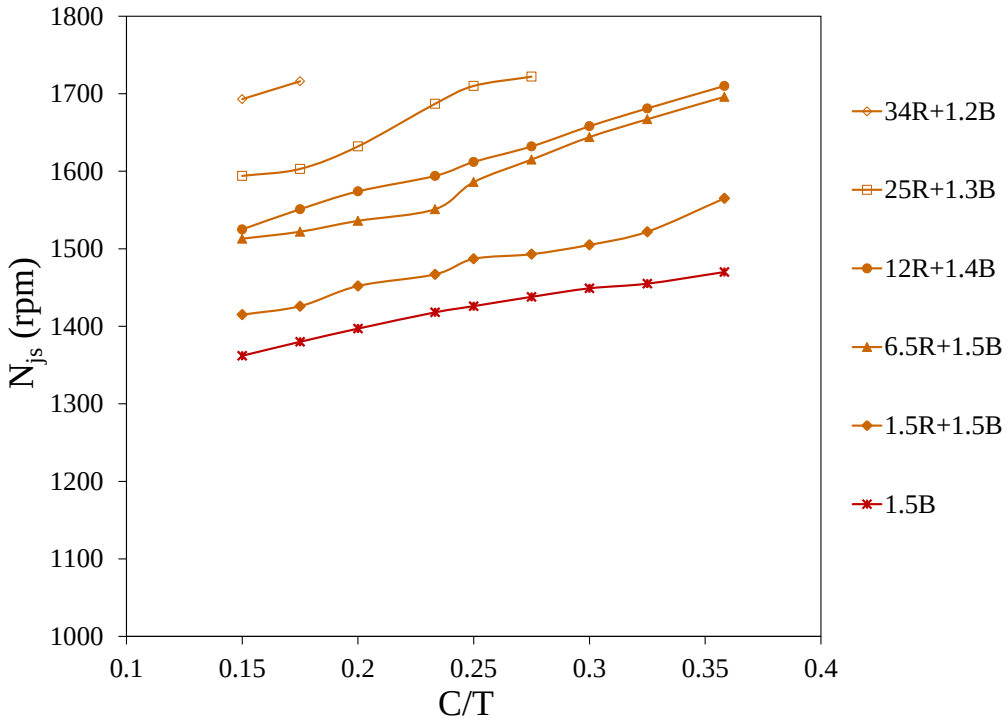

a.

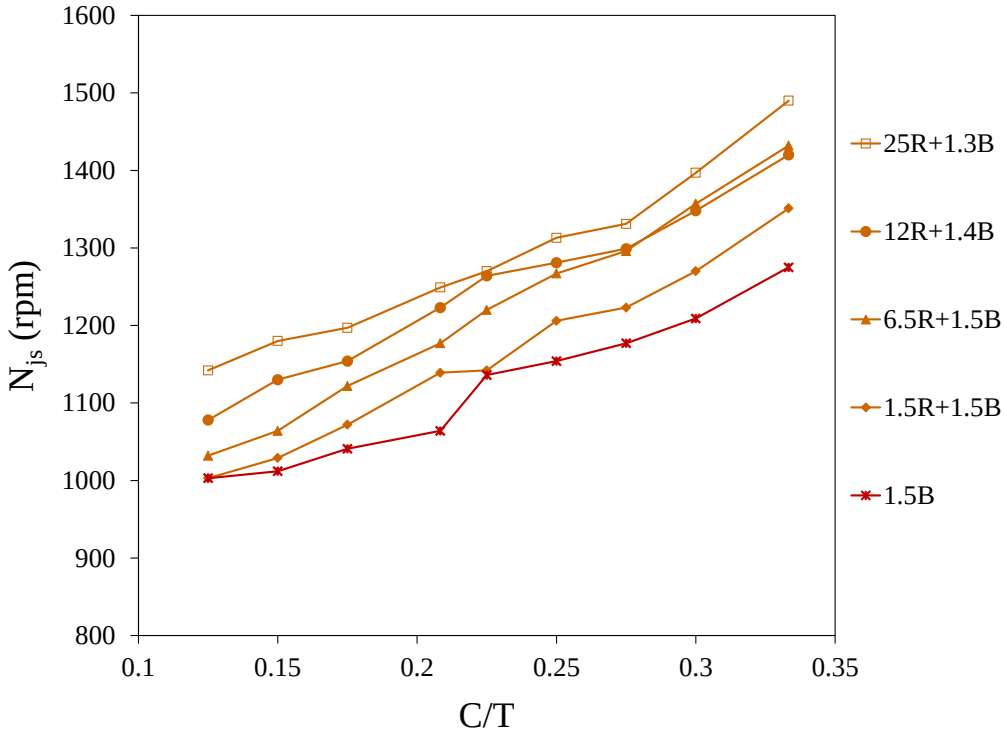

b.

Figure 2-7: At high solids loadings of particles which are larger than the bronze particles, N_{js} increases. The mixtures are resin with bronze a. A310 b. PBT

2.3.3. Effect of particle density for similar sized particles R+LG (density ratio 1:1.8, diameter ratio 1:1) and SG+Ni (density ratio 1:3.6 and diameter ratio 1:1)

The next set of results are for similar sized particles, the first mixture with similar densities (R with LG) and the second mixture with quite different densities (SG with Ni).

Figure 2-8 shows the results for mixtures of R with LG, which are similar to Figure 2-6 and Figure 2-7 where the large particles are less dense than the smaller ones. At solids loadings of R up to 12 wt% the results show a slight tendency to increase, and when the solids loading of R is further increased to 25 wt%, there is a significant increase in N_{js}: 25-27% for the A310 impeller, and 15-20% for PBT impeller.

Figure 2-9 shows a different trend for SG with Ni. In this case there is no significant change in N_{js} as the loading of the SG particles is increased and the N_{js} results are very close to the ones obtained for the unimodal slurry of Ni particles with a solids loading of 1.5 wt%. This is similar to the behaviour of the SG+B mixture at low SG loadings.

The density difference between the SG and Ni is much larger than the density difference between R and LG. This means that in the mixture of SG with Ni, the N_{js} of the mixture is well above the N_{js} of SG and the SG particles are suspended long before the Ni. The momentum transfer as a result of the collisions between the very fast SG particles and the Ni particles is more significant than it is between the R and LG particles, and the N_{js} required to suspend the first 1.5% of Ni is well above the N_{js} required to suspend even a significant loading of SG; therefore, it does not get harder to suspend the mixture as the solids loading of SG particles increases. In this case, the design rule appears to be justified, particularly for the A310, even up to solids loadings of 36 wt %. As is the case for all of the data so far, the A310 is less sensitive to off-bottom clearance than the PBT.

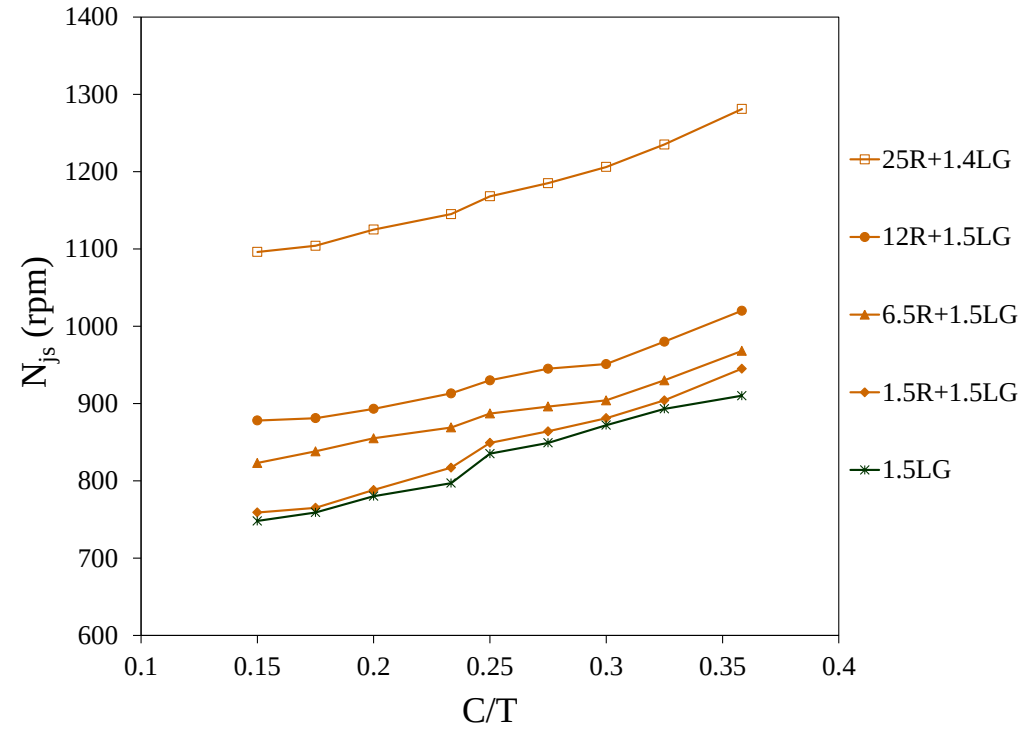

a.

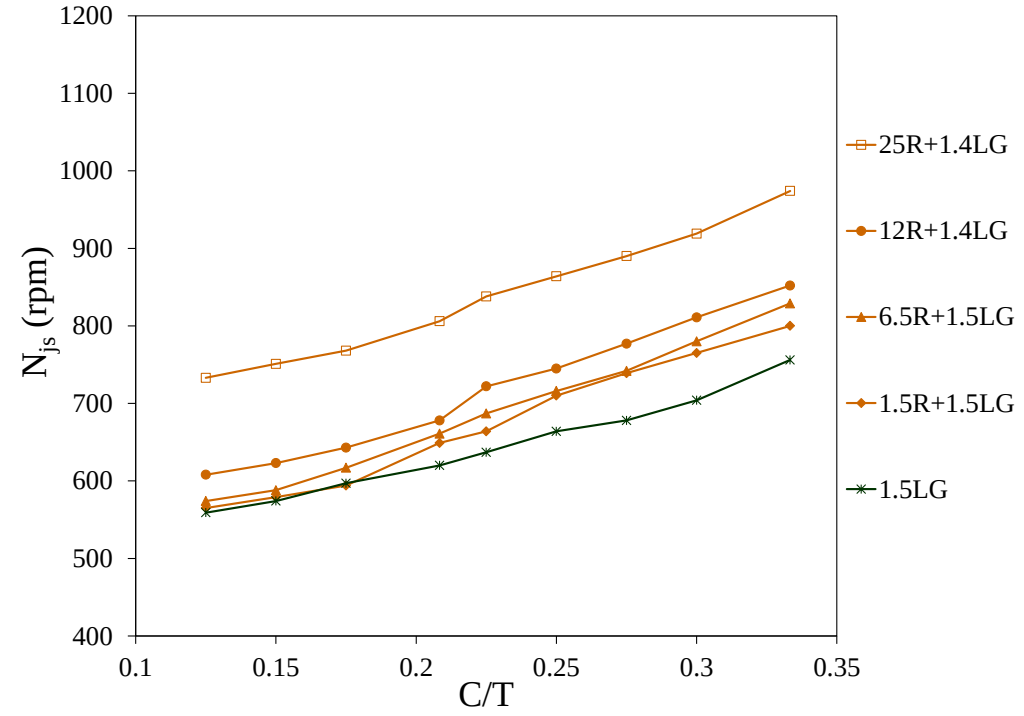

b.

Figure 2-8: Mixtures of particles with similar sizes and densities (R with LG) give steadily increasing N_{js} with increasing solids loading a. A310 b. PBT

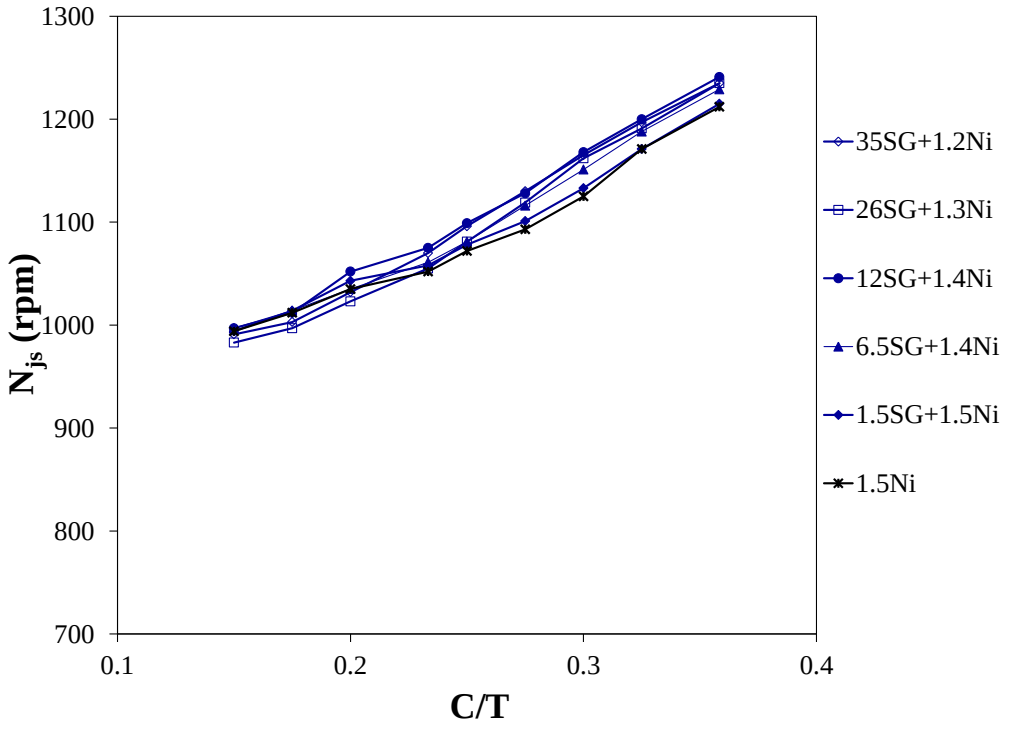

a.

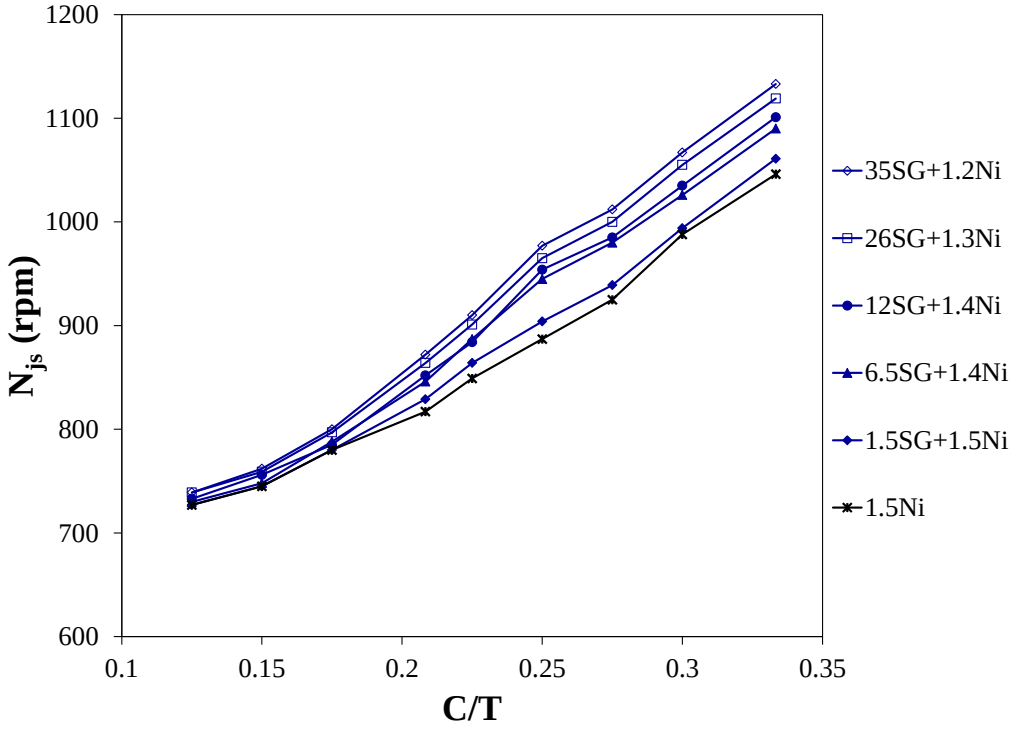

b.

Figure 2-9: Mixtures of particles with similar size, but different densities (SG with Ni) are dominated by the heavier particles a. A310 b. PBT

2.3.4. Design based on maximum N_{js} in a mixture of particles

The data reported in Figure 2-5 through Figure 2-9 consistently shows that selecting the maximum N_{js} from a mixture of particles will underestimate the actual N_{js} of the mixture. For most of the mixtures examined, adding a second particle phase increases N_{js}. The mixture N_{js} can be approximated by the maximum N_{js} only when the second particle phase has a particle diameter either similar to (SG+Ni) or smaller than (SG+B) the dense phase, *and* there is a large difference in N_{js} between the two phases. The design rule is particularly justified for low solids concentrations in mixtures of this kind.

2.3.5. Mechansims

In order to better understand the behaviour of the solids mixtures, related literature on the suspension of mixtures of solids in other geometries was explored: river bed erosion, slurry pipeline flow, and solid-solid mixing. Solid suspension mechanisms proposed for river bed erosion and slurry pipeline flow are similar to the mechanisms proposed for stirred tanks. The literature on slurry flow in pipes and the literature on solid-solid mixing presented two additional interesting mechanisms: the first is based on fluid motion in the boundary layer, the second on particle-particle interactions in the solids bed.

A turbulent boundary layer has three distinct regions: the viscous sub-layer, where velocity gradients are very large and viscosity dominates the flow, the buffer region, and the outer turbulent region, where the mean velocity gradients are much smaller and the flow is dominated by turbulent fluctuations. The slurry pipeline flow literature relates the particle suspension to the hydrodynamic lift near the wall and to turbulent diffusion in the buffer and outer turbulent region (Wilson et al., 2010). Similarly, in stirred tanks if a particle resides completely in the viscous sub-layer, the velocity gradient will roll the particle along the bottom and generate a local lift force which moves the particle away from the wall, reduces the friction at the bottom of the tank, and makes the particles easier to suspend. In the outer turbulent layer, turbulent eddies surround the particle and move it into the higher velocity mean flow, where it is convected toward the wall

and lifted into the bulk of the tank. Molerus and Latzel (1987a) found that the Archimedes number can be used to determine whether a particle is small enough to reside in the viscous sublayer in a stirred tank. For Ar < 40, particles are totally immersed in the viscous sublayer and for Ar ≥ 40 they are larger than the viscous sublayer.

Applying this criterion to the base case, the SG particles at the bottom of the tank are in the viscous sublayer (Ar = 14.7), but the larger B particles (Ar = 820.5) are not. The fast moving SG particles are lifted off the bottom in the viscous sublayer, get underneath the B particles and collide with them. These collisions move the B particles up so that a larger portion of them are exposed to larger scale turbulent eddies which contain more energy, making the solids suspension easier.

The small glass beads are also present in the SG+Ni mixture, which is the only other mixture where N_{js} stayed nearly constant with the addition of a second solids phase. In this mixture, the Ni is very dense, but has Ar=47.6, which is very close to the cutoff. While the SG+Ni mixture shows the same behaviour as the SG+B at low solids loadings, it does not show the same drop in N_{js} at high solids loadings. We attribute this to the size ratio of the particles, which is 1:2 for SG+B, and 1:1 for the SG+Ni. This data confirms that the networking effect is different than the boundary layer lift effect.

All of the other mixtures contain only particles with large Ar. When the particle size ratio is inverted from the base case with mixtures of LG with B and R with B, the Ar for both particles in both mixtures is significantly larger than 40, so these particles are not exposed to the lift forces close to the wall and must rely on turbulent eddies to be suspended. In case of mixtures of R with LG the particle sizes are similar, but both are larger than the viscous sublayer. Again, large scale turbulent eddies are required to suspend these particles and neither one can support the other.

The main drawback of the boundary layer lift theory is the assumption that a viscous sublayer forms at the bottom of a stirred tank which is similar to the

boundary layer at the wall of a pipe. The flow at the bottom of a stirred tank is time varying, with a flow attachment ring near the center of the tank where the flow attaches to the bottom, and a separation ring near the outer walls where the flow changes direction from radially outward to upward. While a boundary layer must be present on all surfaces, and the scale of the boundary layer is very small relative to the flow in the bulk of the tank, it will not have the same uniform thickness in a stirred tank that it does at the walls of a pipe. Application of the Archimedes number criterion to the wide range of conditions encountered in industry would require, at a minimum, changing the fluid in the tank to a higher viscosity to verify the effect of the boundary layer thickness, and preferably targeted testing of a number of other particle classes. This wide range of property variations is outside the scope of this study.

The second mechanism considered is known as the Brazil Nut Effect (BNE), where larger particles segregate to the top of a mixture of particles (e.g. mixed nuts) when the mixture is horizontally sheared. This effect, and the reverse effect, where large particles segregate at the bottom of the mixture (RBNE) is widely discussed in the solids mixing literature. Equation 2-8 gives the cross over point for the BNE. When the diameter ratio equals the square root of the mass ratio, the mixture will be homogeneous; when the diameter ratio is larger, a point is reached where the BNE is observed, and when it is smaller, the RBNE is observed.

Table **2-4** gives the calculations for the BNE. When tested in the lab on dry mixtures of the particles, these predictions were consistent with observations. They are also consistent with the LG+B and the R+B mixture, where the bronze was trapped at the bottom by the larger particles, but not with the B+SG slurry. It is concluded that the BNE criterion cannot be applied to the suspension of mixed slurries in stirred tanks.

Table 2-4: BNE criterion calculations from Equation 2-8

Mixture	d_A/d_B	$\sqrt{m_A/m_B}$	Form of Brazil nut effect
B/SG	2.25	6.35	RBNE
LG/B	3	2.76	BNE
R/B	3.02	2.07	BNE
R/LG	1	0.75	Homogeneous
SG/Ni	1.25	0.74	Homogeneous

2.3.6. Impeller characterization: power consumption (P_{js}), Zwietering constant (S), and the effect of clearance

In this section, the A310 and PBT impellers are compared using the power consumption at the just suspended condition, P_{js} (Equation 2-2). Increases in the impeller speed, the diameter of the impeller, and the density of the slurry all affect P_{js}.

Throughout this paper, the diameter of the impellers is fixed at D=T/3. The density of the slurry depends on the solids loading of the particles in the slurry. The difference in power consumption between the two impellers also depends on the power number of the impeller ($N_{p,A310}$=0.3, and $N_{p,PBT}$=1.27 (Chapple et al., 2002)) and on N_{js}. Figure 2-10 shows the power consumption results for mixtures of SG with B for both the A310 and PBT impellers. While N_{js} for an A310 impeller is always higher than for a PBT impeller for the same conditions, the power consumption for the PBT is significantly higher than for the A310. Both the PBT and the A310 power consumption is sensitive to off-bottom clearance, but the PBT shows a bigger dependence. The increase in power consumption for the PBT is 150% while for the A310 it is 50% from the lowest to the highest clearance.

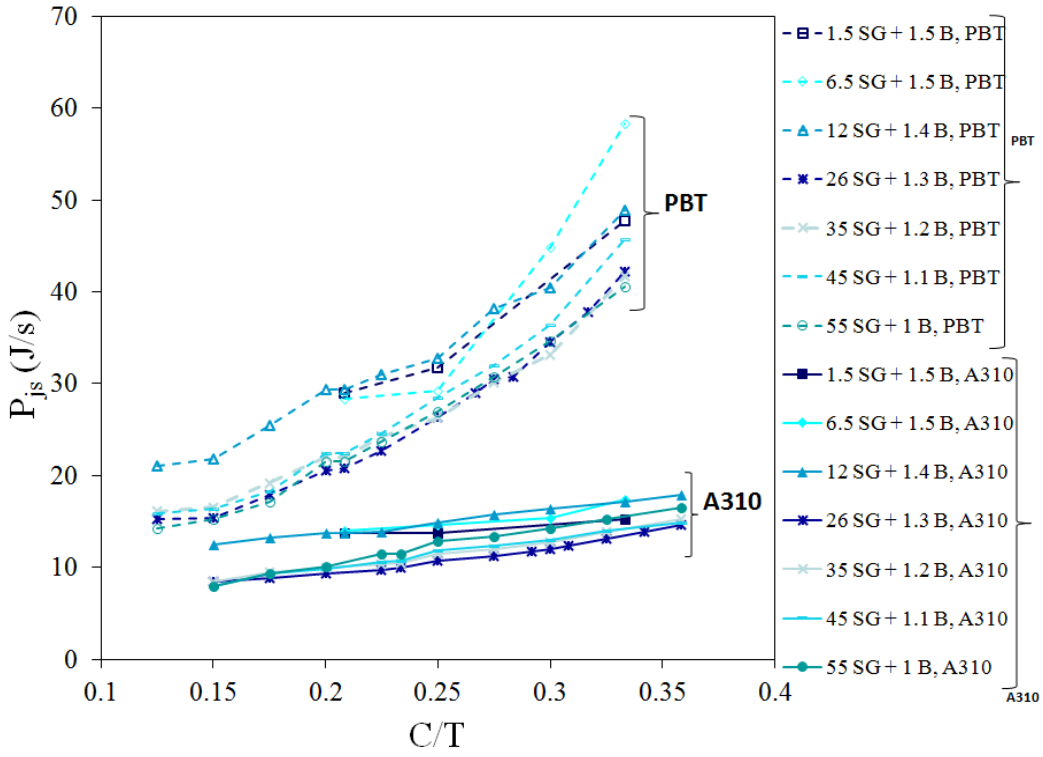

Figure 2-10: Comparison of power consumption by the A310 and PBT impellers for mixtures of SG with B at N_{js}.

Figure 2-11 a and b show the variation in S values for the A310 and PBT impellers for unimodal slurries of the five different particles, SG, B, LG, R and Ni, at 1.5 wt% and ten clearances. The S values for the five different particles were averaged at every clearance for each of the impellers and the results are reported in Table 2-5. The variance on S changes from 0.33 to 0.19 for the PBT and from 0.54 to 0.24 for the A310 over the range of clearances. The full set of data was also fit to linear, polynomial, and power law models ($S \propto (C/T)^k$). The linear model gave the best fit for the A310 data whereas a second order polynomial gave the best fit for the PBT.

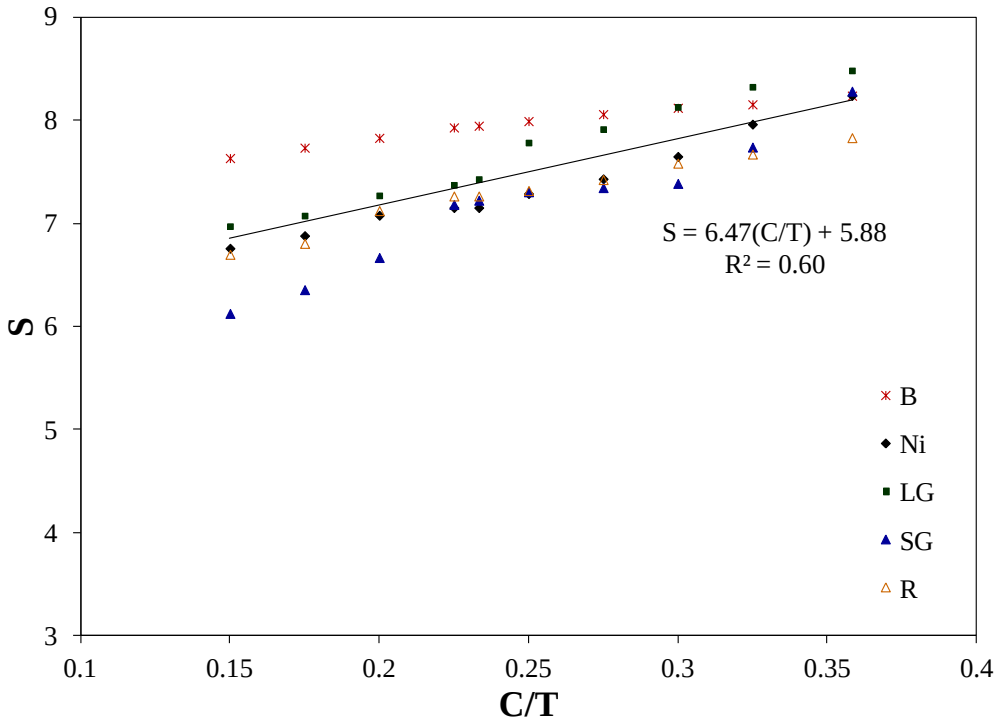

a.

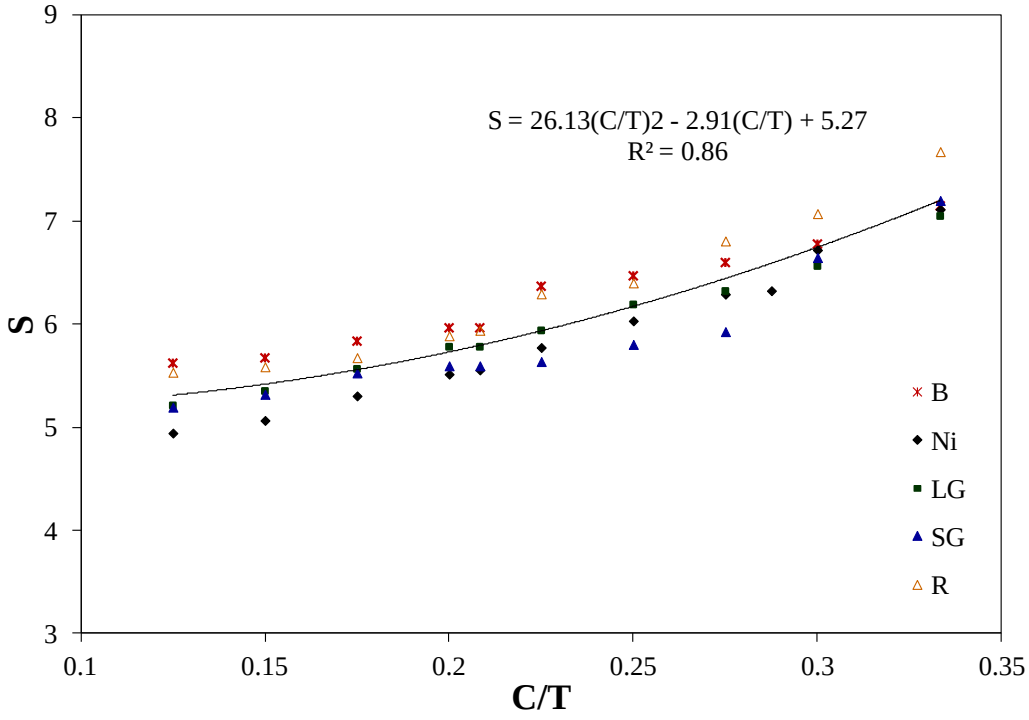

b.

Figure 2-11: Effect of clearance and particle type on S. All particles are tested at 1.5 wt% solids. a. A310 b. PBT

Table 2-5: Calculated S values for the A310 and PBT impellers

Impeller	C/T	S	σ
A310	0.150	6.84	0.54
	0.175	6.97	0.50
	0.208	7.19	0.42
	0.225	7.38	0.32
	0.233	7.40	0.32
	0.250	7.54	0.33
	0.275	7.63	0.33
	0.300	7.77	0.33
	0.325	7.97	0.27
	0.358	8.21	0.24
PBT	0.125	5.30	0.28
	0.150	5.40	0.24
	0.175	5.58	0.20
	0.200	5.75	0.19
	0.208	5.76	0.19
	0.225	6.00	0.32
	0.250	6.18	0.27
	0.275	6.39	0.33
	0.300	6.67	0.19
	0.333	7.15	0.25

Figure 2-11a and b show the trendlines, the equations and the fraction of variance explained by the model, R^2, for both impellers. Within the A310 data, every particle gave a different slope, with only 60% of the variance explained by the model. Since most of the variance in the data is at very low clearances and the A310 is designed for clearances that are larger than T/3, the best conclusion to draw from this result is that the A310 impeller should be used only within the vendor's recommended range of clearances.

The polynomial model provides a good fit for the PBT data, explaining over 85% of the variance and returning a curve which closely follows the trend of the data. The effect of off-bottom clearance on S is small for C/T<0.25, but increases significantly as the secondary circulation loop begins to develop at the bottom of the tank and some of flow at the bottom of the tank is radially inward instead of purely radially outward (see Kresta and Wood, 1993).

The effect of off-bottom clearance is complex and depends on both the impeller type and the particle properties. While a polynomial curve was successfully fit to the PBT data for a single particle type at low solids concentration, this model should not be extended to other impellers, or to mixtures of particles.

2.4. Conclusions

The goal of this research was to examine the complete off-bottom suspension behaviour of mixtures of particles at high solids loadings. The following conclusions can be reached from the experimental results for mixtures of dense and less dense particles:

- The simple design criterion of setting N_{js} equal to the maximum N_{js} among all of the particles in the mixture is not sufficient. In general, increasing the solids loading increases N_{js}.
- When one particle class has an N_{js} much smaller than the other, and when that particle has Ar<40, addition of low concentrations of a second class of particles does not increase N_{js} significantly and the design criterion may safely be applied.
- At very high solids loadings (>25 wt %), particle-particle interactions can dominate and result in significant decrease in mixture N_{js}. Among the five mixtures studied, this was only observed for the SG+B mixture.
- Both the particle diameter ratio and the density ratio have an impact on the solids suspension behaviour.
- P_{js} is lower for the A310 than for the PBT. The power consumption for both impellers increases with off-bottom clearance with the effect being much more dramatic for the PBT. This compares well with a survey of S values from the literature, which showed that axial impellers are much more efficient for solids suspension, and that power consumption increases with increasing off-bottom clearance.

2.5. References

Armenante, P.M., E.U. Nagamine and J. Susanto, 1998. Determination of correlations to predict the minimum agitation speed for complete solid suspension in agitated vessels. Can J Chem Eng. 76, 413-419.

Armenante, P.M. and E.U. Nagamine, 1998. Effect of low off-bottom impeller clearance on the minimum agitation speed for complete suspension of solids in stirred tanks. Chem Eng Sci. 53, 1757-1775.

Baldi, G. and E. Alaria, 1978. Complete suspension of particles in mechanically agitated vessels. Chem Eng Sci. 33, 21-25.

Chapple, D., S.M. Kresta, A. Wall, A. Afacan, 2002. The effect of impeller and tank geometry on power number for a pitched blade turbine. Trans IChemE. 80, A, 364-372.

Chapman, C.M., A.W. Nienow, M. Cooke and J.C. Middleton, 1983, Particle-gas-liquid mixing in stirred vessels. Part-1: particle-liquid mixing. Trans IChemE. 61, 71-81.

Hong, D.C., P.V. Quinn, S. Luding, 2001. Reverse Brazil nut problem: competition between percolation and condensation. Phys Rev Let. 86 (15), 3423-3426.

Ibrahim, S. and A.W. Nienow, 1996. Particle suspension in the turbulent regime: The effect of impeller type and impeller/vessel configuration. Trans IChemE. 74, Part A, 679-688.

Kasat, G.R. and A.B. Pandit, 2005. Review on mixing characteristics in solid-liquid and solid-liquid-gas reactor vessels. Can J Chem Eng. 83, 618-643.

Kresta, S.M. and P.E. Wood, 1993. The mean flow field produced by a 45° pitched blade turbine: changes in the circulation pattern due to off-bottom clearance. Can J Chem Eng. 71, 42-53.

Kuboi, R., I. Komasawa and T. Otake, 1972. Behavior of dispersed particles in turbulent liquid flow. J Chem Eng Japan. 5, 349-355.

Kukukova, A and S M Kresta, 2007. Comparison of the Performance of Different Impeller-Tank Configurations for Solids Suspension. 57th Canadian Chemical Engineering Conference, Edmonton, Oct 28-31, 2007.

Liao, C.C., S.S, Hsiau, T.H. Tsai, C.H. Tai, 2010. Segregation to mixing in wet granular matter under vibration. Chem Eng Sci. 65, 1109-1116.

Machado, M.B., S.M. Kresta, C.F. Joaquim Jr and J.R. Nunhez, 2009. Determination of characteristics of PBT and KPC impellers. 8th World Congress of Chem Eng, Montreal, August 23-27, 2009.

Montante, G. and F. Magelli, 2007. Mixed solid distribution in stirred vessels: experiments and computational fluid dynamics simulations. Ind. Eng. Chem. Res. 46, 2885-2891.

Myers, K.J. and J.B. Fasano, 1992. The influence of baffle off-bottom clearance on the solids suspension of pitched-blade and high-efficiency impellers. Can. J. Chem. Eng. 70, 596-599.

Myers, K.J., J.B. Fasano, and R.R. Corpstein, 1994. The influence of solids properties on the just-suspended agitation requirements of pitched blade and high-efficiency impellers. Can J Chem Eng. 72, 745-748.

Molerus O. and W. Latzel. 1987a. Suspension of solid particles in agitated vessels-I. Archimedes numbers <40. Chem Eng Sci. 42, 1423-1430.

Molerus O. and W. Latzel. 1987b. Suspension of solid particles in agitated vessels-II. Archimedes numbers >40, reliable prediction of minimum stirrer angular velocities. Chem Eng Sci. 42, 1431-1437.

Nienow, A.W., 1968. Suspension of solid particles in turbine agitated baffled vessels. Chem Eng Sci. 23, 1453-1459.

Paul E.L., V.A. Atiemo-Obeng and S.M. Kresta, 2004. Handbook of Industrial Mixing, Science and Practice. John Wiley & Sons, Inc., Hoboken, New Jersey.

Sharma, R.N. and A.A. Shaikh, 2003. Solids suspension in stirred tanks with pitched blade turbines. Chem. Eng Sci. 58, 2123-2140.

Wilson, K.C., R.S. Sanders, R.G. Gillies, C.A. Shook, 2010. Verification of the near-wall model for slurry flow. Powder Technol. 197, 247-253.

Zwietering, Th.N. 1958. Suspending of solid particles in liquid by agitators. Chem. Eng. Sci. 8, 244-253.

Chapter 3 : Prediction of Just Suspended Speed at High Solids Loadings for Mixed Slurries*

3.1. Introduction

In many solid-liquid mixing operations the main objective is mass transfer between the two phases. To maximize the mass transfer the entire surface area of the solids should be exposed. This can be achieved by operating at complete off-bottom suspension conditions. The key operating parameter for this condition is the impeller speed, which is called the just suspended speed (N_{js}). N_{js} is defined as the impeller speed at which no solids remain stationary at the bottom of the tank for more than 1 or 2 seconds (Zwietering, 1958). It is critical to predict N_{js} accurately, because solid-liquid mixing is a power intensive operation. Current correlations are limited to unimodal slurries at low solids loadings, but many industrial slurries are composed of mixtures of solids with varying densities and particle sizes at high concentrations. The gap between research and industry is vast, and the need for an accurate design model for a mixed slurry N_{js} is clear. In this study two models to predict mixture N_{js} are proposed and tested. To understand the behaviour of mixtures we first need to start from the basics and explore the solid suspension mechanisms.

Several mechanisms were suggested for solid suspension, most of which are based on energy and force balances. The most well-known theory was suggested by Baldi et al. (1978). According to this theory the energy of the turbulent eddies should match the energy required to suspend the solids. The turbulent eddies that are in the same order of magnitude as the particle size are capable of suspending the particle. The eddies smaller than the size of the particle do not have sufficient energy, and the larger eddies may convect the particles rather than suspending

* *A version of this chapter has been submitted for publication to Chemical Enginerring Research and Design. This paper is co-authored by Inci Ayranci, Theodore Ng, Arthur W. Etchells III, and Suzanne M. Kresta.*

them. Baldi also mentioned that the mean flow is necessary for moving the particles from the centre towards the walls, where they are carried upwards with the wall-jets (Bittorf and Kresta, 2003).

Molerus and Latzel (1987) suggested a theory based on a force balance where the shear force exerted on a particle by the fluid should be able to overcome the gravity force reduced by the buoyancy in order to suspend the particle. Further investigation of this theory with experimental data showed a limit on Archimedes number (Ar) which is used to determine whether the particles are exposed to the boundary layer effects.

$$Ar = \frac{d_p^3\, g}{\nu^2}\ \frac{(\rho_s - \rho_L)}{\rho_L} \tag{3-1}$$

There are three layers when flow close to a solid surface is considered: viscous sub-layer, buffer layer, and logarithmic layer. The distance of each layer can be defined in terms of the dimensionless distance, y^+. When $y^+<5$, the particle is submerged in the viscous sub-layer, between $5<y^+<30$ it is in the buffer layer, and when $y^+>30$ it is in the logarithmic layer. Based on the analysis of Molerus and Latzel if $Ar<40$ for a fluid-particle system, then the particles are submerged in the viscous sub-layer. These particles are suspended as a result of the boundary layer effects. If $Ar>>40$, then the particle protrude into the logarithmic layer. These particles are carried towards the walls with the mean flow and suspended by eddies which have sufficient energy and size.

These theories suggest that the particles are suspended as a result of the combination of turbulent eddies and mean flow. Ayranci et al. (under review) tested the effect of geometry on the solids suspension mechanisms and showed that the turbulence dominates with a T/3 impeller, but with a T/2 impeller solids suspension occurs as a result of some combination of the turbulence and the mean flow. This shows that there are many parameters that play an active role in solids suspension. Geometry is by far the most important factor. Impeller and tank diameter, impeller type, off-bottom clearance of the impeller, shape of the tank

bottom, and the presence, shape, and clearance of the baffles are some examples that have been studied by many authors (Baldi et al., 1978, Ibrahim and Nienow, 1996, Myers and Fasano, 1992, Armenante and Nagamine, 1998). N_{js} is also a function of particle and liquid properties, such as the particle density, particle diameter and shape, and liquid density and viscosity (Nienow, 1968, Baldi et al., 1978). The behaviour of the particles is different when there are many other particles around them; therefore, solids loading is also very important.

The large number of parameters makes it difficult to determine a design correlation for N_{js}. The first correlation was suggested by Zwietering (1958) and it is still the correlation that is most often used in calculations.

$$N_{js} = S\left(\frac{g(\rho_s - \rho_l)}{\rho_l}\right)^{0.45} \frac{d_p^{0.2}\nu^{0.1}X^{0.13}}{D^{0.85}} \qquad (3\text{-}2)$$

Some of the parameters that affect N_{js} are included in this correlation but the accuracy of the exponents has been questioned by many authors. Nienow (1968) proposed a modified form of the Zwietering correlation for a wider range of particle sizes, density differences, and solids loadings. In the Zwietering correlation the geometrical parameters are represented with the impeller diameter, D, and S which is a constant that includes the impeller and tank geometry. There is an infinite number of possible configurations, and therefore the need for as many S values. Atiemo Obeng et al. (2004) and Ayranci and Kresta (2011) reported the S values for several commonly used geometries. The effect of off-bottom clearance was not included in the Zwietering and Nienow correlations. Many authors showed that off-bottom clearance has a significant effect on N_{js}, and proposed modified forms of the Zwietering correlation (Baldi et al., 1978, Armenante et al., 1998, and Armenante and Nagamine, 1998). Kasat and Pandit (2005) compiled the different exponents on the common parameters suggested by various authors. Their comparison showed that the Zwietering correlation is still the one that predicts most closely, and this is the correlation most often used in industry. The drawbacks of all these correlations related to the current study are

that they are limited to unimodal slurries and to low solids loadings. In industry, however, it is very rare to have a unimodal dilute slurry, as most real slurries are composed of solids with varying densities and particle sizes.

The literature on mixed slurry suspension is only beginning to be developed. Baldi et al. (1978) studied a mixture of glass beads with two particle sizes and found that N_{js} can be predicted using an average particle size, at low solids loadings. For mixed slurries with varying densities and particle sizes this rule is not valid. Montante and Magelli (2007) did a computational study on the distribution of solids for dilute slurries with two solid phases which have different densities but same particle sizes. They showed that the two solids phases are not affected by each other, but this is because the slurries tested were dilute. Recently Ayranci and Kresta (2011) reported experimental work on a wide variety of binary mixtures at high solids loadings (up to 56wt%). Their study showed that the presence of a second solid phase may significantly affect the mixture N_{js}. This effect is amplified for mixtures above 20wt% solids, because at that point the particle-particle interactions start to dominate. The particle sizes and the densities of the two solid phases play an important role in the mixture N_{js}. The work by Ayranci and Kresta (2011) is the first thorough analysis of a suspension of mixed slurries. The next step is to build a model to predict the mixture N_{js}.

The current design heuristic for mixed slurries is to assume that the mixture is composed of only the particles that are hardest to suspend in that slurry. The N_{js} for that slurry is predicted using the Zwietering correlation, and treated as the mixture N_{js}. This design heuristic has many flaws, some of which were shown by Ayranci and Kresta (2011). Of the five mixtures they tested, only one mixture followed the design heuristic up to high solids loadings, and a second mixture followed it up to 13 wt% mixture, but then failed. The other mixtures did not follow the design heuristic. The ratio of the particle size, particle density, and the solids loadings of the two solid phases had an effect on mixture N_{js}. The current design heuristic clearly fails and a more robust model for predicting mixture N_{js} is needed.

In this study we propose and test two models that are based on the power and the momentum required to suspend solids in a stirred tank, which is similar to the general classification of solid suspension mechanisms: an energy and a force balance. The models require the calculation of N_{js} for unimodal slurries for each solid phase in the mixture. As a result, an analysis of the dependence of N_{js} on concentration of solids for unimodal slurries was also performed.

3.2. Model Development

3.2.1. Current Design Heuristic

The current design heuristic is based on the maximum unimodal N_{js} in a mixture:

$$N_{js,mix} = \max(N_{js,1}, N_{js,2}) \tag{3-3}$$

For example, if a mixture N_{js} needed to be determined for a mixture of 1.5 wt% SG with 1.5 wt% B, the N_{js} of the unimodal slurries of the two particles should be calculated and the maximum value should be used as the mixture N_{js}. The unimodal slurry N_{js} is predicted from the Zwietering correlation (Equation 3-2). The unimodal slurry N_{js} was calculated as 318 rpm for 1.5 wt% SG and for 1142 rpm for 1.5 wt% B. The mixture N_{js} is the maximum of the two values, which is 1142 rpm.

3.2.2. Power Model

The power model is proposed based on a hypothesis that the power required to suspend a mixture is the sum of the power required to suspend each of the solid phases in the mixture.

$$P_{js,mix} = P_{js,1} + P_{js,2} \tag{3-4}$$

where $P_{js,mix}$ is the power required to suspend the mixture, and $P_{js,1}$ and $P_{js,2}$ are the power required to suspend the first and the second solid phases, respectively. The power required to suspend each solid phase is calculated at the just suspended condition.

$$P_{js} = \rho_{sl} N_{js}{}^{3} D^{5} N_p \tag{3-5}$$

In combining Equations 3-4 and 3-5 to find N_{js}, the impeller is the same, so the power number, N_p, and the impeller diameter, D, terms cancel out. The mixture N_{js} is thus a function of the densities of the mixed and the unimodal slurries, and the N_{js}'s of unimodal slurries.

$$N_{js,mix} = \left(\frac{\rho_{sl,1} N_{js,1}{}^{3} + \rho_{sl,2} N_{js,2}{}^{3}}{\rho_{sl,mix}} \right)^{1/3} \tag{3-6}$$

In Equation 3-6, $N_{js,1}$ and $N_{js,2}$ are calculated using Equation 3-2. Unimodal slurry N_{js} is a function of solids concentration. In Equation 3-5, ρ_{sl} is the term that includes concentration of solids:

$$\rho_{sl} = \frac{1}{\frac{x_s}{\rho_s} + \frac{x_L}{\rho_L}} \tag{3-7}$$

where x_s is the weight percent of particles and x_L is the weight percent of the liquid phase in the slurry. Incorporating Equation 3-7 into Equation 3-5, and rearranging to isolate N_{js} gives:

$$N_{js} = \left(\frac{x_s}{\rho_s} + \frac{x_L}{\rho_L} \right)^{1/3} \left(\frac{P_{js}}{D^5 N_p} \right)^{1/3} \tag{3-8}$$

The relation between N_{js} and the x_s cannot be explained with a simple exponent. To simplify the expression a hypothetical situation where x_l reaches zero can be considered. In that case N_{js} would be a function of $x_s{}^{0.33}$. Even this exponent would be limited to the case where the concentration is defined in terms of the weight percent of the solid phase, because the relationship would get more complicated if the concentration was defined in terms of Zwietering's mass ratio percent. This shows that concentration and N_{js} cannot be linked through a simple theoretical relation.

It should be noted that the power model does not include any terms to take the particle-particle interactions into account; therefore, it is very likely that the

mixture N_{js} cannot be predicted accurately when in the presence of particle-particle interactions.

3.2.3. Momentum Model

A second hypothesis is that the momentum required to suspend a mixture is equivalent to the sum of the momentum required to suspend each of the solid phases in the mixture.

$$M_{js,mix} = M_{js,1} + M_{js,2} \tag{3-9}$$

where $M_{js,mix}$ is the momentum required to suspend the mixture, and $M_{js,1}$ and $M_{js,2}$ are the momentum required to suspend each individual unimodal slurry. The momentum, M, can be calculated through the dimensionless momentum number (Mo) (Machado et al, 2011):

$$Mo = \frac{\int_0^{D/2} \rho_L V_z^2 2\pi r dr}{\rho_L N^2 D^4} = \frac{M}{\rho_L N^2 D^4} \tag{3-10}$$

The momentum required to suspend each solid phase is calculated at just suspended conditions:

$$M_{js} = Mo\ \rho_{sl}\ {N_{js}}^2\ D^4 \tag{3-11}$$

In combining Equations 3-10 and 3-11 to find N_{js}, the momentum number and impeller diameter are constant, so the terms cancel out. Like the power model, the mixture N_{js} is thus a function of the mixed and unimodal slurry densities and the N_{js} of the unimodal slurries.

$$N_{js,mix} = \left(\frac{\rho_{sl,1} {N_{js,1}}^2 + \rho_{sl,2} {N_{js,2}}^2}{\rho_{sl,mix}} \right)^{1/2} \tag{3-12}$$

In determining the relation between N_{js} and concentration an analysis similar to the power model was performed, and a similar complicated expression was obtained.

3.3. Experimental Procedure

Figure 3-1 shows the experimental setup. A fully baffled (W_b= T/10) cylindrical plexiglass tank with an inner diameter of 24 cm was used for the measurements. The cylindrical tank was placed inside a square tank to prevent optical distortion. In order to maintain stability at high impeller speeds, both tanks were bolted to a steel frame. The just suspended speed was observed visually from the bottom of the tank.

A Lightnin A310 impeller and a four bladed 45° down pumping PBT both with a diameter of D=T/3 were used. The impellers were attached to a shaft with a diameter of 1.27 mm (T/20). The off-bottom clearance was defined as the distance between the bottom of the impeller hub and the bottom of the tank. The blades were flush with the bottom of the hub for both impellers. The dimensionless off-bottom clearance, C/T, was varied from 0.15 to 0.33. Water was used as the liquid phase for all the experiments.

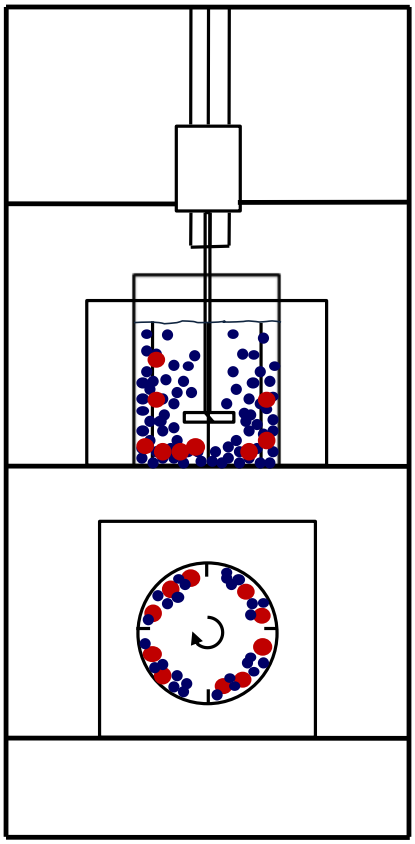

Figure 3-1: The experimental setup with a PBT impeller. N_{js} is determined by visual observation below the tank bottom.

Seven different particles with various physical properties were tested: nickel (Ni), small glass (SG), urea formaldehyde (UF), bronze (B), sand (S), large glass (LG), and ion exchange resin (R). Particle properties are given in Table 3-1. The particles were chosen to give a wide range of densities ($1.3 < SG < 8.9$) and particle sizes ($61\ \mu m < d_p < 841\ \mu m$). The mixtures tested are given in Table 3-2 along with the ranges of solids loadings. For each data set the mass of the more dense particles was kept constant while the mass of the less dense particles increased. A set of experiments where the mass of the dense particle is higher than the mass of the less dense particle was also conducted to validate the models tested for all cases. This set of experiments was for the mixture of R with LG at C/T=0.25.

Table 3-1: Particle properties

Type	Size (μm)	Density (kg/m^3)	Ar	V_t (m/s)	m (mg)
Nickel (Ni)	61–104	8900	47.6	0.139	0.003
Small glass beads (SG)	74–125	2500	14.7	0.066	0.001
Urea formaldehyde (UF)	150-250	1323	25.34	0.044	0.005
Bronze (B)	150–297	8855	820.5	0.225	0.049
Sand (S)	350-500	2656	1247	0.144	0.107
Large Glass beads (LG)	595–841	2500	5378.7	0.177	0.478
Ion Exchange Resin (R)	677	1370	1126.3	0.086	0.213

Table 3-2: Particle mixtures and solids loadings

Less dense particles (wt%)	Denser particles (wt%)	Total solids loading		Density ratio	Particle size ratio
		wt%	vol%		
SG (1.5–26)	B (1.5–1.3)	3–27.3	0.8–12	~1:3.5	~1:2
LG (1.5–26)	B (1.5–1.3)	3–27.3	0.8–12	~1:3.5	~3:1
R (1.5–26)	B (1.5)	3–27.5	1.3–21.8	~1:6.5	~3:1
R (1.5–25)	LG (1.5–1.4)	3–26.4	1.7–20	~1:1.8	~1:1
SG (1.5–26)	Ni (1.5–1.3)	3–27.3	0.77–14.9	~1:3.6	~1:1
UF (1-10)	S (1-5)	2-15	1.1-9.1	~1:2	~1:2

At the beginning of every experiment, the tank was filled with water and particles were weighed and poured into it. The liquid height was then adjusted to give H=T. The shaft was attached to the motor, and the off-bottom clearance was adjusted. Once the desired clearance was achieved, the impeller was started. The impeller speed was increased in steps and the system was left for 2 minutes to reach steady state. After steady state was reached, the particle behavior at the bottom of the tank was observed for 15-45 seconds to determine whether N_{js} was reached. The particles behind the baffles were consistently the last particles to be suspended. The just suspended speed was reached when no particles remained stationary at the bottom of the tank for more than 1 or 2 seconds (Zwietering, 1958). After that the motor was switched off, and the off-bottom clearance was

adjusted for the new measurement. More details about the experimental setup and the procedure are given in Ayranci and Kresta (2011).

3.4. Results and Discussion

The results are divided into two major parts. In the first part the two models for mixture N_{js} are tested using experimental data. The current design heuristic is used to provide a baseline for comparison. Next the performance of the power and momentum models is tested for mixtures of solids.

The second part focuses on the prediction of mixture N_{js} by combining the Zwietering correlation for the unimodal slurries with the power model for the mixed slurries. The off-bottom clearance and solids concentration were varied in the experiments. The effect of these parameters on N_{js} is analyzed, and a modified Zwietering correlation is proposed based on the information obtained from this analysis. In the last subsection the prediction of mixture N_{js} using the modified Zwietering correlation and the power model is tested.

3.4.1. Prediction of Mixture Njs

3.4.1.1. Test of Current Design Heuristic

Figure 3-2a and b compare the prediction of $N_{js,\,max}$ using the Zwietering correlation for the more difficult to suspend solids with the experimental data for mixture N_{js}. In the Zwietering correlation, S is a function of impeller and tank geometry and particle properties. Figure 3-2a and b represent the best possible predictions using the current form of the Zwietering correlation since the S values were obtained for the specific particles and the geometries used here (Ayranci and Kresta, 2011). According to the current design heuristic, the largest unimodal slurry N_{js} in the mixture is used as the mixture N_{js}. For each mixture the wt% of the more difficult to suspend solids remains constant as the wt% of the easier to suspend solids increases. The prediction of mixture N_{js} is constant because the N_{js} of the easier to suspend solids does not change enough with increasing concentration to overtake $N_{js,max}$. In Figure 3-2a the mixture N_{js} for R with LG at C/T=0.15 remains constant even though the concentration of R changes at each

experimental point and the experimental N_{js} does in fact increase. The current design heuristic fails to capture the physics behind the solids suspension. The standard deviation between the measured and the predicted values for all of the mixtures at varying off-bottom clearances is 10% for the PBT and 12.6% for the A310. The fact that the trend does not follow the experimental data is of greater concern.

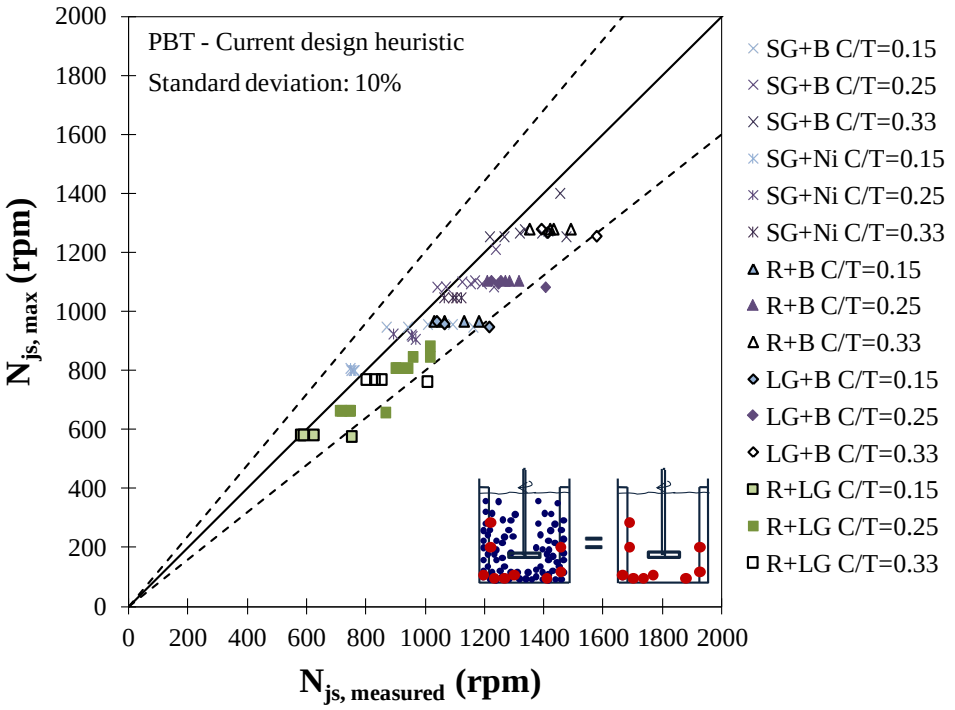

a.

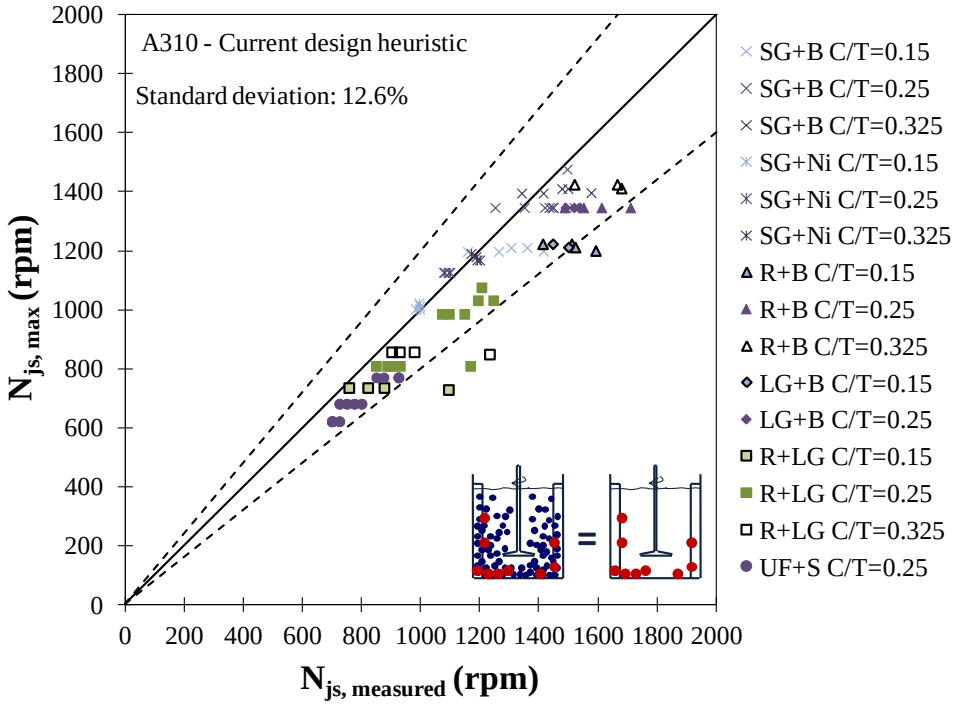

b.

Figure 3-2: The parity plot between the current design heuristic and the experimental data. The current design heuristic uses the maximum N_{js} in the mixture, calculated using the Zwietering correlation. a. PBT b. A310

3.4.1.2. Power Model and Momentum Model

To find the mixture N_{js} through the power or momentum models, the slurry densities are first calculated from Equation 3-7. The unimodal slurry N_{js}'s are known from the experiments. The mixture N_{js} is then calculated from Equation 3-6, power model, and from Equation 3-12, momentum model.

Figure 3-3a and b show the power model parity plots for the PBT and the A310. The predicted N_{js}'s follow the parity line closely. Most of the data is within ±20% of the parity line. This indicates that the physics of the solids suspension is captured up to 20 wt % solids for all six mixtures. Beyond 20 wt % solids, particle particle interactions can become quite strong. For the LG+B, R+B, and R+LG mixtures N_{js} increases with increasing solids and the model captures N_{js} up to the highest loading tested – 27 wt % solids. The data for UF+S goes up to only 10 wt % solids. For the SG+B mixture there is an unexpected drop in N_{js} above 20 wt% SG (Ayranci and Kresta, 2011) and for the SG+Ni N_{js} is constant. The power model cannot predict these effects because there is no term for particle-particle interactions. Based on this information the data points above 20 wt% SG for both SG+B and SG+Ni mixtures were eliminated from the data set shown in Figure Figure **3-3** a and b. The resulting standard error is 9.6% for the PBT and 9% for the A310. The mixture N_{js} can be predicted accurately with the power model up to 27 wt% solids for a range of off-bottom clearances, with two separate impellers, in the absence of particle-particle interactions.

Figure 3-4a and b show that the momentum model captures the physics, but over-predicts the mixture N_{js}, leaving more data points outside the ±20% range. Again the same data points with particle-particle interactions were eliminated from the figures. The standard error of the momentum model prediction is 17.3% for the PBT and 15.7% with the A310.

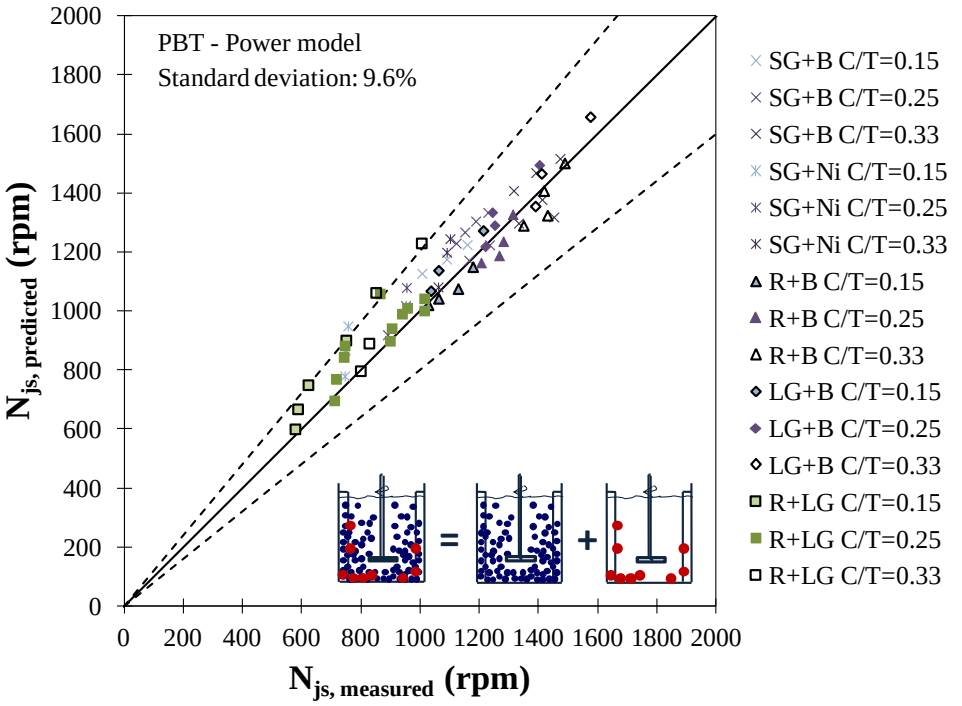

a.

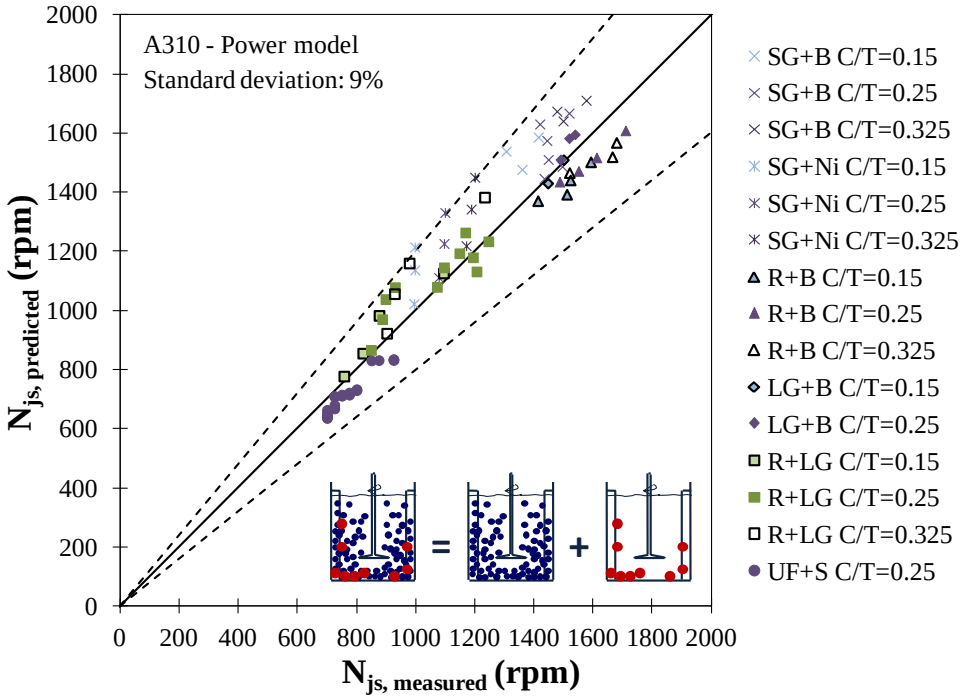

b.

Figure 3-3: The parity plot for the power model at varying clearances for all mixtures with the a. PBT b. A310.

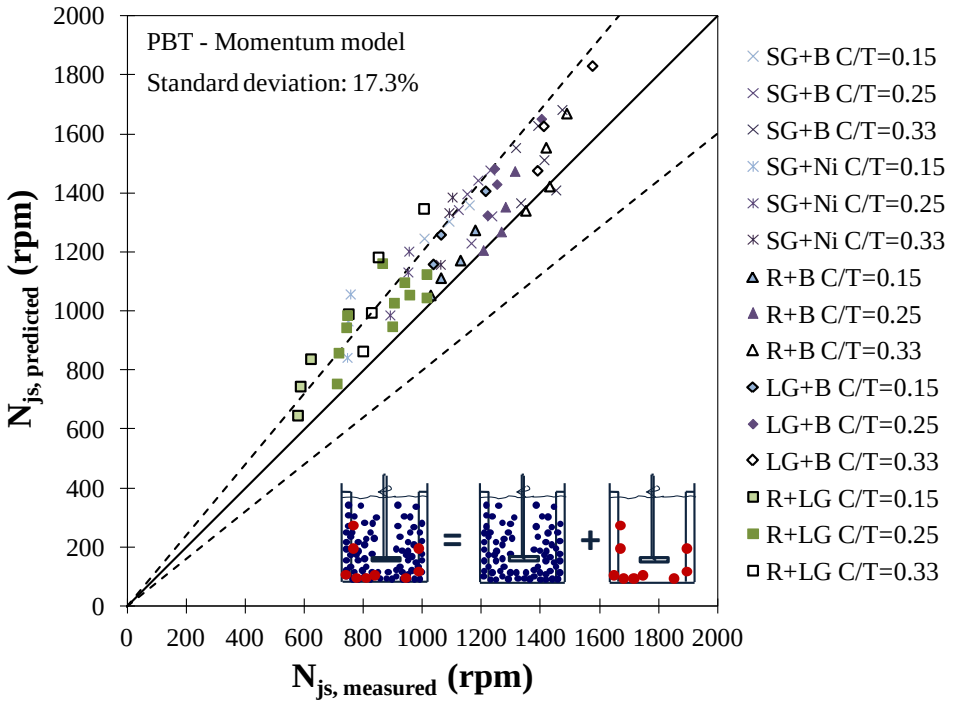

a.

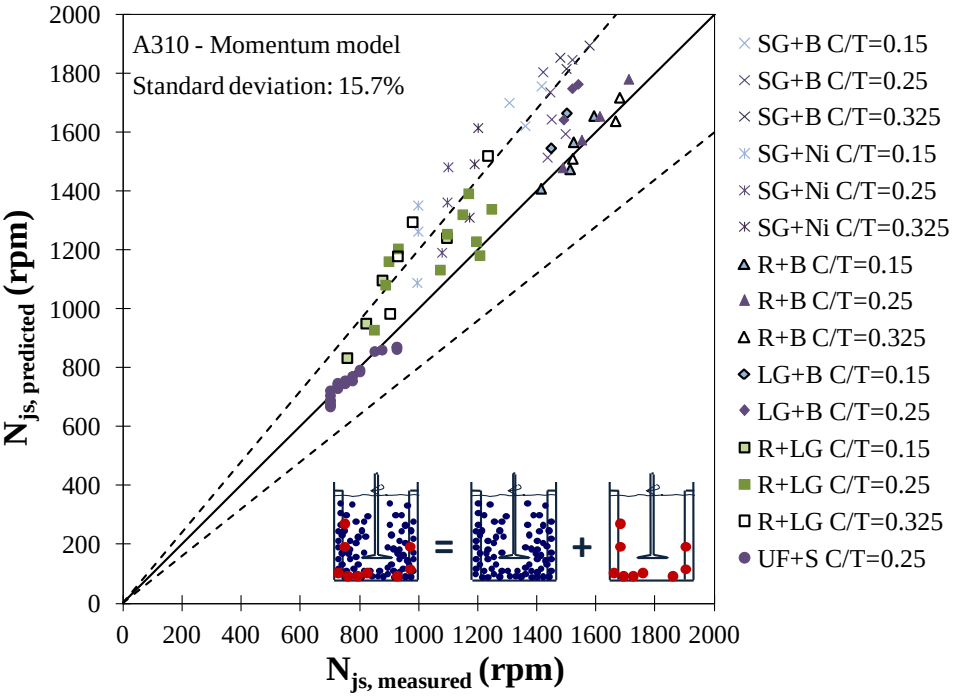

b.

Figure 3-4: The parity plot for the momentum model at varying clearances for all mixtures with the a. PBT b. A310.

In Figure 3-5 comparison of the power and momentum models with both the PBT and the A310 shows that the momentum model consistently over-predicts

mixture N_{js}. The standard deviation between the two models is 6.4% when the data for both impellers is combined. The power model clearly better predicts mixture N_{js} for all cases.

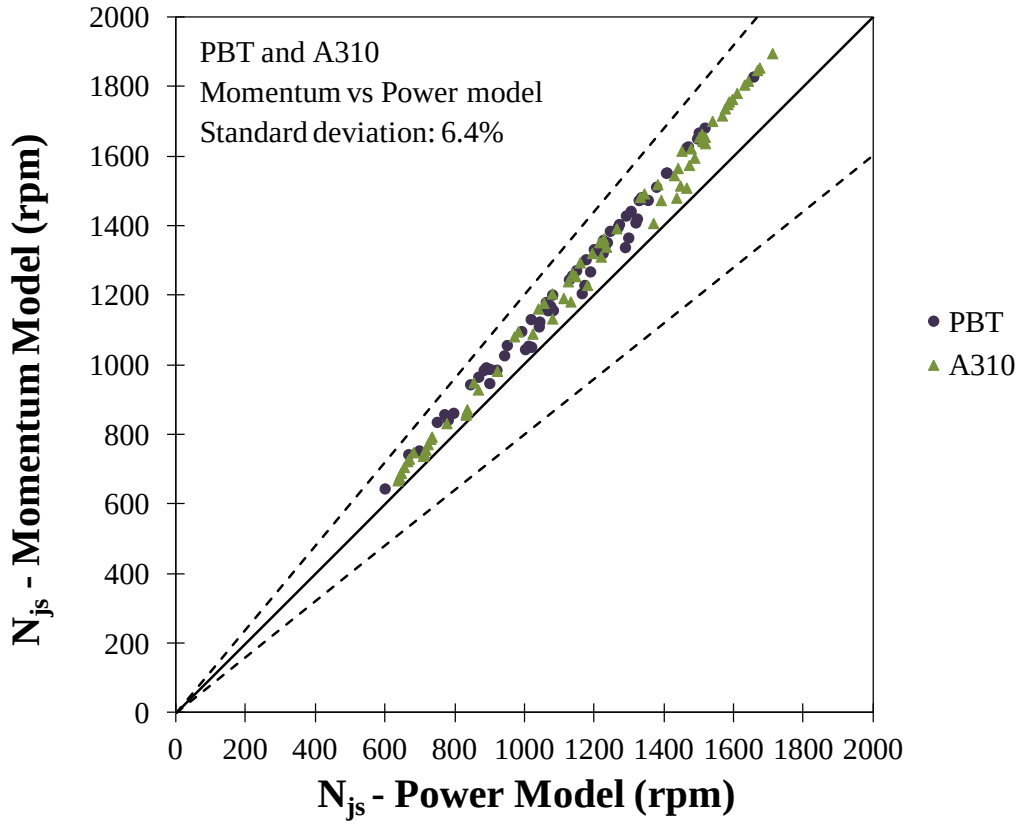

Figure 3-5: Comparison of the momentum model and the power model at varying clearances for all particles with the PBT and A310.

3.4.2. Prediction of mixture N_{js} without experimental data

It should be noted that the mixture N_{js} predictions up to this point were done using experimental data for the unimodal slurry N_{js}'s. Experimental data is not always available, so the Zwietering correlation must also be used. In Figure 3-6 the mixture N_{js} predictions using the power model and the Zwietering correlation are shown. While some data points follow the parity line, most of the mixture N_{js} data flattens out as the solids loading increases. The comparison of this plot, Figure 3-6, with the current design heuristic, Figure 3-2a, which also does not rely on any experimental data, shows that there is no significant improvement from the current design heuristic to the power model prediction: the

improvement due to use of the power model is lost when the Zwietering correlation is used to predict unimodal N_{js}'s in the model. In the experiments for each mixture the off bottom clearance and the solids concentration were varied, so these two effects are analyzed next to test whether the correlation can be improved.

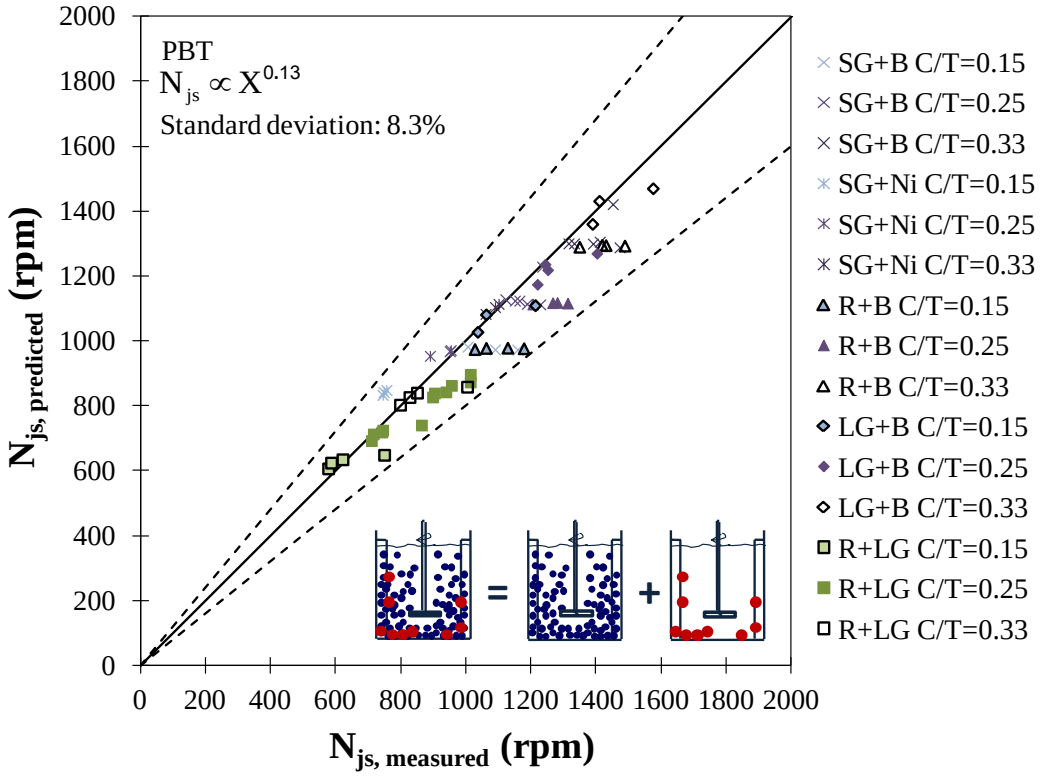

Figure 3-6: The prediction of mixture N_{js} without any experimental data using the power model and the current form of the Zwietering correlation with the PBT.

3.4.2.1. The effect of off-bottom clearance on N_{js}

The effect of off-bottom clearance is not explicitly included in the Zwietering correlation but it is known to affect N_{js} significantly. The qualitative effect of clearance on N_{js} is shown in Ayranci and Kresta (2011). The high velocity discharge stream from the impeller slows down as it moves away from the impeller and entrains more fluid. At high clearances N_{js} must increase to compensate for the greater velocity decay from the impeller to the tank bottom. Ayranci and Kresta (2011) reported the N_{js} of several mixtures at increasing solids loadings and at ten clearances for two impellers which were also used in this

work, an A310 and a PBT both with diameters of D=T/3. The N_{js} data was plotted against C/T. Additional analysis of an expanded data set is done here. Linear, exponential, and power-law fits were applied to the data. The standard deviations showed no significant difference between the three fits. The linear fit is shown in Figure 3-7a and b since it has a slightly smaller standard deviation.

$$N_{js} = k\left(C/T\right) + n \qquad 3\text{-}13$$

In Figure 3-7a and b the slope is plotted as a function of solids concentration. The data for the two impellers falls in different ranges, and there are also variations for different mixtures. The slopes fall in the 1200-2500 range for the PBT impeller, and the 400-1200 range for the A310 impeller. The standard deviation of the slopes for a fixed concentration of any kind of mixture is 15-25% for the PBT and 15-36% for the A310 impeller. It is concluded that the slope depends on the solids concentration, the type of solids used and the type of the impeller. When the exponent on C/T was allowed to vary in a power law fit, similar results were observed. This shows that there is no way to quantify the effect of off-bottom clearance on N_{js}. In the Zwietering correlation the off-bottom clearance is lumped into S. Since the effect of off-bottom clearance cannot be modeled explicitly, the S values that were used in the calculations for Figures 3-2, 3-6, 3-8, 3-10 and 3-11 match exactly with the geometries and the particles tested. Using the S values that exactly match the geometry under consideration is the recommended way to account for the effect of off-bottom clearance.

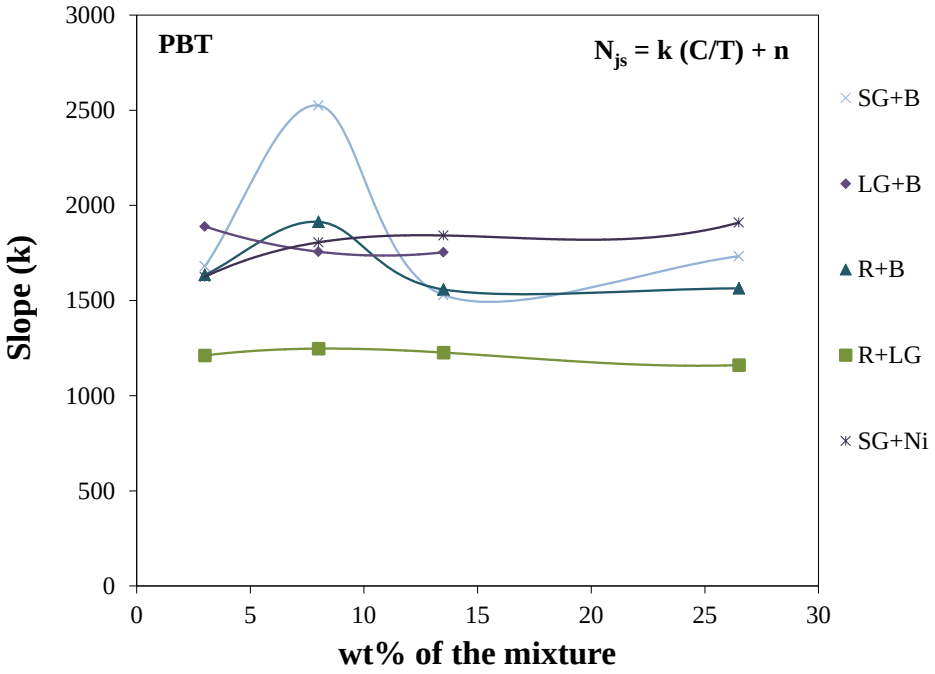

a.

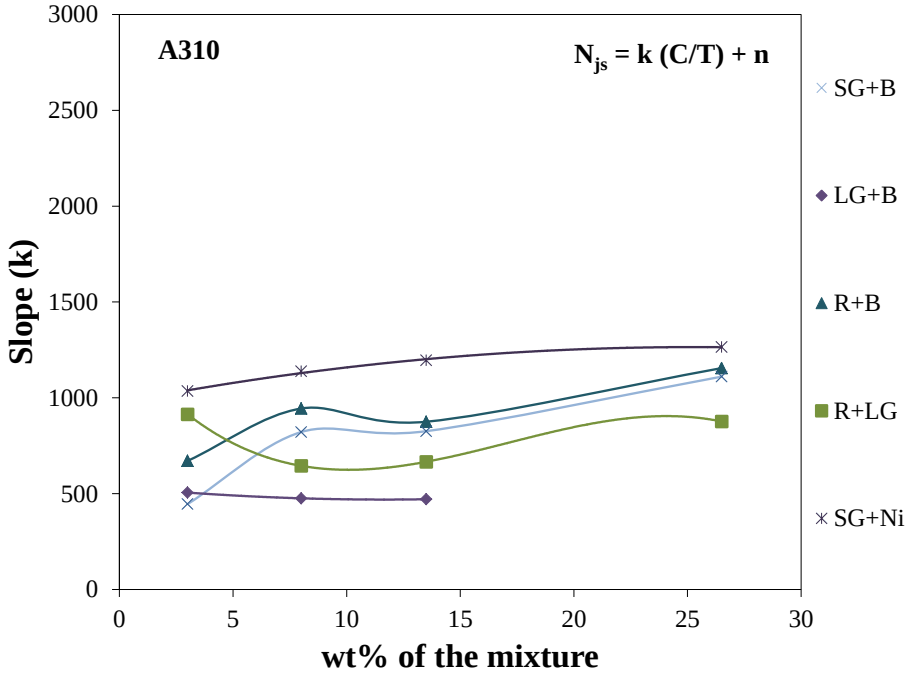

b.

Figure 3-7: The effect of C/T on N_{js} for a. PBT, and b. A310. The slope ranges from 1200-2500 for the PBT, and from 400-1200 for the A310 with no consistent trend.

3.4.2.2. Exponent on Concentration for Unimodal Slurries

The concentration dependence of the Zwietering correlation is not considered reliable above 10 wt% solids. Most industrial applications and the data in this work employ slurries well above 10 wt%, so an analysis of the effect of concentration on unimodal slurry N_{js} is needed. Figure 3-8 shows the parity plot for the PBT using the current exponent of 0.13 on concentration for unimodal slurry N_{js} predictions. Given S values from Ayranci and Kresta (2011) the N_{js} of some of the slurries can be predicted, but most of the data falls out of the ±20% range. It is clear that the current exponent of 0.13 is not a good predictor. An exponent that better represents the data set over the full range of solids loadings is required. In this section the effect of concentration on unimodal slurry N_{js} is tested to find an exponent that may better represent the reality.

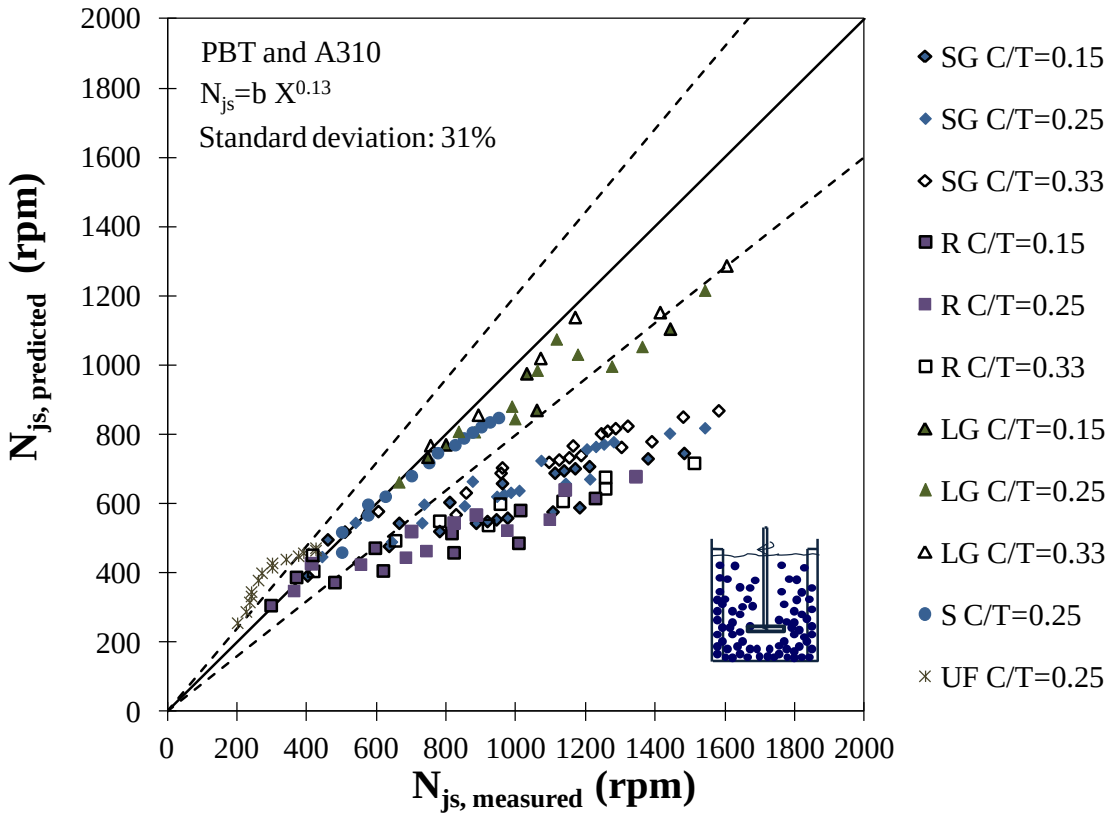

Figure 3-8: The comparison of the Zwietering predicted N_{js} and the experimental N_{js} for the PBT impeller. The exponent on concentration is 0.13as it is in the original Zwietering correlation.

In Figure 3-9a and b the exponent on concentration was calculated for each data set by applying a power-law fit to N_{js} as a function of concentration in the form of Zwietering's mass ratio percent (X).

$$N_{js}=b\,X^{a} \tag{3-14}$$

Table 3-3a and b give the resulting exponents. In each table there are two groups: the first group is SG and R, the second group is LG, S, and UF. When the data is combined for the two impellers, the mean exponent for the first group (SG and R) is 0.33±0.01, for the second group (LG, S and UF) it is 0.18±0.01, and the average exponent for all particles is 0.24±0.01.

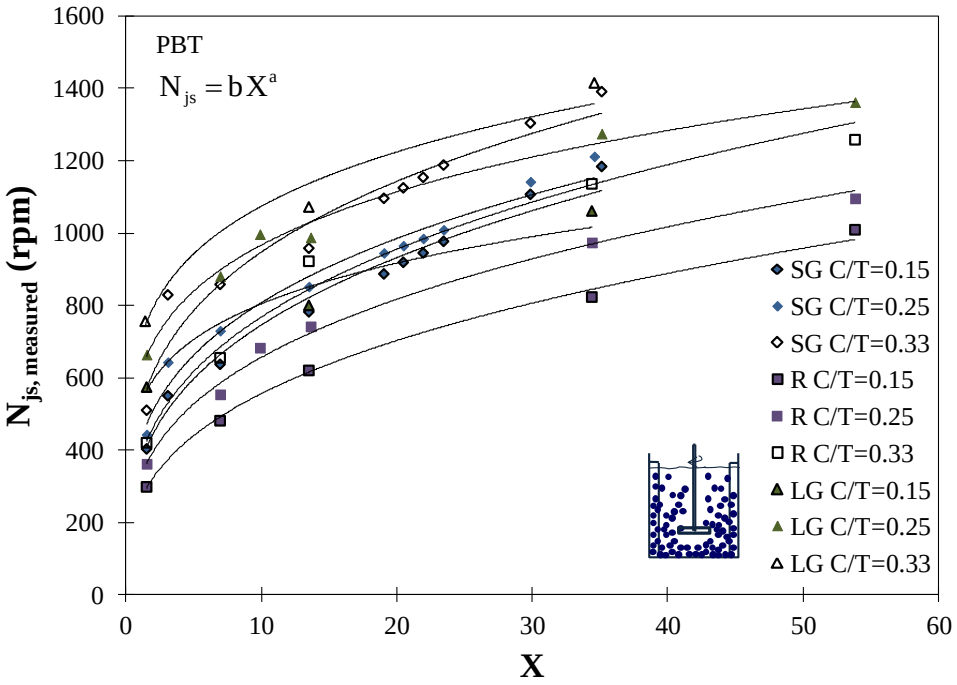

a.

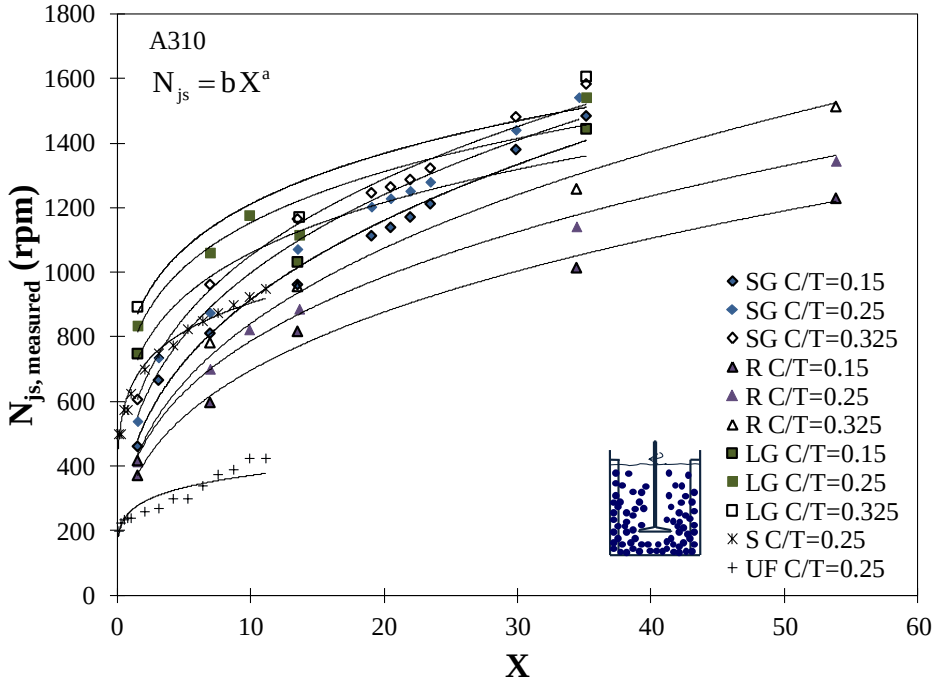

b.

Figure 3-9: The measured N_{js} at increasing concentrations (X) for all particles at varying off-bottom clearances a. PBT b. A310. Values of the exponent, a, are given in Table 3-3.

Table 3-3a: Exponent on concentration using Zwietering mass percent ratio (X) for the PBT. All $R^2 > 0.91$.

Particles	C/T	Exponent
SG	0.15	0.32
	0.25	0.30
	0.33	0.27
R	0.15	0.34
	0.25	0.32
	0.33	0.32
LG	0.15	0.19
	0.25	0.20
	0.33	0.19

Table 3-3b: Exponent on concentration using Zwietering mass percent ratio (X) for the A310. All $R^2 > 0.91$, except for UF at 0.86.

Particles	C/T	Exponent
SG	0.15	0.32
	0.25	0.31
	0.325	0.31
R	0.15	0.32
	0.25	0.33
	0.325	0.37
LG	0.15	0.20
	0.25	0.19
S	0.25	0.15
UF	0.25	0.15

Figure 3-10a, b and c show the modified Zwietering prediction of unimodal slurry N_{js} using the three different exponents on concentration for both the PBT and the A310. The exponent of 0.18 works for LG up to 26 wt%, for S up to 10wt%. The situation is different for UF. Within all the particles the power-law fit for UF resulted with the smallest R^2 value (R^2=0.86). In Figure 3-10a when the exponent of 0.18 used, the N_{js} for UF can be predicted only up to 0.25 wt%. The exponential fit results in a larger R^2; however, applying an exponential fit also does not provide a better prediction. The unimodal slurry N_{js} cannot be predicted

for the UF within 20% error; however, N_{js} is over-predicted, which overall results in a conservative design. The standard deviation from parity line with the exponent of 0.18 is 19.1%. When the UF data is not included the standard deviation drops to 5.5%.

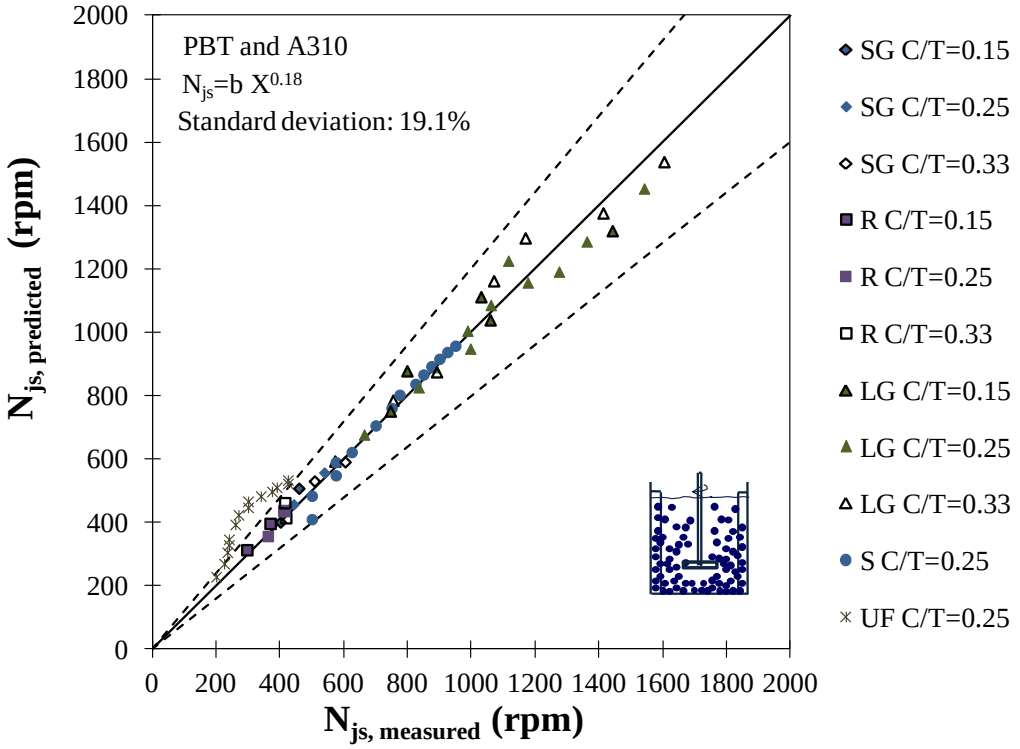

a.

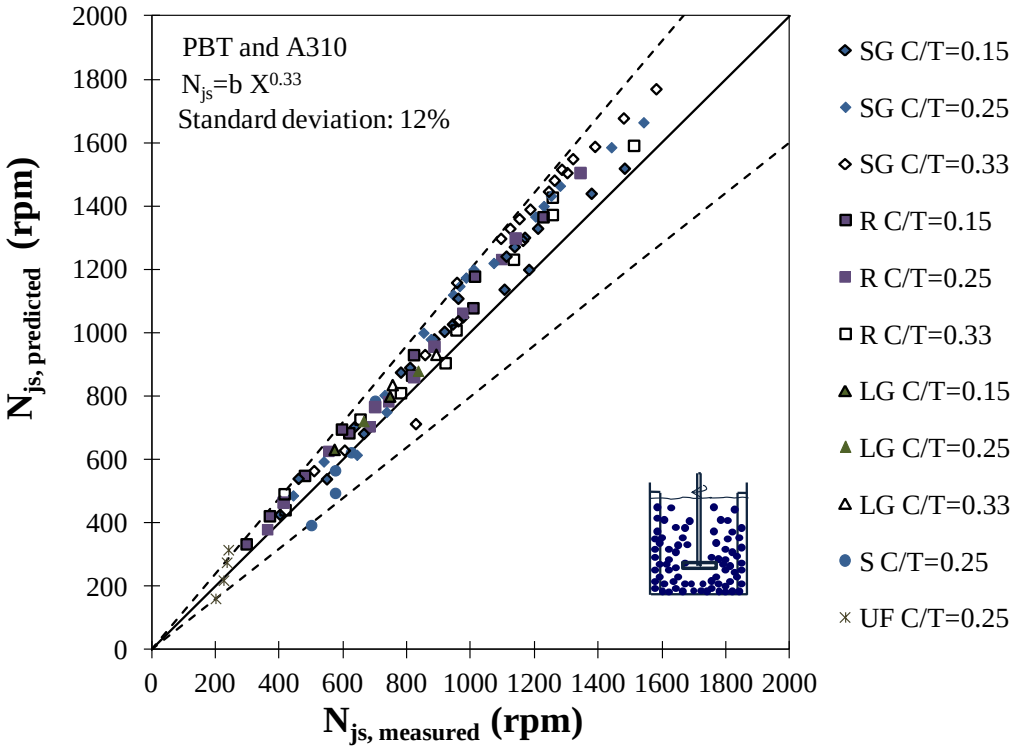

b.

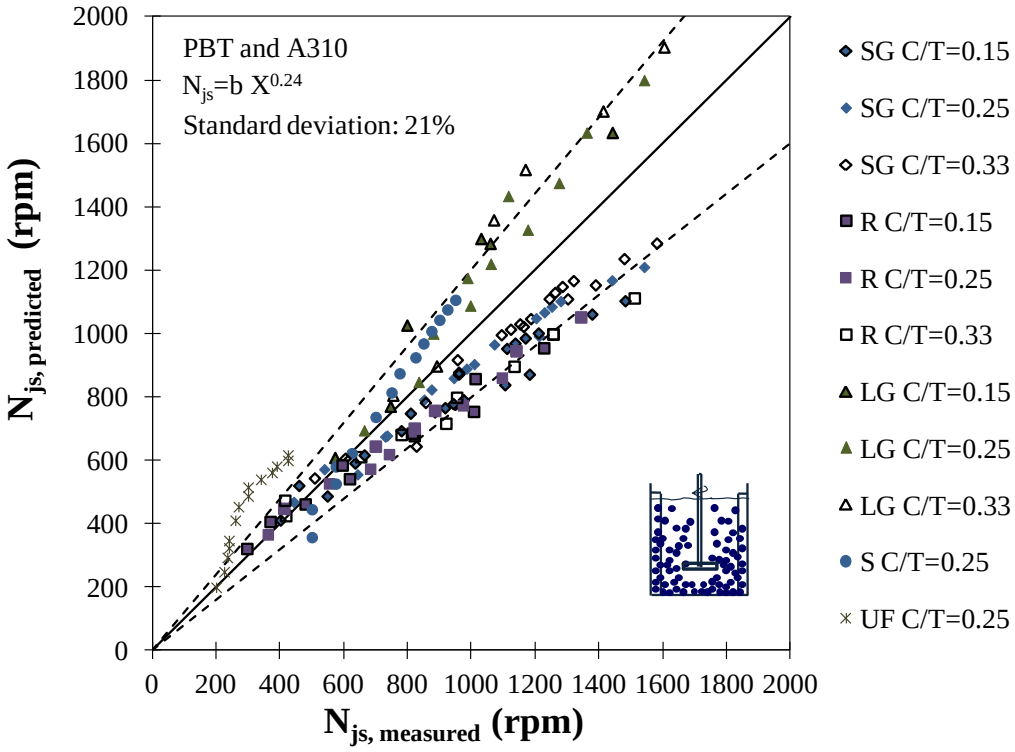

c.

Figure 3-10: The effect of exponent on concentration on the prediction of unimodal slurry N_{js} for a PBT. Exponents are a. 0.18 b. 0.33 c. 0.24

The exponent of 0.33 represents SG and R up to 35 wt% solids, over a range of off-bottom clearances with a standard deviation of 12%. The predictions with an exponent of 0.24 fall mid-way between the two exponents. The unimodal slurry N_{js} can be predicted within the ±20% error bars using this exponent; however, it should be noted that the data has a standard deviation of 21%. All three exponents are quite different than the previously suggested exponents in the literature. This is because the current data set extends to significantly higher concentrations, up to 35 wt%.

The properties of the particles were explored to attempt to find a basis for the two exponents. The density and size of the particles does not provide an explanation because both groups have the same ranges of particle densities (ρ_{SG}= $\rho_{LG}\approx \rho_S$, $\rho_R\approx \rho_{UF}$), and particle sizes ($d_{p,R}\approx d_{p,LG}$). Next the settling velocity (V_t), individual mass, and the Ar of the particles were analyzed, as given in Table 3-1. According to Bittorf and Kresta (2003) the fast settling particles V_t>0.173 m/s show different behaviour than those with slower settling velocity, V_t where the terminal velocity can be calculated from:

$$V_t=1.73\left(\frac{g\,\Delta\rho\,d_p}{\rho_L}\right)^{1/2} \tag{3-15}$$

for $1000<Re_p<35x10^4$ (Atiemo-Obeng et al., 2004).The V_t for the particles in the descending order is $V_{t,\,LG} > V_{t,\,S} > V_{t,\,R} > V_{t,\,SG} > V_{t,\,UF}$. Only LG has a V_t larger than this limit ($V_{t,\,LG}$=0.177 m/s). While S has the next largest V_t, UF has the smallest V_t, and neither of the two particles is counted as fast settling.

Next the individual mass of the particles was calculated. The heavier the particle, the harder it is to suspend the particle since it has more inertia. The individual mass of the particles in descending order is: $m_{LG} > m_R > m_S > m_{UF} > m_{SG}$. Once again LG leads the sequence with the biggest mass, but the order of the particles does not overlap with the particle grouping for the exponents on concentration.

Last the Archimedes number of each particle was explored. According to Molerus and Latzel (1987) if Ar<40, the particles are completely submerged in the viscous sub-layer, and if Ar>>40, the particles are protruding into the logarithmic layer. Different mechanisms apply for solids suspension based on the position of the particle. As given in Table 3-1 LG, S, and R protrude into the logarithmic layer with Ar>>40, and SG and UF are submerged in the viscous sub-layer with Ar<40. This analysis also leads to a different grouping than the exponents on concentration.

Combining this information we see that LG exceeds the V_t limit, it is the heaviest particle, and it has the largest Ar. This explains why LG does not follow the same trend as the SG and R. S and UF however, are not strongly in one extreme, and tend to be closer to R and SG in some cases explored above, rather than LG. This analysis showed that there is no clear explanation for why the particles group into two distinct concentration exponents.

Up to this point the concentration of solids was analyzed in terms of the Zwietering mass ratio percent. In the broader literature the concentration of solids is defined using three different terms: Zwietering mass ratio percent (X), weight percent (X_w), and volume percent (X_v).

$$X = \frac{m_s}{m_L} \times 100 \tag{3-16}$$

$$X_w = \frac{m_s}{m_s + m_L} \times 100\% \tag{3-17}$$

$$X_v = \frac{V_s}{V_s + V_L} \times 100\% \tag{3-18}$$

To determine which one represents solids suspension in stirred tanks the best, the experimental N_{js} was plotted against X, X_w, and X_V. All three gave similar results. The average exponent on concentration for all the particles using X is 0.23, using X_w is 0.25, and using X_V is 0.24. X incorporates both the weight percent and volume percent because it includes both the mass of solids and the effect of the solids density on the liquid volume. Thus, X indirectly measures both

the probability of interactions and the particle inertia. X_w is intuitively easy to use, and encompasses the inertia of particles relative to the entire slurry i.e. the more dense or heavy the particles are, the larger the inertia. X_V gives information about how close the particles are to each other. In slurry pipeline flow solids concentration is always defined in terms of X_v. The mean exponents for the three different concentration terms are quite similar to each other, indicating that any one of the three could be used, but it seems that X and X_v represent the solids concentration slightly better. The Zwietering mass ratio percent, X, was chosen for the rest of the analysis in this paper.

3.4.2.3. Prediction of mixture N_{js} in case of no experimental data

The power model is successful in predicting mixture N_{js} when the unimodal slurry N_{js} is predicted accurately; therefore, it is crucial to improve the Zwietering correlation. While the effect of off-bottom clearance can be incorporated by using the correct S values for the specific geometry and particles, a correction on the exponent on concentration is essential. The analysis showed that there are three exponents that could work: 0.18, 0.24 and 0.33. In Figure 3-11a, b, and c the power model prediction of mixture N_{js} is shown when the unimodal slurry N_{js}'s were calculated with an exponent of 0.18, 0.24 and 0.33 on concentration.

In Figure 3-11a, with an exponent of 0.18 on concentration, most of the data points fall on top of the parity line and the standard error is small, 6.8%. It should however be noted that some data points, which are marked on the figure, are still under-predicted, indicating that the physics cannot be captured completely. The mixtures that include LG, which follows an exponent of 0.18, are aligned with the parity line nicely, but the others fail. This again shows that once the unimodal slurry N_{js} is predicted correctly, the power model is capable of predicting the mixture N_{js}.

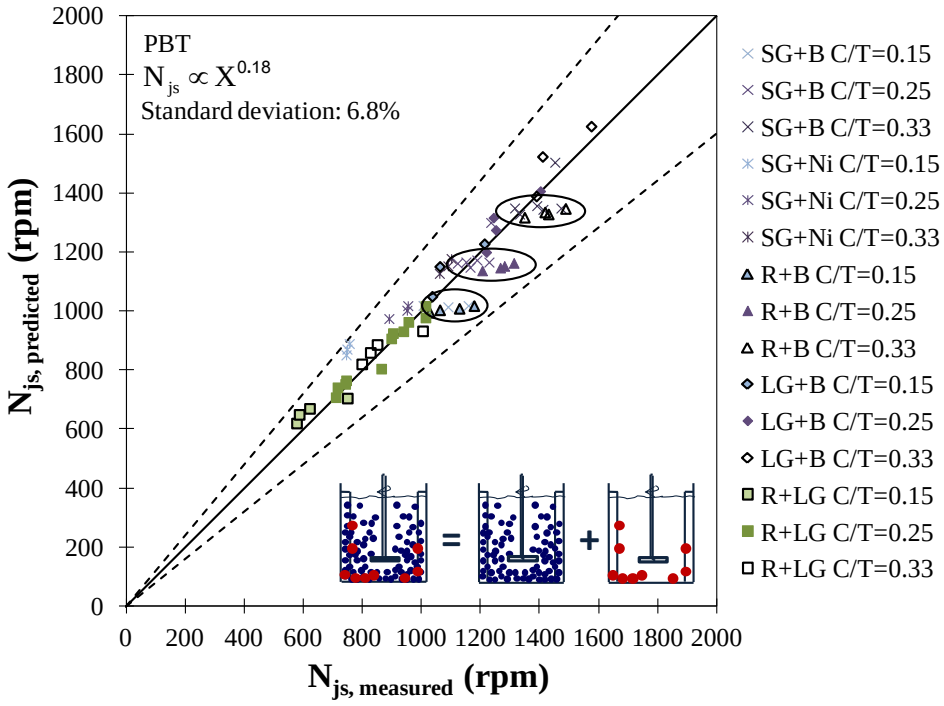
PBT
$N_{js} \propto X^{0.18}$
Standard deviation: 6.8%
$N_{js,\ predicted}$ (rpm)
$N_{js,\ measured}$ (rpm)
0
200
400
600
800
1000
1200
1400
1600
1800
2000
SG+B C/T=0.15
SG+B C/T=0.25
SG+B C/T=0.33
SG+Ni C/T=0.15
SG+Ni C/T=0.25
SG+Ni C/T=0.33
R+B C/T=0.15
R+B C/T=0.25
R+B C/T=0.33
LG+B C/T=0.15
LG+B C/T=0.25
LG+B C/T=0.33
R+LG C/T=0.15
R+LG C/T=0.25
R+LG C/T=0.33

a.

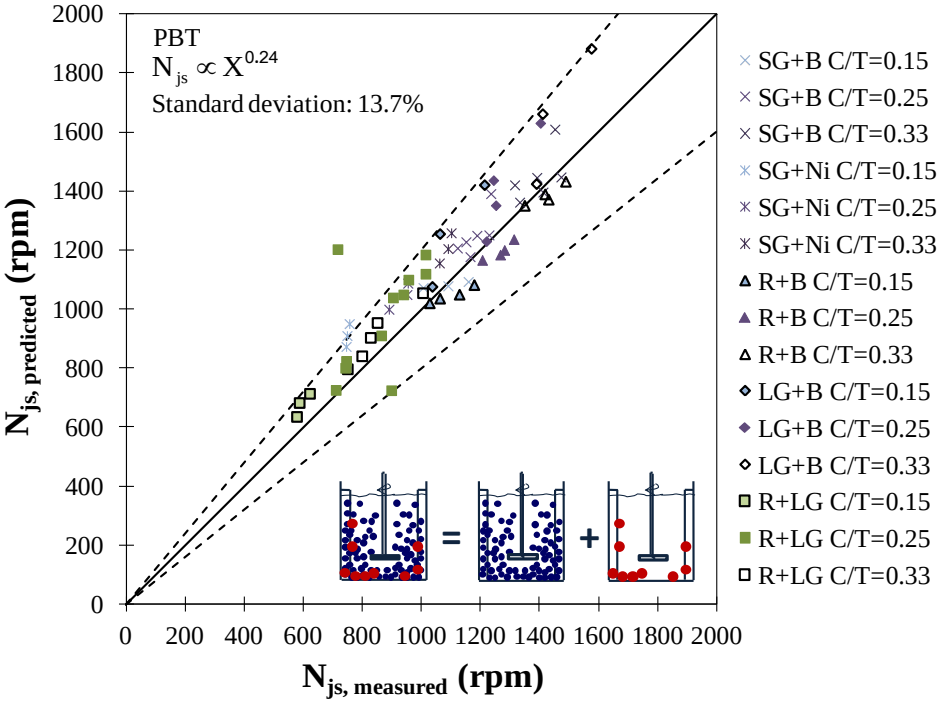
PBT
$N_{js} \propto X^{0.24}$
Standard deviation: 13.7%
$N_{js,\ predicted}$ (rpm)
$N_{js,\ measured}$ (rpm)
0
200
400
600
800
1000
1200
1400
1600
1800
2000
SG+B C/T=0.15
SG+B C/T=0.25
SG+B C/T=0.33
SG+Ni C/T=0.15
SG+Ni C/T=0.25
SG+Ni C/T=0.33
R+B C/T=0.15
R+B C/T=0.25
R+B C/T=0.33
LG+B C/T=0.15
LG+B C/T=0.25
LG+B C/T=0.33
R+LG C/T=0.15
R+LG C/T=0.25
R+LG C/T=0.33

b.

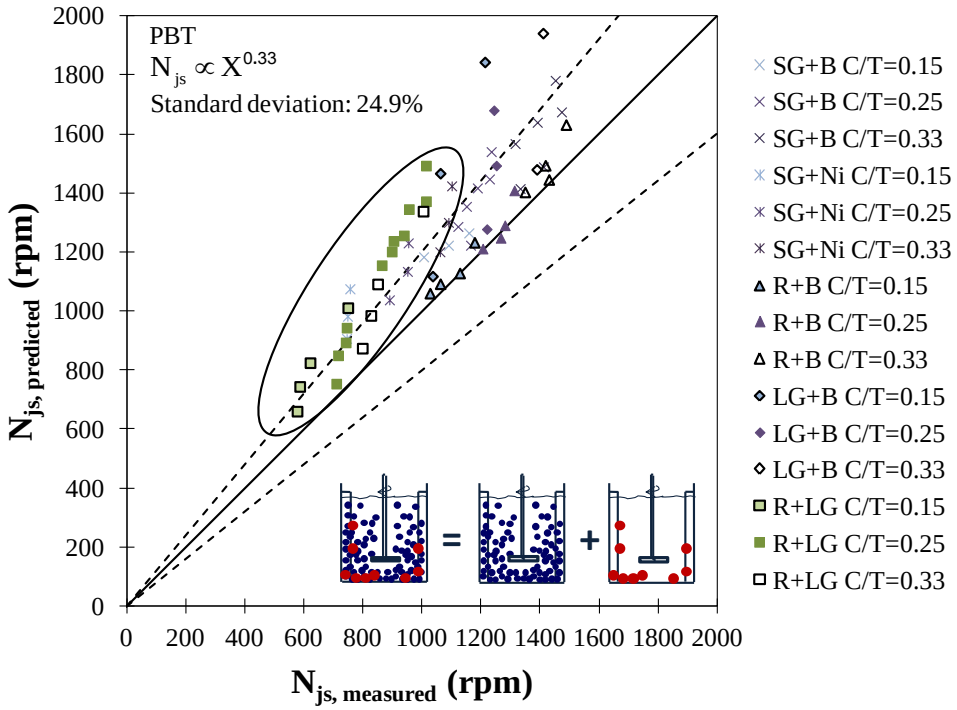

c.

Figure 3-11: The prediction of mixture N_{js} by power model with the PBT. The unimodal slurry N_{js}'s were determined by modified Zwietering correlations. The exponent on concentration term is a. 0.18 b. 0.24 c. 0.33.

In Figure 3-11c, when an exponent of 0.33 is used the data mostly follow the correct trend, but this time the mixture N_{js} is over-predicted. There are many data points above the +20% error lines. The standard deviation is 24.9%. Once again the mixtures with particles that follow an exponent of 0.33 follow the parity line, but the others fall outside of the trend. Since the exponent of 0.18 under-predicts and 0.33 over-predicts, an exponent in between these limits can better represent the entire data set.

Figure 3-11b shows the prediction of mixture N_{js}, using the particle-averaged exponent, 0.24, for unimodal slurry prediction. Almost all the data is within the ±20% error lines, and they tend to follow the trend, but the data is quite scattered. The standard deviation is 13.7%, which is very similar to the one calculated for the power model prediction through experimental unimodal slurry N_{js}'s.

3.5. Conclusions

The objective of this study was to propose and test two models to accurately predict the mixed slurry N_{js}. The analysis of the experimental data for several mixtures at varying off-bottom clearances and solids loadings with two impeller geometries led to the following conclusions:

- The current design heuristic is inadequate for the prediction of mixture N_{js} since it ignores the addition of a second solid phase, and cannot represent the physics.
- The power model, as given below, predicts mixture N_{js} accurately for both the PBT and the A310 impellers up to 27 wt% solids over a range of off-bottom clearances. The momentum model consistently over-predicted N_{js} and was discarded.

$$N_{js,mix} = \left(\frac{\rho_{sl,1} {N_{js,1}}^3 + \rho_{sl,2} {N_{js,2}}^3}{\rho_{sl,mix}} \right)^{1/3}$$

- The effect of off-bottom clearance on N_{js} depends on the type of the particle, the solids loading, and the type of the impeller and could not be reduced to a single term.
- The effect of concentration on N_{js} also proved to be complicated. Three possible exponents on concentration: 0.18, 0.24, and 0.33 were examined. While the exponent of 0.18 represents the LG up to 26 wt% solids and S up to 10wt% solids, the exponent of 0.33 represents the SG and R up to 35 wt% solids over a range of off-bottom clearances. The average exponent of 0.24 represents the entire data set within ±20%, but the data is scattered. Since the effect of concentration is quite complicated, the authors recommend carrying out experiments to determine the unimodal slurry N_{js} when applicable. If experiments are not possible, then one of these exponents could be chosen. It should be noted that a theoretical basis could not be found to explain why the particles follow different exponents.

3.6. References

Armenante, P.M., Nagamine E.U., and Susanto J., 1998. Determination of correlations to predict the minimum agitation speed for complete solid suspension in agitated vessels. Can J Chem Eng. 76, 413-419.

Armenante, P.M. and Nagamine E.U., 1998. Effect of low off-bottom impeller clearance on the minimum agitation speed for complete suspension of solids in stirred tanks. Chem Eng Sci. 53, 1757-1775.

Ayranci, I., and Kresta S.M., 2011. Design rules for suspending concentrated mixtures of solids in stirred tanks. Chem. Eng. Res. Des. 89, 1961-1971.

Ayranci, I., M.B. Machado, D.S. Nobes, J.J. Derksen and S.M. Kresta. The effect of geometry on the mechanism for off-bottom solids suspension in a stirred tank. Chem Eng Sci *(under review)*

Baldi, G., Conti, R., and Alaria E., 1978. Complete suspension of particles in mechanically agitated vessels. Chem Eng Sci. 33, 21-25.

Bittorf, K.J., and Kresta,S.M., 2003. Prediction of cloud height for solid suspensions in stirred tanks. Chem. Eng. Res. Des. 81, 5, 568-577.

Ibrahim, S. and Nienow A.W., 1996. Particle suspension in the turbulent regime: The effect of impeller type and impeller/vessel configuration. Trans IChemE. 74, Part A, 679-688.

Kasat, G.R. and Pandit A.B., 2005. Review on mixing characteristics in solid-liquid and solid-liquid-gas reactor vessels. Can J Chem Eng. 83, 618-643.

Machado, M.B., Nunhez, J.R., Nobes D., and Kresta, S.M., 2011. Impeller Characterization and Selection: Balancing Efficient Hydrodynamics with Process Mixing Requirements. AIChE Journal, DOI: 10.1002/aic.12758.

Molerus O., Latzel, W., 1987. Suspension of solid particles in agitated vessels. Part. Sci. and Tech., 5(3), 235-260.

Montante, G. and Magelli F., 2007. Mixed solid distribution in stirred vessels: experiments and computational fluid dynamics simulations. Ind. Eng. Chem. Res. 46, 2885-2891.

Myers, K.J. and Fasano J.B., 1992. The influence of baffle off-bottom clearance on the solids suspension of pitched-blade and high-efficiency impellers. Can. J. Chem. Eng. 70, 596-599.

Nienow, A.W., 1968. Suspension of solid particles in turbine agitated baffled vessels. Chem Eng Sci. 23, 1453-1459.

Atiemo-Obeng, V.A., Penney, W.R., Armenante, P., 2004. Solid-liquid mixing. In: Paul E.L., Atiemo-Obeng V.A., and Kresta S.M., eds. Handbook of Industrial Mixing, Science and Practice. John Wiley & Sons, Inc., Hoboken, New Jersey.

Zwietering, Th.N. 1958. Suspending of solid particles in liquid by agitators. Chem. Eng. Sci. 8, 244-253.

Chapter 4 : Effect of Geometry on the Mechanisms for Off-Bottom Solids Suspension in a Stirred Tank*

4.1. Introduction

Complete off-bottom suspension is the most common process requirement for solid-liquid mixing. The impeller speed at this condition is called the just suspended speed (N_{js}), and is defined as the impeller speed at which no particles remain stationary at the bottom of the tank for more than one or two seconds (Zwietering, 1958). Using this criterion Zwietering proposed a correlation for N_{js}:

$$N_{js} = S\left(\frac{g\left(\rho_S - \rho_L\right)}{\rho_L}\right)^{0.45} \frac{X^{0.13}\, d_p^{0.2}\, \nu^{0.1}}{D^{0.85}} \qquad 4\text{-}1$$

Many later papers provided measurements and tested other correlations for N_{js} (Nienow, 1968, Baldi et al., 1978, Armenante et al., 1998), but the Zwietering correlation is still the most widely accepted form for design. There are a number of valid criticisms of this correlation:

- The Zwietering constant, S, varies with impeller type, impeller diameter, off-bottom clearance, the shape of the tank bottom, the baffle geometry, and the particle type.
- The effect of viscosity is questionable since the original experiments did not use a wide range of viscosities.
- When there is only one particle, N_{js} drops to zero, which is non-physical.
- The correlation is only applicable to low solids loadings (<10 wt%) and unimodal slurries.

---

* *A version of this chapter has been submitted for publication to Chemical Engineering Science. This paper is co-authored by Inci Ayranci, Marcio Machado, Adam Madej, David S. Nobes, Jos J. Derksen, and Suzanne M. Kresta.*

In addition to the issues listed above, Grenville et al. (2010) showed that S changes on scale-up.

The Zwietering correlation does not successfully predict either the effect of geometry or scale. When the geometry is kept constant and the tank is scaled up, $D^{0.85}$ does not fully capture the effect of scale and S changes. When the scale is kept constant and D changes, S must also change. In order to make progress, a better understanding of the mechanism of solids suspension is required. Since the definition of complete off-bottom suspension is based on conditions at the bottom of the tank, it is not surprising that the impeller diameter alone does not provide enough information. Additional variables such as power number and the off-bottom clearance of the impeller provide more information, but they are not necessarily good predictors of the critical flow condition at the bottom of the tank. To make progress, more information is needed about the critical conditions at the bottom of the tank at the just suspended point and how the tank geometry affects solids suspension.

Baldi et al. (1978) suggested that turbulent eddies are the cause of solids suspension in a stirred tank. Eddies have a range of sizes and energies. Eddies that are close to the particle size are most likely to suspend the particles. This is often generalized to the idea that more solids can be suspended if there is more turbulence or the idea that constant power per volume is a reasonable scale-up rule. Both of these statements are flawed. To illustrate the problem consider two impellers: the Rushton turbine and the A310 impeller. The Rushton turbine is a radial impeller which provides intense turbulence, and the A310 is an axial impeller which provides mostly flow (Zhou and Kresta, 1996). The A310, however, is known to be better for solids suspension with a much lower P_{js} than the Rushton turbine (Ayranci and Kresta, 2011). There are two reasons for the failure of the Rushton turbine in suspending solids. First is the location of the turbulence. The Rushton turbine generates turbulence around the impeller, not at the tank bottom. The A310 directs all of the turbulence it generates towards the bottom. Second is the direction of the flow. The Rushton turbine discharges the

fluid radially towards the walls where it divides into two circulation loops one above and one below the impeller. The loop below the Rushton turbine reaches the tank bottom and flows towards the centre of the tank where the particles tend to drop out with no means of resuspension. The discharge of the A310 goes directly to the tank bottom and then turns outwards towards the walls. Once it reaches the walls, the baffles direct the fluid and solids upwards, making the solids suspension more efficient.

Next consider two tanks, both with A310 impellers, but different shapes of tank bottom: one has a flat bottom and one has a dished bottom. With the flat bottomed tank, the last point of suspension is at the tank walls, as described above, while with a dished bottom it is in the centre. If the baffles are profiled to fit close to the tank bottom in the dished tank, N_{js} is much higher than if they are left as rectangular baffles (Myers and Fasano, 1992). The just suspended speed is clearly sensitive to both the overall flow patterns and the details of the flow close to the bottom of the tank.

Important outcomes of these examples can be summarized as:

- N_{js} depends on the conditions at the bottom of the tank.
- Changing the impeller geometry completely changes the bottom conditions.
- Details of the flow close to the bottom can make a large difference to N_{js}.

These outcomes highlight an important point also emphasized by Thorpe and Stevenson (2003): if the turbulence is not sufficient for solids suspension and other parameters such as the flow pattern have an effect, then some mechanism in addition to turbulence must also play a role in solids suspension.

The hypothesis is further developed using an example with a much simpler geometry. First, the turbulent velocity is broken into two components: the mean velocity and the root mean square of the turbulent fluctuating velocity. Some combination of the velocity components provides the required conditions for

solids suspension. To form a better hypothesis of which mechanisms might determine the solids suspension condition, the contribution from each of these velocity components should be well understood.

Consider flow over a flat plate with a single particle. When the particle is sitting on the plate as shown in Figure 4-1a the forces acting on the particle are gravity (F_G), buoyancy (F_B), drag (F_D), and lift (F_L). In Figure 4-1b the mean flow on the particle is isolated from the turbulence. The mean flow needs to go over the sphere. This imposes both boundary layer and form drag on the particle and it starts to roll or slide along the plate. A pressure difference will develop between the top and bottom of the particle due to the asymmetry of the flow. The pressure difference applies a lift force on the particle. If $F_L > F_G$, the particle lifts off the plate. The lift forces that are caused by the shear and rotation of the particle are known as the Saffman force, F_S, and the Magnus force, F_M, respectively. In Figure 4-1c the turbulence is isolated from the mean flow. The eddies formed in a turbulent flow have different energies and sizes. The smallest eddies will not affect the particle. The largest eddies will have a convective effect and act similarly to the mean flow. A range of intermediate sized eddies will have sufficient energy to suspend the particle when they hit it, and will also have a size that is similar to the particle size. This is shown as the turbulence force, F_T in Figure 4-1c. In this simple case, illustrated with a single particle on a flat plate, both the mean flow and the turbulence can play a role in suspending the sphere.

In a stirred tank with an axial impeller, the solids are carried towards the walls by the mean radial velocity where they meet baffles and the associated vertical wall jets which work as elevators for the particles at the tank walls (Bittorf and Kresta, 2003). The particles that are carried towards the walls are easier to suspend and circulate in the tank, which explains the importance of selecting an axial flow impeller for solids suspension. At the same time as the mean radial velocity convects particles toward the walls, the axial component of fluctuating velocity lifts the particles off the bottom of the tank and into the strong circulating flow. In a hypothetical case where only turbulence is present in the

tank without any mean flow, the turbulent eddies can suspend the particles; however, this is a short term suspension since the particles are suspended only slightly from the bottom by the intermediate sized eddies. Each particle settles quickly and is resuspended at some later time, failing on average to lift all particles from the bottom of the tank. Since there is no mean flow the particles are not carried towards the walls and they are not circulated throughout the tank.

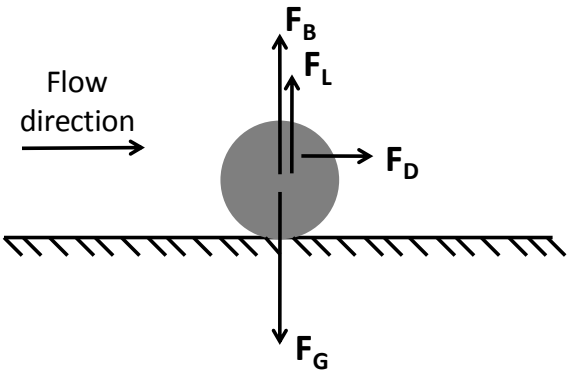

a.

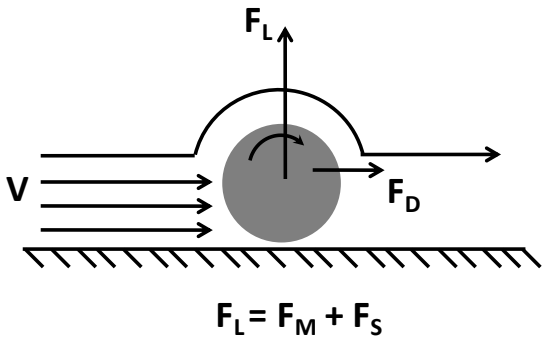

b.

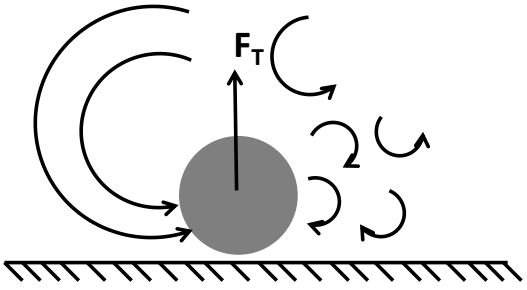

c.

Figure 4-1: Effect of mean velocity and turbulence on a particle on a flat plate. a. the forces effective on the particle b. mean velocity isolated from turbulence c. turbulent eddies isolated from the mean flow.

Now consider a second hypothetical case where there is only mean flow and no turbulence. The particles are easily carried towards the walls. They are slightly lifted as a result of the combination of drag and lift forces; however, this does not provide complete suspension at the bottom. The particles pile up at the periphery of the tank in low velocity regions. At the walls the radial mean flow is redirected into axial mean flow. This suspends many particles that are at the top layer of the pile; however, a significant fraction of the particles remain stationary at the periphery since there is no turbulence to push them up and out of the stagnant zone they are in. These thought experiments suggest that the complete off bottom suspension condition in a stirred tank could easily require contributions from both velocity components.

Solids suspension has been extensively studied in two other research areas: slurry pipeline flow and river sediment transport. In both flows, the effects of mean flow, turbulence, and near wall lift have been considered. These results are considered next and their applicability to stirred tanks is discussed.

Thorpe and Stevenson (2003) compared solids suspension in stirred tanks and slurry pipeline flow in terms of the definition of suspension and the form of the correlations. The deposition velocity, the minimum solid transport rate below which the particles start accumulating at the pipe wall, is analogous to N_{js} in stirred tanks. The main mechanisms for solids suspension in slurry pipelines are turbulent diffusivity (fluctuating velocity) and near wall lift. In the core region turbulent diffusion provides solids suspension. Near the wall, the turbulence is diminished in the viscous sub-layer. In the horizontal plane close to the viscous sub-layer there is downwards flux of particles; however, there is no upward flux of particles caused by the turbulence since it is not effective any more. The balance of the flux of particles is supported by another mechanism which is the near wall lift (Wilson, 2005). This is where the Saffman and Magnus forces become important because they are the vertical forces that act on the particle in the viscous sub-layer. Recently, Wilson et al. (2010) reported the importance of the ratio of the particle size to the thickness of the viscous sub-layer. When the

particle size is small the particles are submerged in the viscous sub-layer. For larger particles, no particles remain in the viscous sub-layer. The thickness of the viscous sub-layer changes according to the mean flow. Higher mean flow results in a thinner viscous sub-layer. This affects the importance of near wall lift, since the ratio of the particle size to viscous sub-layer thickness changes. Turbulence, near wall lift, and the mean flow are all active in providing solids suspension for slurry pipeline flows.

Molerus and Latzel (1987) reported boundary layer effects in stirred tanks. Based on the wall friction on pipeline flow they related a shear Reynolds number for the boundary layer to the Archimedes number (Ar), and defined limits on Ar to determine whether the particle is submerged in the viscous sub-layer.

$$\mathrm{Ar} = \frac{g(\rho_s - \rho_L)d_p^3}{\nu^2 \rho_L} \qquad 4\text{-}2$$

Molerus and Latzel showed that the particles are submerged in the viscous sub-layer if Ar<40. Larger particles extend beyond the viscous sub-layer, and therefore, different mechanisms apply for these particles. It seems that the Ar does not include a velocity term. The thickness of the viscous sub-layer, however, decreases with an increase in velocity. To test the validity of the argument of a limit on Ar to determine the position of the particle with respect to the viscous sub-layer the details of the Ar should be analyzed. Ar is the ratio of gravitational forces to viscous forces.

$$\mathrm{Ar} = \frac{(\rho_s - \rho_L)\, g\, d_p}{\frac{\mu_L\, U}{x}} \qquad 4\text{-}3$$

The velocity, U, is present in this initial form of the Ar, but not in the final form, so it cancels out in the derivation. Since the focus is on the viscous sub-layer, the length scale, x, can be assumed to be the thickness of the viscous sub-layer, δ, and the velocity, U, becomes U^*, the shear velocity. If $\delta \geq d_p$, then the particle is submerged in the viscous sub-layer. The limiting point is when $\delta = d_p$. Applying this limit and the assumptions to Equation 4-3 gives

$$Ar = \frac{(\rho_s - \rho_L)\, g\, d_p}{\frac{\mu_L\, U^*}{d_p}} \quad 4\text{-}4$$

The U^* is still present in the equation. In slurry pipeline flow a dimensionless particle diameter, d^+ is used to determine whether the particle is submerged in the viscous sub-layer (Wilson et al., 2010).

$$d^+ = \frac{\rho_L\, d_p\, U^*}{\mu_L} \quad 4\text{-}5$$

If $d^+<9$, then the particle is completely submerged in the viscous sub-layer, and if $d^+>27$, then the particle is significantly larger than the viscous sub-layer and starts to protrude into the logarithmic layer. The near wall lift applies when $9<d^+<27$. Since d^+ is dimensionless, it can be interpreted as some ratio of δ to the particle diameter. There are three layers when flow close to a solid surface is considered: viscous sub-layer, buffer layer, and logarithmic layer. The distance of each layer can be defined in terms of the dimensionless distance, y^+. When $y^+\leq5$, the particle is submerged in the viscous sub-layer, between $5\leq y^+<30$ it is in the buffer layer, and when $y^+>30$ it is in the logarithmic layer (Davies, 1972):

$$y^+ = y\frac{U^*}{\nu} \quad 4\text{-}6$$

When $y^+=5$, $y=\delta$. Applying these boundary conditions in Equation 4-6 gives

$$\delta = 5\frac{\nu}{U^*} \quad 4\text{-}7$$

To combine this back to the particle size remember that the particle is submerged in the viscous sub-layer when $d_p = \delta$, and based on Equation 4-7 when $d_p = 5\frac{\nu}{U^*}$. Substituting this information in Equation 4-5 shows that $d^+=5$ when the particle is the same size as the viscous sub-layer. Since the limiting d^+ is known, 5, it can be substituted in Equation 4-5 to obtain an expression for U^*.

$$U^* = 5\,\frac{\mu_L}{\rho_L\, d_p} \quad 4\text{-}8$$

When this U^* is replaced in Equation 4-4, the final form of the Ar, given in Equation 4-2, is obtained with a constant. This scaling argument shows that the

limit on the Ar does include the effect of velocity on the thickness of the viscous sub-layer for the fixed condition of particles being submerged in the viscous sub-layer.

The limit based on d^+ can be improved with different assumptions. Further investigation of the Ar criterion and d^+ showed that they can be linked. The Ar is based on the particle shear Reynolds number, and d^+ is the same as the particle shear Reynolds number. Combining the two cases the relation between Ar and d^+ is:

$$d^+ = \sqrt{\frac{2}{3}\mathrm{Ar}} \qquad 4\text{-}9$$

This relation applies only for the cases where $\delta = d_p$. The particles are submerged in the viscous sub-layer when Ar<40. This corresponds to $d^+<5$. Note that this limit is the same as the limit based on flow close to a solid surface. There is no limit for stirred tanks at which the particles penetrate beyond the logarithmic layer. For slurry pipelines this limit is $d^+>27$. This limit can loosely be used for the stirred tanks: a particle is exposed to near wall lift when $5<d^+<27$, and it penetrates beyond the logarithmic layer when $d^+>27$. An exact quantitative upper limit cannot be given for stirred tanks because of the complexity of boundary layer development at the bottom of a stirred tank.

River sediment transport is another area where solids suspension has been widely discussed. The motion of solids is caused by the mean flow over a bed of sediment. At very low velocities no sediment moves. At higher velocities individual particles start rolling and sliding intermittently along the bed. As the velocity is further increased the drag and lift on the particles increases; some particles start to make short jumps, leave the bed for a short time and return either to come to rest or to continue in motion on the bed and undergo further jumps. If the mean velocity increases slightly, the particles jump more frequently and some of the grains are incorporated into the main body of the flow by the upward

components of the turbulence. They may then stay in suspension for appreciable lengths of time (Vanoni, 2006).

The size of the unsuspended sediment particles determines the surface roughness of the bed, which in turn affects the flow velocity distribution and its sediment transport capacity. If the bottom boundary is smooth, turbulence will be suppressed in the viscous sub-layer near the bed and the capacity of turbulence to suspend solids will be dramatically decreased. This is rarely the case in rivers. Most boundaries in alluvial rivers are hydraulically rough; therefore, there is no viscous sub-layer formation. Turbulence becomes the main mechanism in solids suspension from the bed (Garcia, 2008). The effect of bottom roughness on N_{js} in a stirred tank was studied by Ghionzoli et al. (2007). Their study showed that the N_{js} of particles which have a diameter smaller than 10 η, where η is the Kolmogoroff length scale, is reduced on a rough bottom while the N_{js} for larger particles stays the same. The bottom roughness determines the turbulent eddy size and allows the turbulence to be the controlling mechanism for solids which are well matched to the defining eddies.

This analysis of related research areas shows that mean flow and turbulence are the main mechanisms for solids suspension. It seems that both of these mechanisms are necessary for solids suspension: either one of them acting alone may not be sufficient to suspend the solids throughout the volume of a stirred tank. In some cases one of the mechanisms may dominate. At the larger scale, the mean flow carries the particles towards the walls. In the boundary layer, the velocity gradient due to the mean flow rolls and/or slides the particles and lifts them out of the viscous sub-layer so that they can be carried towards the walls by the bulk flow. At the same time turbulent eddies of a similar size and inertial energy to the particles lift particles for short periods of time, again exposing them to the bulk flow. Larger eddies may act as an additional convective effect, but those eddies which have a large scale should also have a directional preference which will scale with the mean velocity, so they are lumped with the mean flow. We hypothesize that both the mean flow and the turbulent eddies are necessary for

solids suspension, but if there is sufficient turbulence with the required eddy size, then the eddies will be the main mechanism that suspend the particles. If there is sufficient mean flow, the turbulence will still contribute to solids suspension, but the mean flow will dominate.

To test this hypothesis, experiments were designed to apply gradual changes to the flow field using constant solid species and solids concentration to compare the critical flow conditions at the just suspended speed. The desired changes are small enough to keep the circulation pattern the same, but large enough to observe a difference in the decay of the impeller discharge stream. Varying the off-bottom clearance of an A310 impeller was chosen as the best way to achieve this objective. If convection across the tank bottom (mean flow) is the dominant mechanism for solids suspension, then all of the mean radial velocity profiles, properly scaled to N_{js}, should collapse onto a single profile for all clearances. In this case the turbulent eddies are still necessary, but their contribution is not sufficient to obtain complete off-bottom suspension. If it is the turbulent eddies which dominate, then the axial rms (root mean square) velocity profiles should collapse onto a single profile for all clearances, and the mean flow profiles will most likely be scattered.

The analysis of the dominant mechanism requires the analysis of a collapse in the velocity profiles. This collapse is based on the differences between the single phase velocity profiles and the velocity profiles scaled to N_{js}. The analysis can be done by visual inspection and by inspecting the change in standard deviation. Both these analyses are done to test the hypothesis. An additional analysis based on the particle-eddy interactions is also included.

4.2. Experimental Procedures

To test the hypothesis stated above a three-step plan was prepared. First, the N_{js} of four slurries (three at low and one at high solids loading) was measured at varying off-bottom clearances. Second, single phase velocity profiles, the mean radial velocity and the axial fluctuating velocity, were measured using PIV

(particle image velocimetry) and calculated with LES (large eddy simulations) over a horizontal plane close to the tank bottom for the same range of geometries. Third, the velocity profiles were scaled to the just suspended condition at every clearance to identify whether a single critical flow condition exists at the bottom of the tank.

4.2.1. N_{js} experiments

N_{js} was measured as a function of off-bottom clearance in a flat bottomed cylindrical tank with an inner diameter of 0.24 m, shown in Figure 4-2. The tank was equipped with four baffles (W_b=T/10). The liquid level in the tank was equal to the tank diameter (H=T). Two Lightnin A310 impellers with diameters D=T/3 and D=T/2 were used. The A310 was chosen for this study because it generates a purely axial flow and is efficient for solids suspension in terms of the power consumption at N_{js}. The off-bottom clearance, C/T, was varied from 0.15 to 0.358 for the T/3 impeller, and from 0.125 to 0.333 for the T/2 impeller to ensure that the impeller stream reached all the way to the tank bottom in all cases. The liquid phase was tap water in all experiments. The cylindrical tank was placed in a square tank in order to minimize the optical distortion, and these two tanks were bolted onto a platform which is open in the middle, in order to leave the bottom of the tank visible from below. More details about the experimental setup and the procedure are given in Ayranci and Kresta (2011).

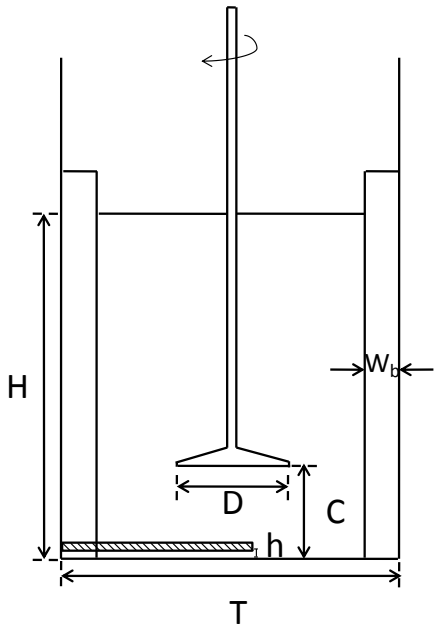

Figure 4-2: Cross-section of the cylindrical tank used for N_{js} and PIV experiments, and LES simulations. The dashed plate represents the position of the calibration plate 4 mm above the bottom of the tank. The measurement plane is 3.5-4.5 mm from the bottom of the tank and is 2mm thick.

The just suspended speed, N_{js}, is determined visually by watching the bottom of the tank. N_{js} is the impeller speed at which no particle remains stationary at the bottom of the tank for more than 1 or 2 seconds (Zwietering, 1958). The impeller speed was increased gradually, and after the system reached steady state (1 to 2 minutes) the bottom of the tank was observed. Four slurries were used in the experiments; unimodal slurries of small glass beads (SG), large glass beads (LG), and bronze (B) at low solids loadings and a mixture of small glass beads with bronze at high solids loadings. The specifications of the particles are given in Table 4-1. The solids loadings of the unimodal slurries of SG, LG and B were 1.5 wt%, and the SG+B mixture loading was 26 wt% SG with 1.3 wt% B. The mixture is at a high solids loading where the presence of particles may start to affect the flow field so the single phase velocity data should be considered with some caution. The data for the B slurry is available only for the T/3 impeller, because air entrainment was excessive with the T/2 impeller.

Table 4-1: Specifications of the particles used in the N_{js} experiments

Type	Density (kg/m^3)	Size (μm)	Ar	Shape
Small glass beads (SG)	2500	74-125	14.7	Spherical
Bronze (B)	8855	150-297	820.5	Spherical
Large glass beads (LG)	2500	595-841	5378.7	Spherical

4.2.2. PIV experiments

A stereoscopic PIV system was used to measure velocity profiles close to the tank bottom. The PIV was composed of two high-resolution cameras (14bit, 2048×2048 pixels) which capture images of a seeded flow field illuminated with the double pulse of an Nd:YAG laser (532nm, 10Hz, 400mJ of energy per pulse). The flow facility is a 240 liter glass walled holding tank (1200 mm length × 500 mm height × 400 mm width) in which a 240mm diameter glass cylinder served as the mixing tank. The cameras viewed the region-of-interest from below.

The PIV measurements followed a procedure outlined by Madej et al. (2011). The water in the holding tank was evenly seeded with tracer particles (hollow glass spheres, Potters Industries). The mean particle size of the tracer particles was 11 μm and their specific gravity was 1.1. They were sufficiently small and light to perfectly follow the flow, so the measured particle velocities match the liquid velocity. The light sheet had a thickness of ~2mm to capture the out-of-plane component of the flow. The stereoscopic PIV system hence resolved the three components of the flow over a 2mm thick, two dimensional plane. For each operating condition, 2 000 image pairs were recorded and the time interval between the two images was set between 700 μs and 1000 μs, depending on the off bottom clearance of the impeller. The lower time interval was used for lower clearances, since the velocities at the bottom were higher when the clearances were lower. The sampling frequency between each image pair was between 1.6 Hz and 2.5 Hz.

In order to determine the camera scaling and the image overlap a target was placed 4 mm above the bottom of the tank. Using the target data the images

were dewarped and the camera scaling was calibrated. This allowed the positioning of the 2mm thick measurement plane 3.5-4.5 mm above the bottom of the tank. Image overlap was further enhanced using a self-calibration of the data to locate the position of the laser sheet as it overlaps with the target. The calibration plate had a diameter of 20 cm and, as shown in Figure 4-2, it was positioned such that images can be taken from the centre of the tank to the tank wall. Here, only data from the mid-baffle plane is reported.

A three-dimensional cross-correlation PIV algorithm was used to determine the particle displacement over the time interval between the two images. From these displacement vectors, velocity vectors were calculated using commercial software (Davis 7.4, LaVision). The resulting data field is an instantaneous snap-shot of the three components of velocity over the measurement plane. Velocity data processing was carried out using interrogation cell sizes of 64x64 pixels for the preliminary step and 32x32 pixels with 50 % overlap for the final step. At this final interrogation window size, the determined velocity vector is an average over a physical region of 1.116 mm x 1.116 mm in plane by the thickness of the light sheet of ~ 2mm.

The glass tank used for the PIV measurements has the same dimensions as the tank used for the N_{js} experiments, with the same ranges of off bottom clearances. Measurements were carried out at a fixed Reynolds number of 48000.

$$\mathrm{Re} = \frac{ND^2}{\nu} \qquad 4\text{-}10$$

A fixed rotational speed was used at all clearances: 200 rpm for the A310 T/2 and 450 rpm for the A310 T/3 impeller. This avoided shaft vibration and air entrainment at high rotational speeds which would have made the PIV experiments more difficult. The measured velocities were then scaled to complete off bottom suspension conditions using the N_{js} determined for each off-bottom clearance.

$$V_{scaled} = V_{measured} \frac{N_{js}}{N_{expt}} \quad (4\text{-}11)$$

Several authors have shown that velocity profiles below the impeller scale exactly with the tip speed (πND) (Nouri et al, 1987, Zhou and Kresta, 1996). The range of clearances used here falls within a range where this scaling can also be applied at the bottom of the tank (Kresta and Wood, 1993). This was validated through some test experiments.

4.2.3. LES simulations

A lattice-Boltzmann method was used to discretize the Navier-Stokes equations and a force-field technique was employed to represent the effect of impeller, shaft, baffles and tank wall on the fluid. In the lattice-Boltzmann method, the fluid flow can be considered as a many-particle system where all the particles follow the laws of conservation of mass and momentum (Derksen and Van den Akker, 1999). The particles reside on a uniform cubic lattice. At every time step, particles move to neighboring lattice sites, collide, and exchange momentum.

LES was chosen because of its flexibility in adapting to complex geometries, providing detailed information and using less computer resources compared to DNS (direct numerical simulations). In LES, small scale eddies are filtered out and the large scale eddies are resolved. The effect of the small scale eddies on the large scale is modeled using a subgrid-scale model. For this modeling, the Smagorinsky model with a constant of $c_s = 0.1$ was used.

A force-field technique was used to represent the cylindrical tank wall, rectangular baffles, and revolving impeller and shaft in the cubic lattice. These are defined by points on the surface. These points do not need to coincide with the lattice sites. The forces acting on the flow are calculated in such a way that the fluid has prescribed velocities (Derksen and Van den Akker, 1999) at these surface points. Applying the boundary conditions results in the desired curved surface for the tank wall, the rectangular baffles, and the rotating impeller and shaft.

A computational domain with 200^3 grid nodes was used. The Reynolds number was 48000, which is the same as in the PIV experiments. The simulations were performed for an A310 impeller with a diameter of D=T/3 at C/D=0.45, 0.675, 0.75, and 0.9. The entire tank was simulated and the three velocity components were computed. The averages were taken for several horizontal planes.

4.3. Results and Discussion

The results are presented in five major sections. First the effect of particle properties, solids loadings and geometry (impeller diameter and off-bottom clearance) on N_{js} are presented. Next the velocity profiles for the T/3 and the T/2 impeller are evaluated to determine the solids suspension mechanism for each impeller and to examine whether the dominant mechanism depends on the impeller diameter. After the analysis of the experimental data, the hypothesis and the conclusions are compared with the LES results. Finally, the power consumed by the two impellers is compared to better understand the interaction between the observed mechanisms and power consumption.

4.3.1. N_{js} results

Figure 4-3 shows the N_{js} results for the T/2 and T/3 impellers for unimodal slurries of B, LG and SG at 1.5 wt% and the mixed slurry of 26 wt% SG with 1.3 wt% B, all at varying off-bottom clearances. Within the unimodal slurries the B has the highest density and also the highest N_{js}. The LG and SG have the same density, but LG has a higher N_{js} since it is 7 times larger than the SG. The mixed slurry has the highest solids loading, so it has a higher N_{js} than the LG and the SG, but lower than the B because of particle-particle interactions as explained in Ayranci and Kresta (2011). These trends are consistent for both impeller diameters, and as expected, N_{js} is smaller for the larger impeller diameter. As predicted by the Zwietering equation, an increase in the particle density, particle size or solids loading - in the absence of particle-particle interactions - results in an increase in N_{js} .

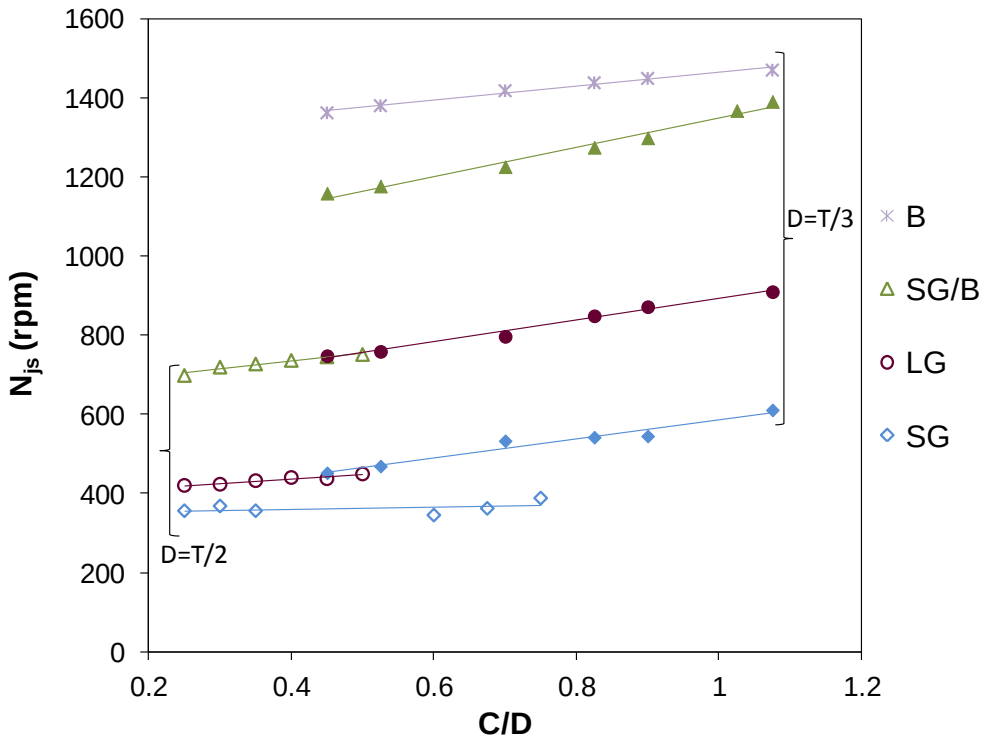

Figure 4-3: The effect of impeller diameter, particle diameter, particle density, and solids loading on N_{js}. B, LG and SG are at 1.5 wt% and the mixture of SG+B is at 27wt% total solids loading with 1.3 wt% B. Solid and hollow symbols represent D=T/3 and D=T/2, respectively.

The effect of off-bottom clearance on N_{js} is more complex, as shown in Figure 4-4. At off-bottom clearances, C/D, larger than 0.35, the particles collect close to the tank walls, and are suspended from there when N_{js} is reached. At off-bottom clearances smaller than 0.35 the particles collect in the centre of the tank as well as at the tank walls. This is because the A310 impeller cannot develop purely axial flow below the hub at low C/D and the discharge of the impeller is quickly deflected to produce a swirling radial flow. Figure 4-4 shows sample experimental observations of this behaviour for a slurry of 1.5wt% SG with 1.5wt% B with the D=T/2 impeller. At C/D=0.25 the particles collect both in the centre and at the periphery of the tank, but when the off-bottom clearance is increased to C/D=0.5 there is no accumulation in the centre: all the particles are at the periphery of the tank. These two deposition patterns will be helpful for understanding some of the later results.

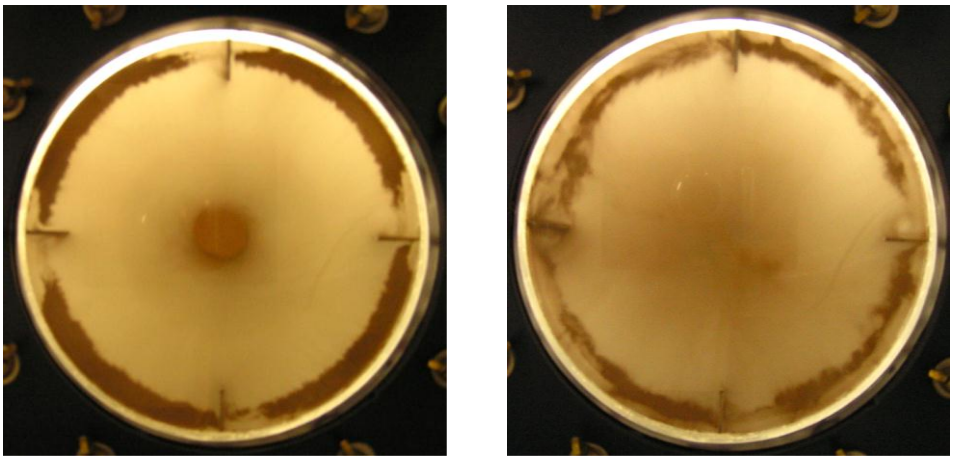

a. b.

Figure 4-4: The effect of off-bottom clearance on the solids suspension pattern for the A310 D=T/2 a. C/D=0.25 b. C/D=0.5

4.3.2. Solids suspension mechanisms with the T/3 impeller

The evaluation of the dominant solids suspension mechanism is based on a hypothesis that solids suspension occurs due to a combination of mean flow and turbulent eddies, and at the complete off-bottom suspension condition one of these mechanisms, either the turbulence or the mean flow, should dominate for a fixed set of particles and tank geometry. For a purely axial impeller, the flow pattern stays the same as the off-bottom clearance is increased and thus the velocity component which is dominant at the point of off-bottom suspension should also remain the same. If this hypothesis holds, a set of velocity profiles should collapse onto a single curve for all off-bottom clearances when the measured profiles are scaled to N_{js} at the respective clearances. This hypothesis is evaluated based on both the visual inspection of scaled velocity profiles for mean radial velocities, V_r, and axial rms velocities, v_z', and the reduction in normalized standard deviation for scaled V_r or v_z' over the range of clearances at each point in the profile. A comparison of estimated eddy sizes with particle sizes was also made to further probe the mechanisms. The analysis starts with the measured velocity profiles.

The measured V_r and v_z' at seven off-bottom clearances were normalized with the tip speed of the impeller and are shown in Figure 4-5 a and b. The

profiles in each graph show similar trends for increasing off-bottom clearances, but they do not follow a definite order. In Figure 4-5a the V_r profile for the highest clearance, C/D=1.075, is 12 % lower than the other clearances in the 40-100 mm area. This is because the discharge of the impeller loses a significant amount of momentum by the time it reaches the bottom of the tank when the impeller is more than one impeller diameter away from the tank bottom. While the data for this clearance in the centre blends in with the rest, it cannot sustain similar level of velocities in the 40-100 mm area. This clearance was eliminated from the rest of the figures because it violates the basic assumption of having a constant circulation pattern. In Figure 4-5a another irregularity is seen for C/D=0.675 and C/D=0.75 in the 95-120 mm area. While the circulation pattern remains to be the same as the rest of the clearances tested, a transition is seen. The maximum radial velocity can be sustained longer at these off-bottom clearances. In Figure 4-5b for these two clearances the position of the peak velocity is slightly shifted, and after 40 mm $v_z^{'}$ is slightly higher than the rest of the data. The remaining profiles for both V_r and the $v_z^{'}$ are quite close to each other at varying off-bottom clearances when normalized with tip speed. This indicates that the expected collapse with either one of the velocity profiles may be difficult to determine by inspection when the profiles are scaled. To allow a more objective assessment, the collapse was also analyzed in terms of $\Delta\sigma$, the point by point difference between the standard deviation of the scaled velocity profiles and the measured velocity profiles for each slurry.

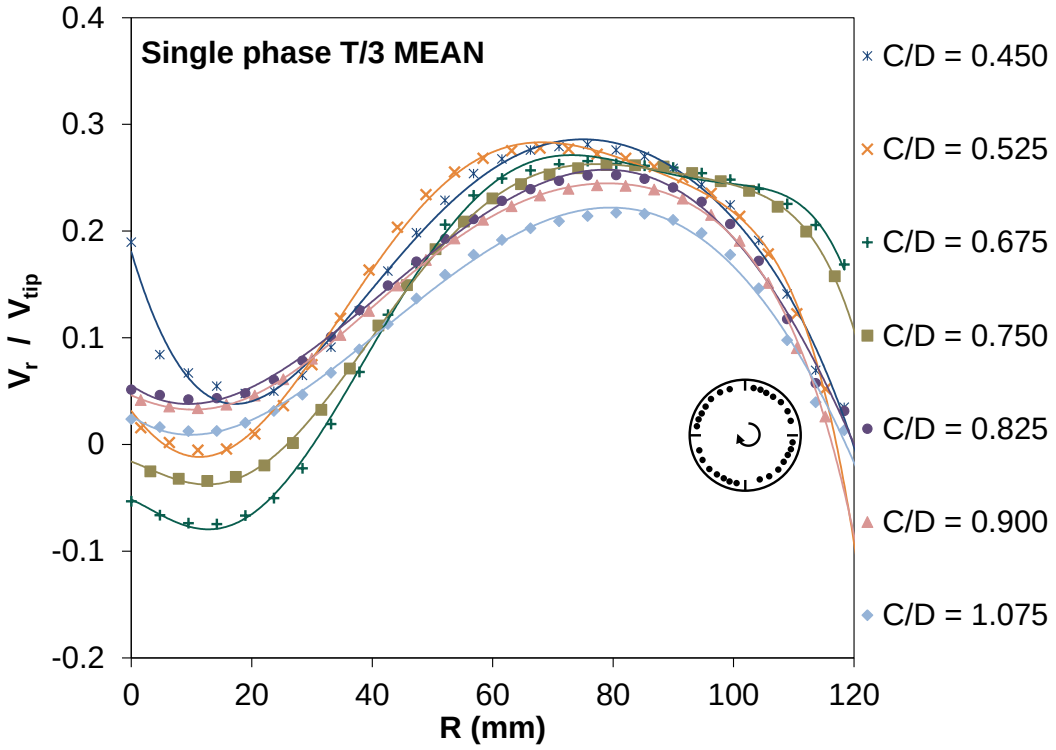

Figure 4-5a: Measured mean radial velocity profiles normalized with the tip speed of the impeller: A310 T/3.

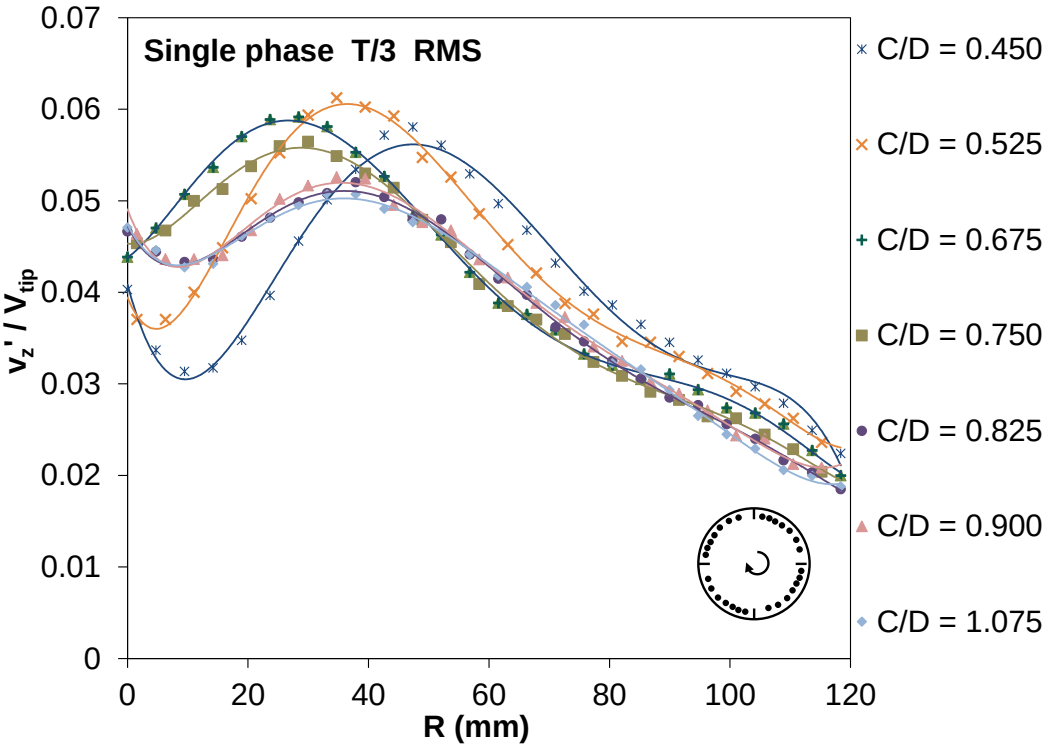

Figure 4-5b: Measured axial rms velocity profiles normalized with the tip speed of the impeller: A310 T/3.

The measured velocity profiles were scaled to N_{js} for four slurries: SG, LG, B, and the mixture of SG with B. For all four slurries the last point of suspension is at the tank walls. The SG slurry results were representative and are reported here. The scaled V_r profiles in Figure 4-6a are scattered over most of the profile but collapse from 40-65 mm, which is right after the tip of the blade, for all clearances when compared to the measured velocities in Figure 4-5a. The scaled v_z' profiles in Figure 4-6b are scattered over the first 40 mm, which is the area below the impeller blades. From 40 mm to the tank walls the v_z' profiles collapse, and the collapse becomes more significant after 80 mm. The v_z' profiles collapse over most of the radius and the collapse is more significant than the small part in V_r. This shows that some level of mean flow is necessary, but a certain level of turbulence is required for solids suspension. The turbulence is the dominant mechanism for solids suspension with the T/3 impeller.

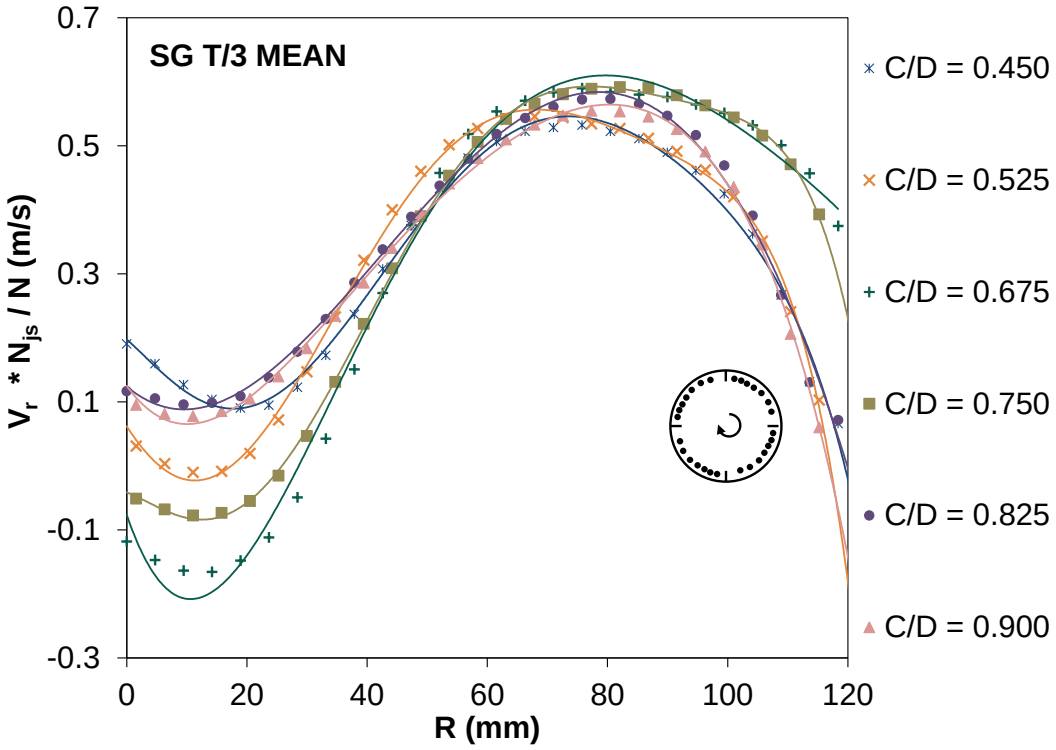

Figure 4-6a: Scaled mean radial velocity profiles for 1.5 wt% SG with the A310 T/3.

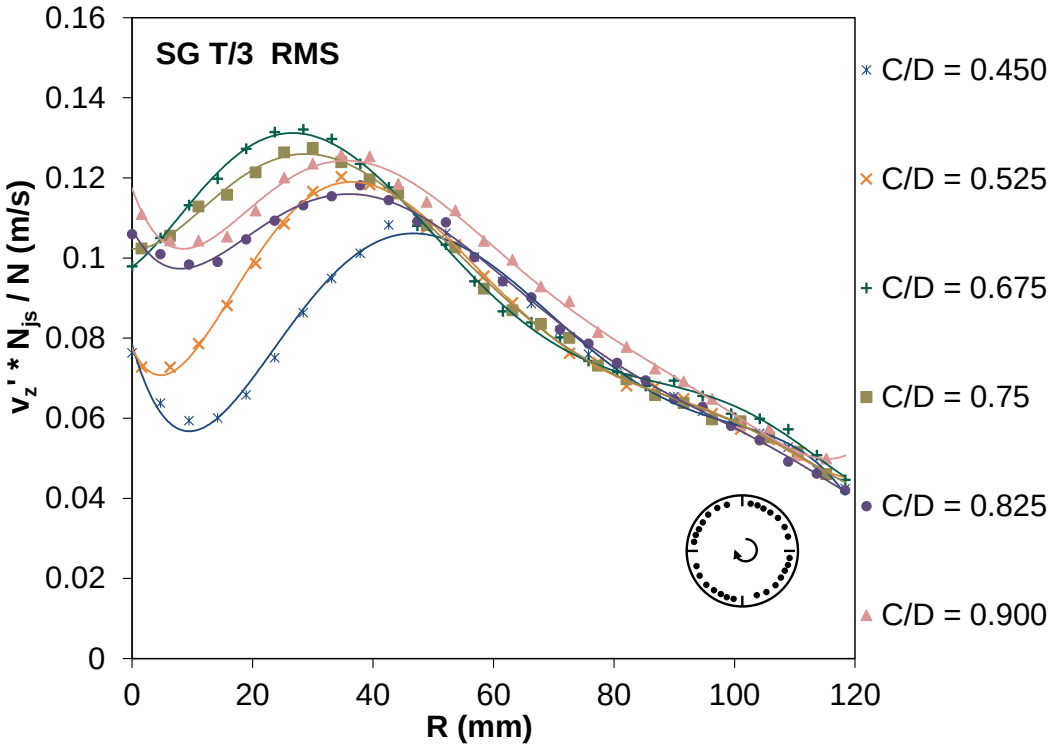

Figure 4-6b: Scaled axial rms velocity profiles for 1.5 wt% SG with the A310 T/3.

While we categorize some parts of these figures as collapsed, the collapse is not perfect and the measured profiles are quite close to each other for varying clearances, so it is prudent to analyze the data from another perspective to verify that this initial conclusion is correct.

The normalized standard deviation (σ) of the velocities for all six clearances was calculated at each radial position for both velocity components (V_r and v_z').

$$\sigma = \sqrt{\frac{\sum_{n=1}^{n=6}\left(\frac{x_n - x_{mean}}{x_{mean}}\right)^2}{6-1}} \qquad 4\text{-}12$$

Here n signifies the off-bottom clearance. For each impeller there are six off-bottom clearances. x_n is either V_r or the v_z' at the n^{th} off-bottom clearance, x_{mean} is the mean of the velocities at all off-bottom clearances. This calculation is repeated

for every radial position and the difference between the normalized standard deviation of the measured and the scaled results, $\Delta\sigma$, is calculated as:

$$\Delta\sigma = \left[\sqrt{\frac{\sum_{n=1}^{n=6}\left(\frac{x_n - x_{mean}}{x_{mean}}\right)^2}{6-1}}\right]_{scaled} - \left[\sqrt{\frac{\sum_{n=1}^{n=6}\left(\frac{x_n - x_{mean}}{x_{mean}}\right)^2}{6-1}}\right]_{measured} \qquad 4\text{-}13$$

The change in normalized standard deviation, $\Delta\sigma$, is reported in Figure 4-7a and b for V_r and v_z' and for all four particle species. Values above zero indicate that the profiles are more scattered, and values below zero indicate that profiles have collapsed. The results confirm the conclusions made from Figure 4-6. Turbulence is clearly the dominant mechanism for all four slurries for the T/3 impeller. The collapse of the mean radial velocity is erratic, actually becoming more scattered in the area immediately below the impeller blades (0-40 mm) where very large or very small $\Delta\sigma$ are seen. This is not surprising because the mean V_r over all clearances is close to zero in this area, and in the $\Delta\sigma$ calculations the velocities are divided by the mean of the velocities. The profiles show more agreement over the middle region (40-80 mm), increasing again from 80-120 mm. This shows that the hypothesis holds true for the T/3 impeller: both the mean flow and the turbulent eddies are necessary for solids suspension, but the turbulent eddies dominate. A certain level of turbulence should be reached at the bottom of the tank with the contribution of some mean flow in order to achieve complete off-bottom suspension.

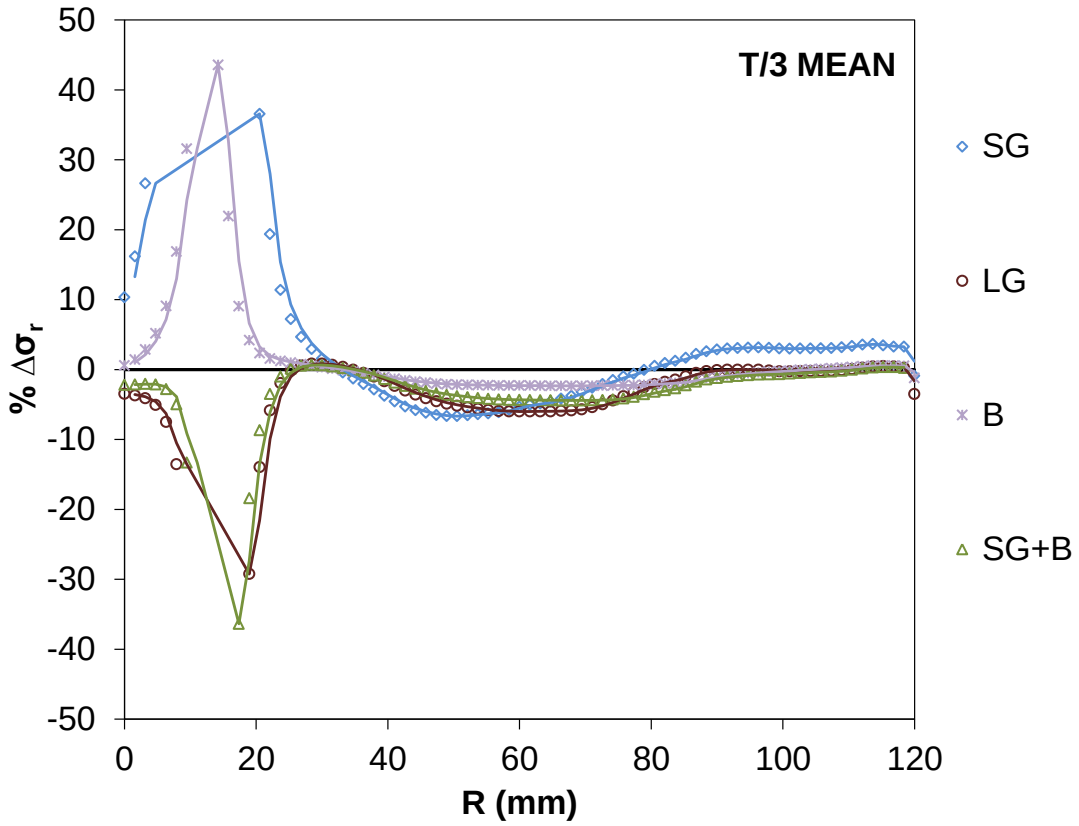

Figure 4-7a: The difference between the normalized standard deviation of the scaled and the measured mean radial velocity for each particle species with the A310 T/3.

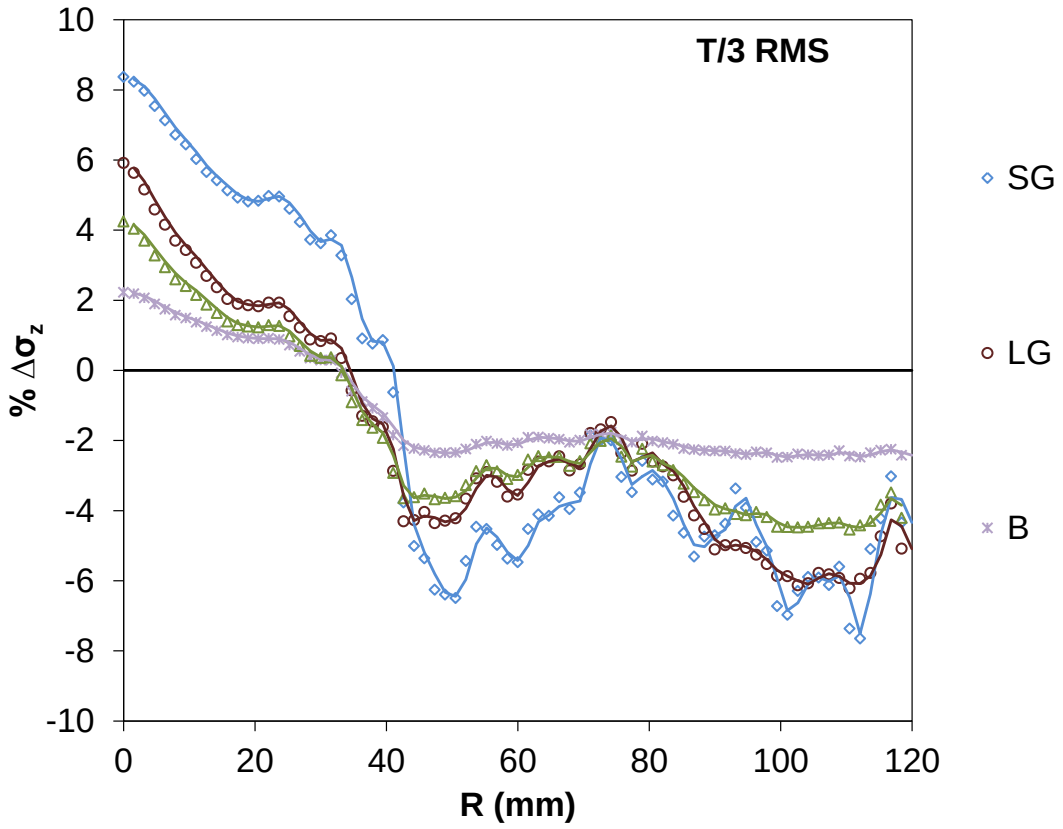

Figure 4-7b: The difference between the normalized standard deviation of the scaled and the measured axial rms velocity for each particle species with the A310 T/3.

A final analysis was done based on the size of the smallest eddies – the Kolmogoroff length scale (η). A minimum and a maximum η can be estimated at the bottom of the tank using the following scaling arguments. An axial flow impeller generates turbulence at the bottom of the tank, with the smallest eddy sizes, the Kolmogoroff scale, following the relationship:

$$\eta_{est} = \left(\frac{\nu^3}{\varepsilon}\right)^{1/4} \qquad 4\text{-}14$$

where ν is the kinematic viscosity and ε is the energy dissipation. The energy dissipation can be estimated from:

$$\varepsilon = A\frac{v_z'^3}{L} \qquad 4\text{-}15$$

where A is 1.0 for isotropic turbulence, v_z' is the axial rms velocity, and L is the integral length scale. Two integral length scales might be considered: the size of the trailing vortices close to the impeller, L=D/10, and the size of the circulation layer at the bottom of the tank, L=T/5. Since the trailing vortices are at the impeller, and the eddies get larger towards the bottom of the tank (Tatterson et al., 1980), the length scale at the bottom of the tank should be larger than D/10. Similarly, the length scale at the bottom of the tank should be smaller than the circulation layer close to the bottom of the tank, L<T/5. Based on these two limiting length scales and the measured v_z', a maximum and a minimum limit on the Kolmogoroff length scale of the eddies can be estimated:

$$\eta_{min} = \left(\frac{\nu^3}{A \frac{v_z'^3}{D/10}} \right)^{1/4} \qquad 4\text{-}16$$

$$\eta_{max} = \left(\frac{\nu^3}{A \frac{v_z'^3}{T/5}} \right)^{1/4} \qquad 4\text{-}17$$

The v_z' in Equations 4-16 and 4-17 was determined from the scaled velocity profiles for each particle. Over the sections where the profiles collapsed the maximum v_z' was used in Equation 4-16 to estimate η_{min}, and the minimum v_z' was used in Equation 4-17 to estimate η_{max}. Table 4-2 shows the results. For SG, the range of smallest eddy sizes overlaps the range of particle sizes so the particles are much smaller than the most energetic eddies and will be swept up mainly by turbulent convection from eddies much larger than the particles. For LG, the particles are much larger than the smallest eddies (about 10x) but substantially smaller than the integral scale (10-80x), so the particle-eddy interaction at the particle scale may be expected to be quite strong. For B, the particles are 3-4 times η, and again the potential for particle-eddy interaction is quite strong.

Table 4-2: The range of Kolmogoroff length scales for each particle species as observed for two impeller diameters

Particle type	Impeller diameter	Minimum v_z' (m/s)	Maximum v_z' (m/s)	L_{min} (m)	L_{max} (m)	η_{min} (μm)	η_{max} (μm)
SG	T/3	0.04	0.10	0.008	0.048	53	165
LG	T/3	0.07	0.10			53	115
B	T/3	0.10	0.30			23	83
SG	T/2	0.10	0.28	0.012	0.048	27	83
LG	T/2	0.33	0.10			24	83

4.3.3. Solids suspension mechanisms with the T/2 impeller

Following the same procedure that was used for the T/3 impeller, the collapse of the scaled velocity profiles for the D=T/2 A310 was first evaluated visually, and then using $\Delta\sigma$. Figure 4-8a and b show the measured V_r and the v_z' for six clearances, normalized with the tip speed of the impeller. There are two regions in both figures: a low clearance region, C/D≤0.35, and a high clearance region, C/D>0.35. The high clearances region is comparable to the off-bottom clearances in T/3 profiles. In the high clearance region the particles collect around the periphery of the tank, and in the low clearance region the particles settle out in the centre of the tank as well as around the periphery. While this initially suggests that the mean radial flow must be small at the centre of the tank for low clearances Figure 4-8a shows that the normalized mean radial flow is actually larger than what it is in the high clearance region. Some other effect is dropping particles out in the centre of the tank at low clearances.

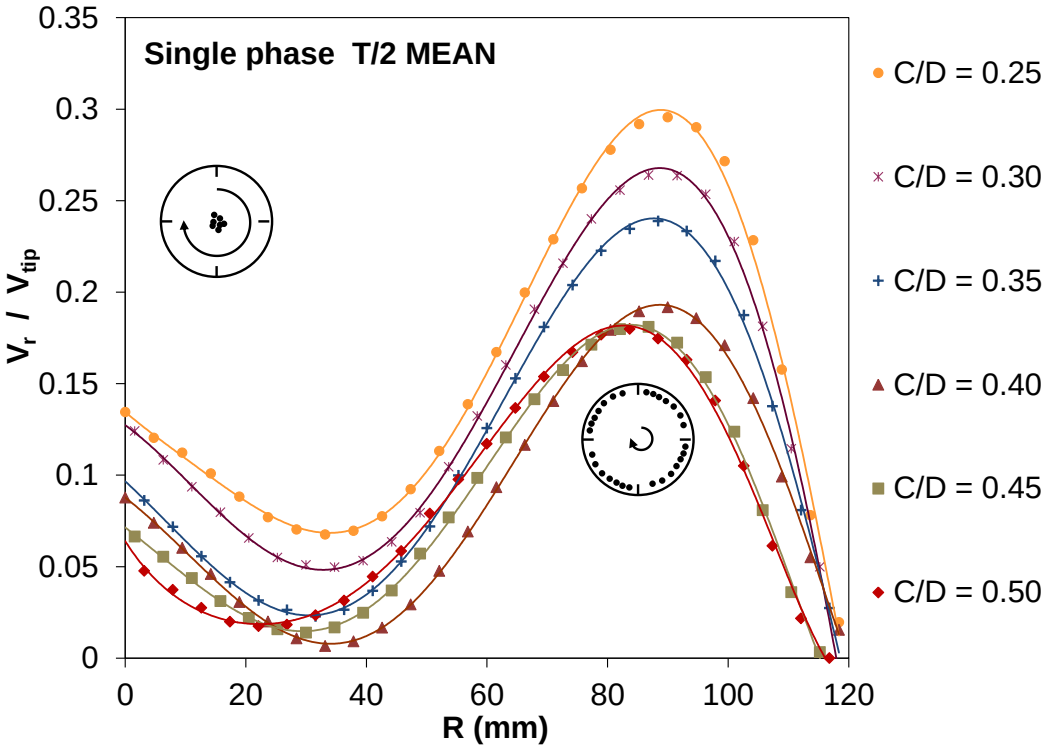

Figure 4-8a: Measured mean radial velocities normalized with the tip speed of the impeller: A310 T/2.

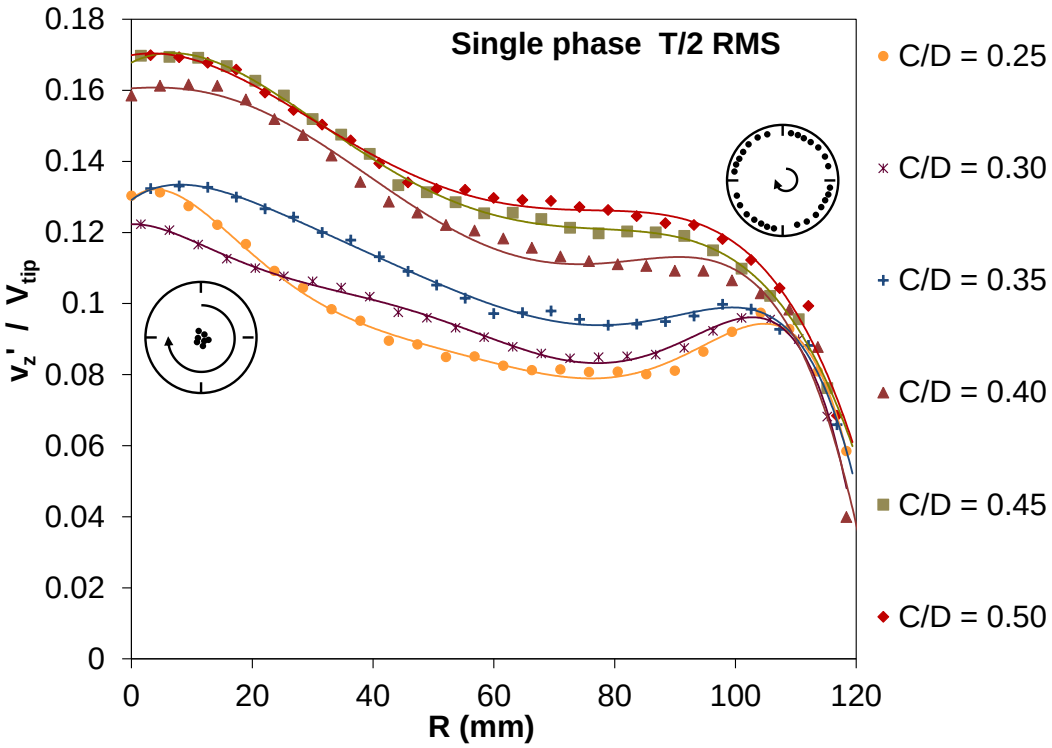

Figure 4-8b: Measured axial rms velocities normalized with the tip speed of the impeller: A310 T/2.

This additional effect is a strong rotational flow below the impeller. This swirl diminishes when there is sufficient distance between the impeller and the tank bottom, but when the impeller is close to the tank bottom, $C/D \leq 0.35$, the swirl is contained between the impeller and the tank bottom causing particles to drop out. This requires the analysis of the theta velocities. The profiles are not shown here, but an analysis is provided. From 0-30 mm in theta velocity profiles a forced vortex is evident, followed by free vortex out to the tank walls. In the 0-30 mm area the scaled theta velocities increase up to 0.16 with a steep slope. This high velocity causes the particles drop out in the centre immediately below the 20 m diameter hub. As the off-bottom clearance increases, $C/D > 0.35$, the theta velocity drops showing free vortex behaviour all along the radius.

The measured velocities were scaled to N_{js} for three slurries: SG, LG, and the mixture of SG with B. For all of the slurries the last point of suspension at low clearances is both at the centre of the tank and at the tank walls, and at high clearances it is only at the tank walls. The LG slurry results are representative and are shown in Figure 4-9 a and b. Visual inspection indicates that with the T/2 impeller the contribution of both mean flow and turbulent eddies is necessary, but neither of them dominates. The data does not show any collapse in either the low clearance or the high clearance region. This indicates that the hypothesis does not hold true for the T/2 impeller.

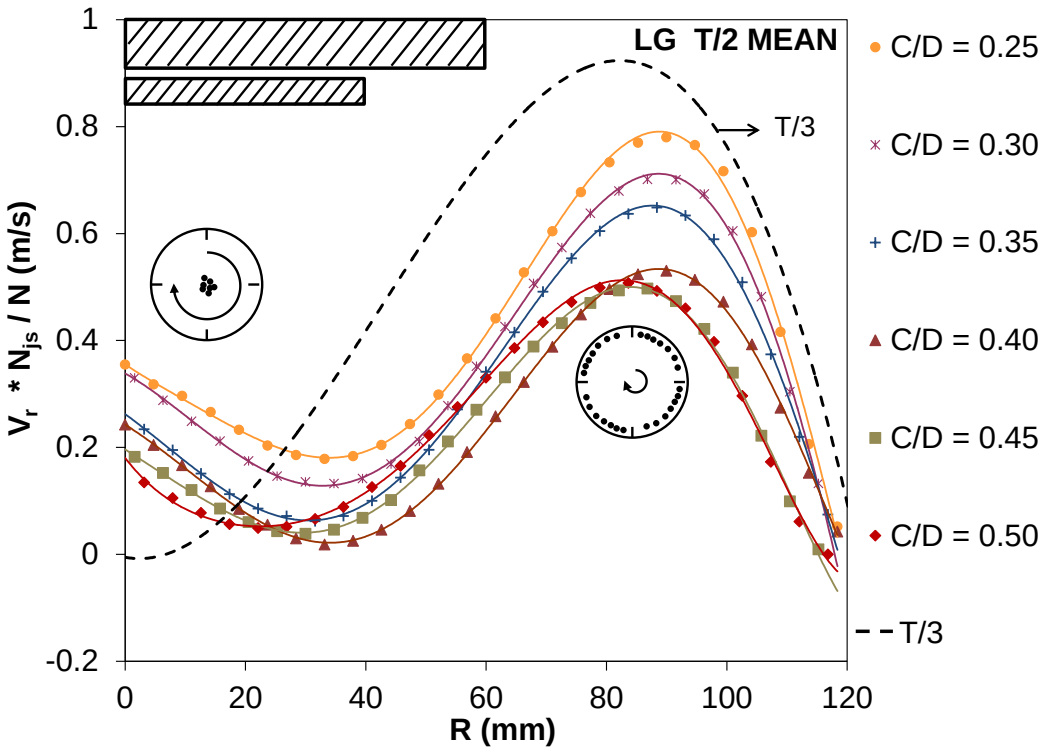

Figure 4-9a: Scaled mean radial velocity profiles for 1.5 wt% LG with the A310 T/2.

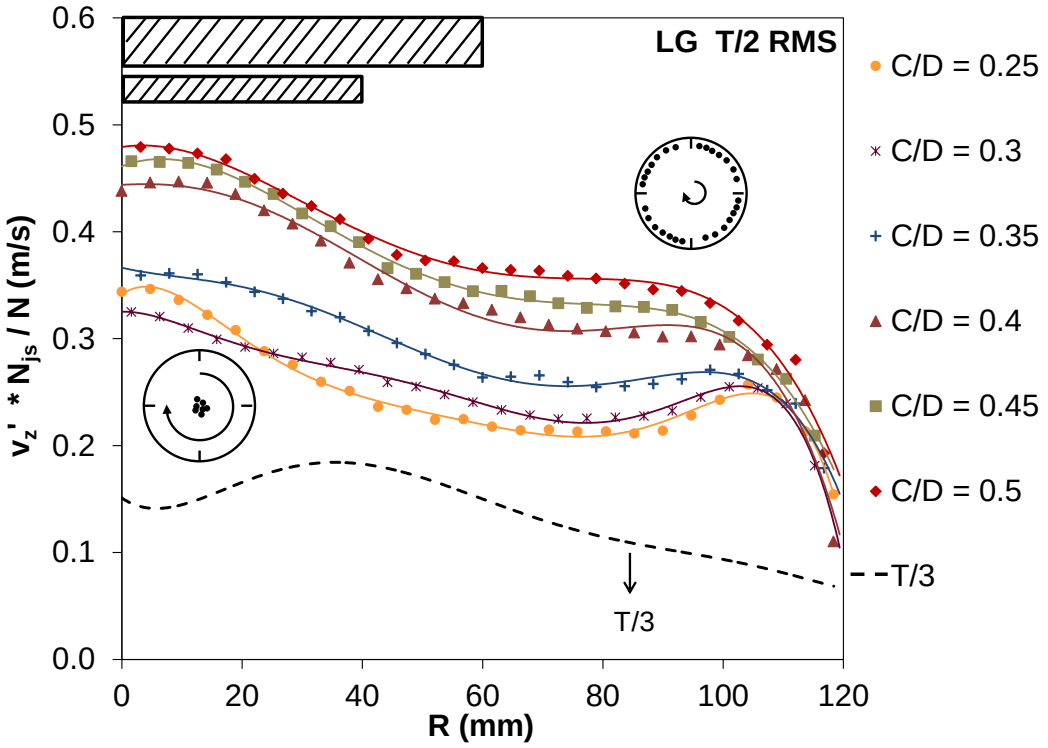

Figure 4-9b: Scaled axial rms velocity profiles for 1.5 wt% LG with the A310 T/2.

The $\Delta\sigma$ results are shown in Figure 4-10a and b. $\Delta\sigma$ is always negative for V_r, and is always positive for v_z', suggesting that mean flow is the principle mechanism for the T/2 impeller, but this does not agree with the visual inspection of the velocity profiles, which are nearly unchanged. The same conflicting result was observed for LG, SG and the mixture of SG with B.

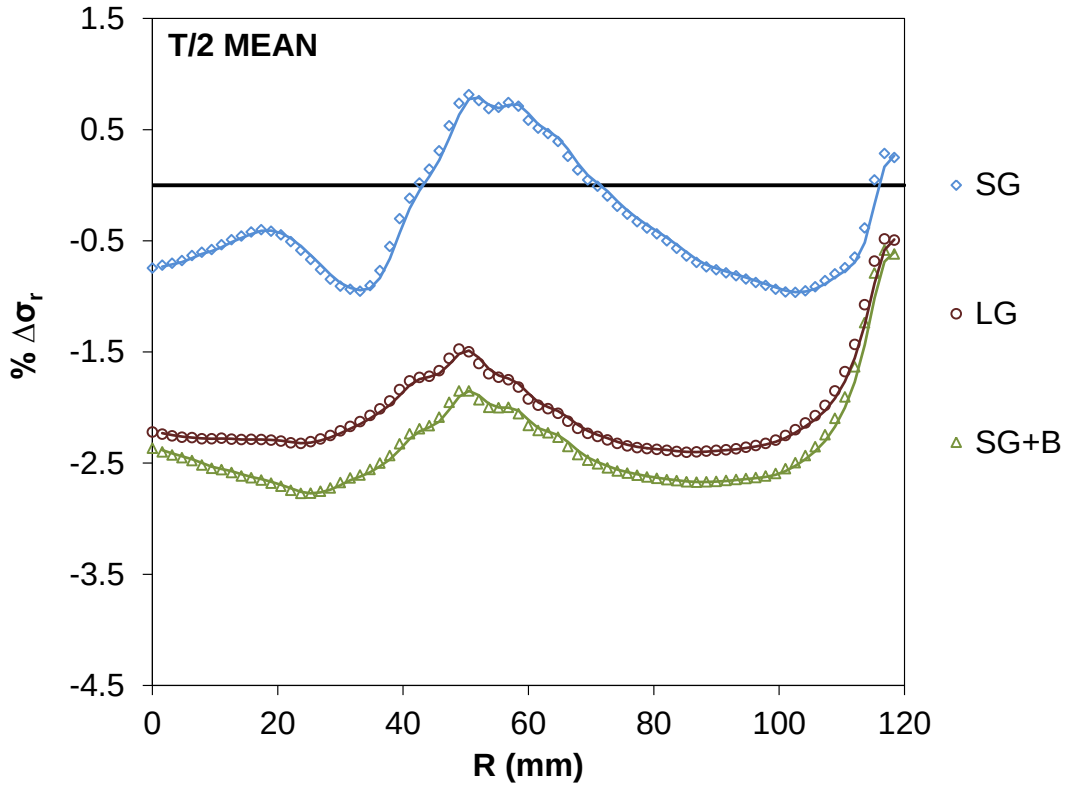

Figure 4-10a: The difference between the normalized standard deviation of scaled and the measured mean radial velocity profiles for each particle species: A310 T/2.

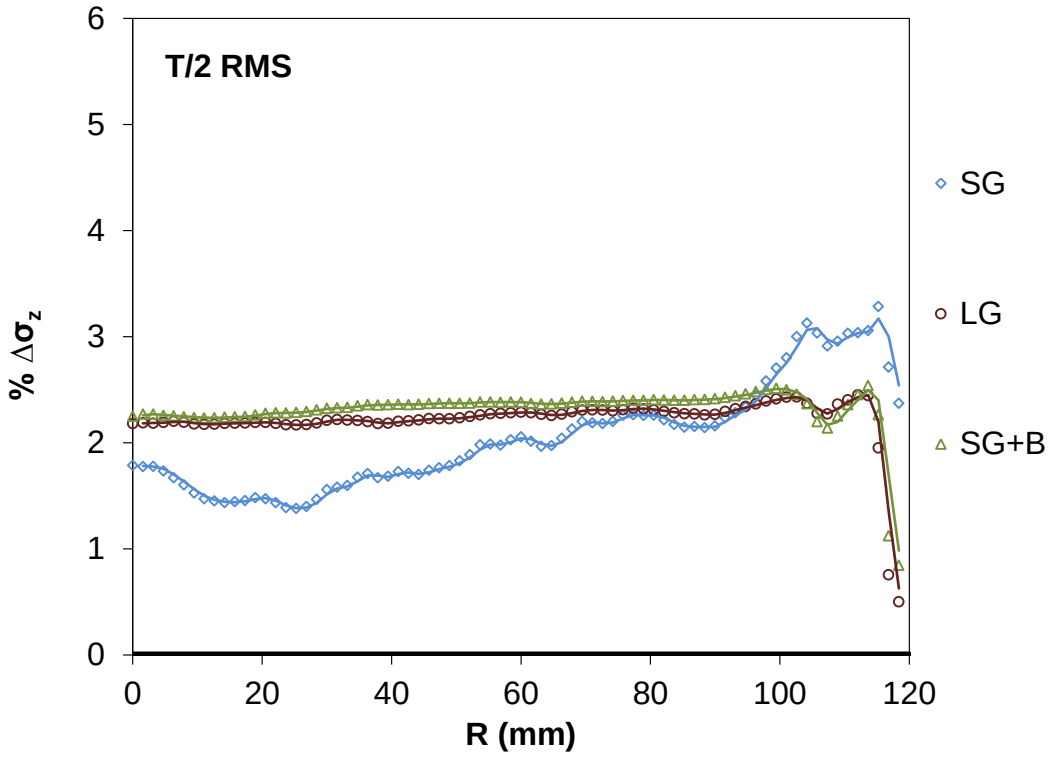

Figure 4-10b: The difference between the normalized standard deviation of scaled and the measured axial rms velocity profiles for each particle species: A310 T/2.

The two impellers can be directly compared by plotting the velocity profiles for the T/3 mean and rms scaled for N_{js} of the LG directly on top of the plots for the T/2 impeller. This is shown in Figure 4-9a and b as dashed lines. Considering first the mean velocity profiles, the T/3 result falls above the two results for the D=T/2 impeller at both high and low clearances. The dropping V_r close to the centre of the tank is much smaller for the T/3 impeller, extending out to only 8 mm, while the T/2 impeller retains this trend out to 40 mm. This is a direct effect of the change in impeller diameter. For both impellers, the maximum radial velocity occurs at about 80 mm, but for the T/2 impeller this is a sharp peak, while for the T/3 impeller, it is a broad peak which extends from roughly 60-100 mm. Again, this is a direct effect of the impeller geometry. The larger impeller has less space to reach the peak, so the slope of the profile on either side must be steeper. Overall, the mean radial velocities are of a similar magnitude, with the T/2 impeller having a significantly less favorable configuration for

removing solids from the bottom of the tank. The more surprising results are found by comparing the fluctuating velocity profiles. The LG particles can be suspended when the scaled fluctuating velocities are in the 0.8-1.8 range and there is some mean flow present with the T/3 impeller. For the T/2 impeller, the rms velocity is 3-4 times larger than the required rms velocity. This is because of the shape of the radial velocity profiles with the T/2 impeller and proves that the contribution of mean flow is certainly important. In order to achieve the required minimum convective effect with the mean velocity, the T/2 impeller generates much more turbulence as a secondary effect.

As a last note, consider the high and low clearance cases. The low clearance case, where particles tend to collect at the centre of the tank, has a higher mean velocity and a lower rms velocity in this region. This suggests that some other mechanism is drawing particles into the centre of the tank, and the mean velocity has to be increased to compensate for this effect. The rms velocity cannot convect the particles away from the centre, so it plays a less critical role for this particular configuration.

An estimation of the size of the smallest Kolmogoroff eddies was also made for the T/2 impeller, as given in Table 4-2. There is no significant collapse of the velocity profiles for this impeller, so the minimum and maximum v_z' were taken close to the tank walls, from 100-120 mm. The SG particles are similar in size to the smallest eddies, while the LG particles fall in the centre of the most energetic eddy size range. Note that the maximum Kolmogoroff eddy size is smaller than for the T/3 impeller due to the increase in the rms velocity. This will lead to an increase in power consumption with no improvement in solids suspension conditions.

The mean and rms velocity results reveal several things: solids suspension for the T/3 impeller is determined by the rms velocity limit, and the profiles collapse nicely to show this. The T/2 impeller, on the other hand, is limited by an unfavorable mean radial velocity profile. Overcoming the limitations of this

profile requires a significant increase in the rms velocity beyond what is required to suspend the particles. For the low clearance case, some additional three dimensional effect is driving particles toward the centre of the tank, and this effect has to be overcome by further increasing the mean velocity.

4.3.4. LES results

In the final stage of analysis, single phase velocity profiles were obtained using LES at the same conditions as the PIV experiments for the T/3 impeller. The advantage of LES is that the flow field in the entire tank is calculated and the data for every grid point is stored. This allows us to investigate the velocity profiles at different horizontal measurement planes. In this section, the critical flow condition hypothesis is tested for a final time using the LES results, and the LES and the PIV results are compared. Second, the sensitivity of the velocities to the position of the measurement plane was analyzed using the high resolution LES data.

4.3.4.1. Solids suspension mechanisms with the T/3 impeller and comparison of the LES and PIV data

Figure 4-11a and b show the scaled V_r and $v_z^{'}$ for the T/3 impeller. Both the V_r and the $v_z^{'}$ profiles are scattered; there is no visible collapse of the profiles. The visual inspection does not show a clear trend for a dominant solids suspension mechanism. Figure 4-12a and b show the $\Delta\sigma$ for V_r and $v_z^{'}$. The $\Delta\sigma$ for V_r is mostly negative, while the $\Delta\sigma$ for $v_z^{'}$ is negative only from 75-105 mm. This suggests that the mean flow is the dominant mechanism for the T/3 impeller. The $\Delta\sigma$ analysis leads to a different conclusion than both the visual inspection and the PIV results.

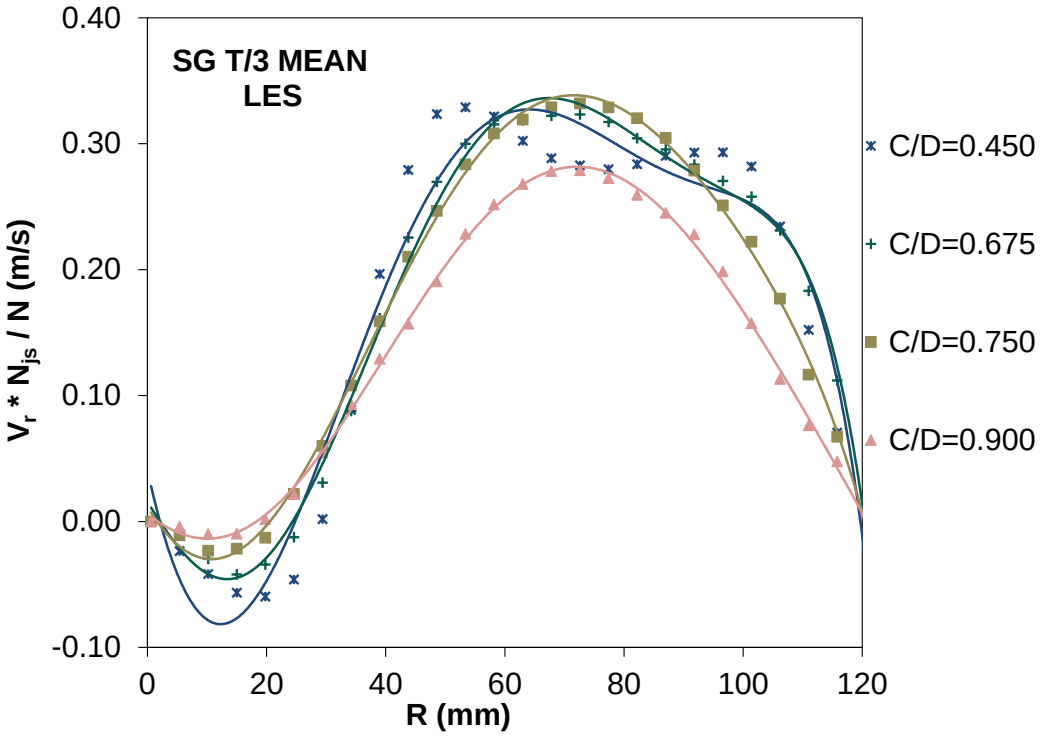

Figure 4-11a: LES results for the scaled mean radial velocity profiles for 1.5 wt% SG: A310 T/3.

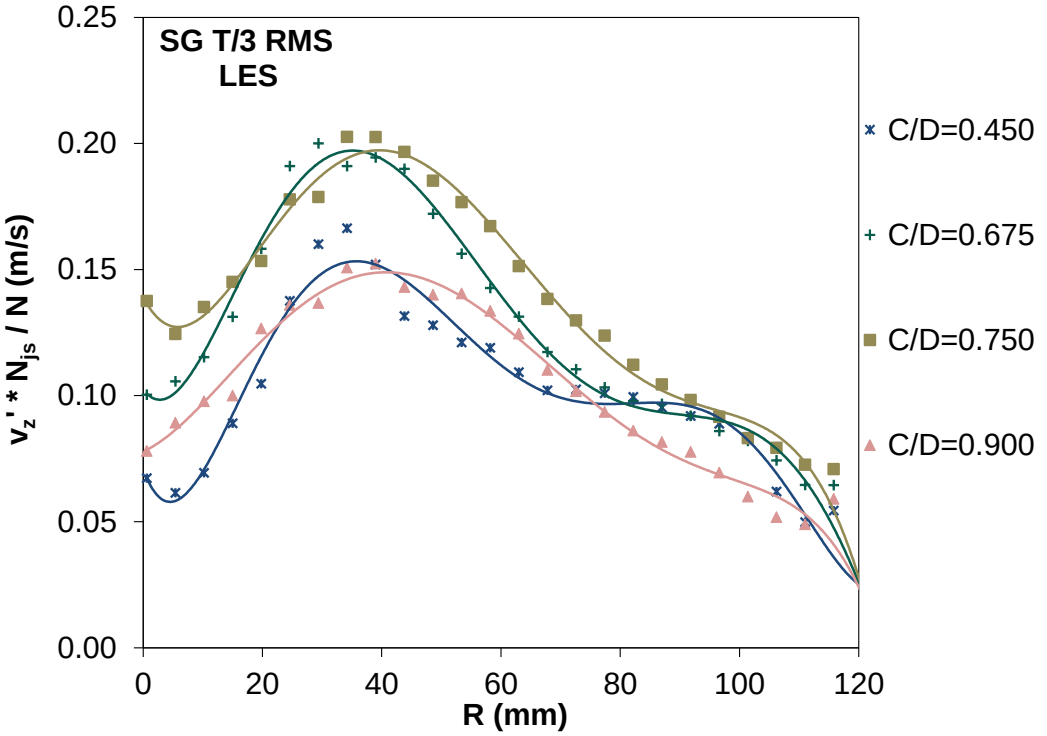

Figure 4-11b: LES results for the scaled axial rms velocity profiles for 1.5 wt% SG: A310 T/3.

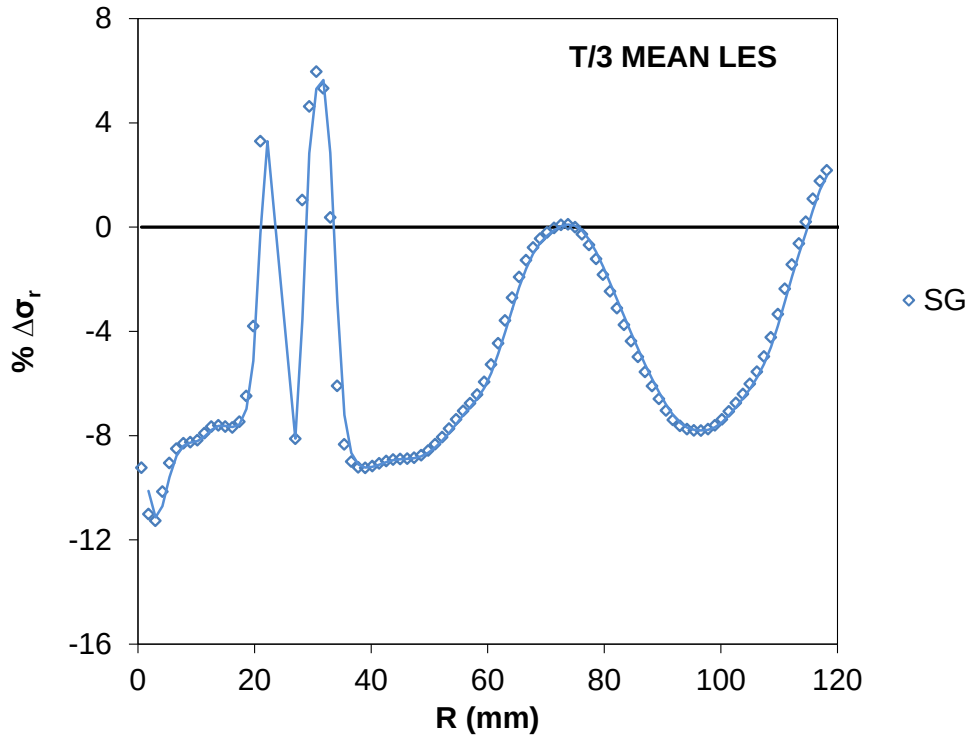

Figure 4-12a: The difference between the normalized standard deviation of the scaled SG and the single phase mean radial velocities according to LES.

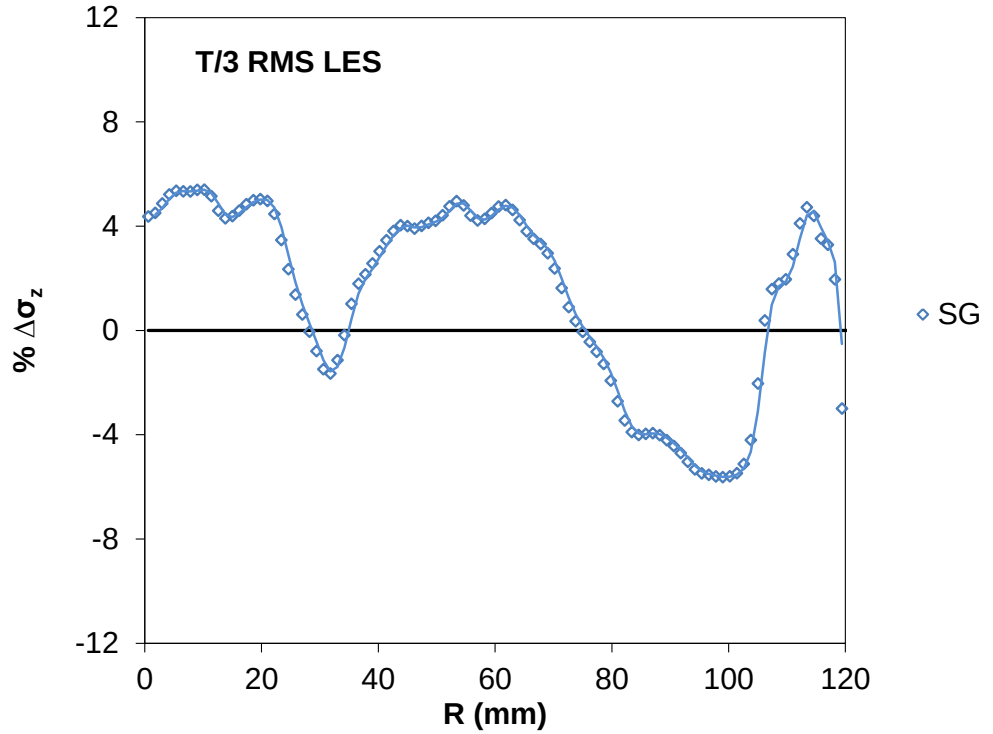

Figure 4-12b: The difference between the normalized standard deviation of the scaled SG and the single phase radial mean velocities according to LES.

The shapes of the scaled velocity profiles with LES, Figure 4-11a and b, are similar to the PIV profiles, Figure 4-6a and b, but there are some differences in both the flow details and in the magnitude of the velocities. In Figure 4-11a, V_r calculated using LES is zero in the centre of the tank while it is between -0.1 and 0.2 m/s in the PIV measurements, giving a mean of zero. In a mathematical sense V_r must approach zero at the bottom centre of the tank because there is no point source of mass at R=0. Capturing an exact zero velocity at the centre of the tank would require measurements with a longer time average as well as high resolution in both time and space close to the centre of the vessel, and a thoughtful consideration of the best time averaging scheme to apply if a slow precessing vortex structure is present in this region. This detailed flow analysis is beyond the scope of work considered here.

In the LES results, the magnitude of V_r is under-predicted, and the magnitude of v_z' is over-predicted. The LES profiles are located 4.2 mm above the bottom of the tank, which is a region where wall effects may have a substantial impact on the accuracy of LES predictions.

4.3.4.2. The effect of distance from the bottom of the tank on velocities

The LES profiles in Figure 4-11a and b were taken 4.2 mm above the bottom of the tank. In the PIV experiments the axial position of the measurement plane was 3.5 to 4.5 mm above the bottom of the tank, and the thickness of the plane was 2 mm. Close to the bottom of the tank the velocities may vary significantly, so it is interesting to consider how sensitive the results may be to small errors in positioning. This analysis cannot be done with the PIV data since it was only at one vertical position, but LES data was recorded for all horizontal planes along the vertical axis.

Figure 4-13a shows the scaled mean radial velocity profiles at a fixed impeller off-bottom clearance, C/D=0.75, at various distances from the bottom of the tank. As the plane moves away from the bottom of the tank the radial

velocities vary slightly close to the centre of the tank and close to the tank walls, but they all collapse on to a single profile at around the maximum V_r.

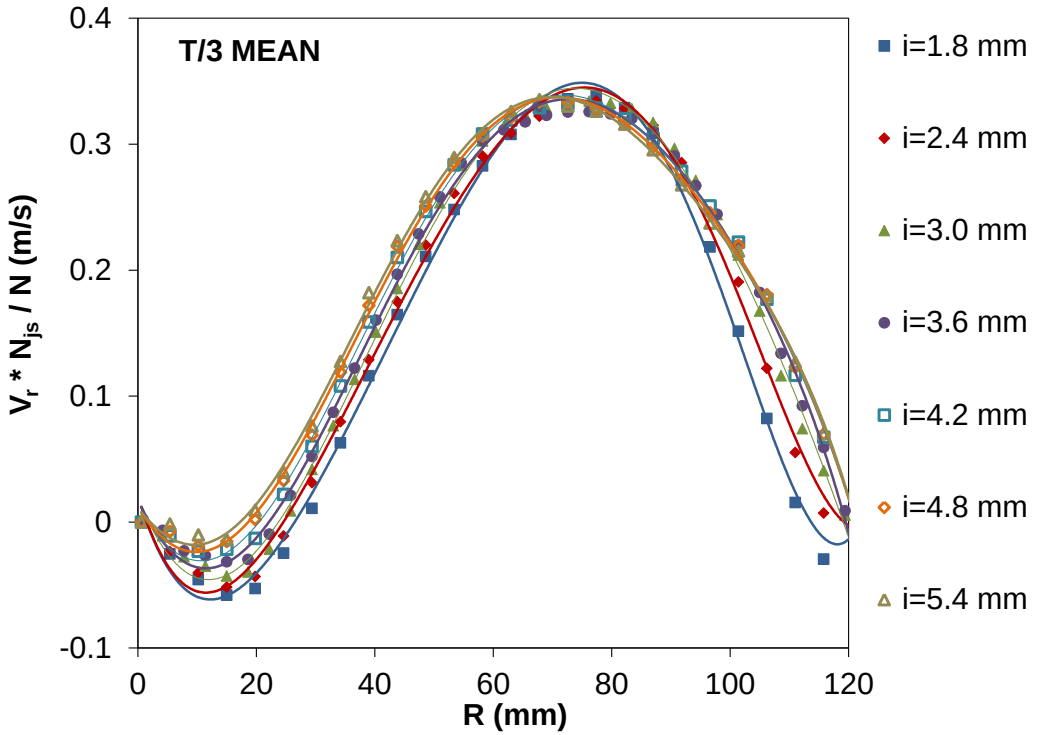

Figure 4-13a: The effect of the position of the measurement plane on radial mean velocities. Mean radial velocities were obtained with LES and scaled with N_{js} data for 1.5 wt% SG with the A310 T/3 at C/D = 0.75.

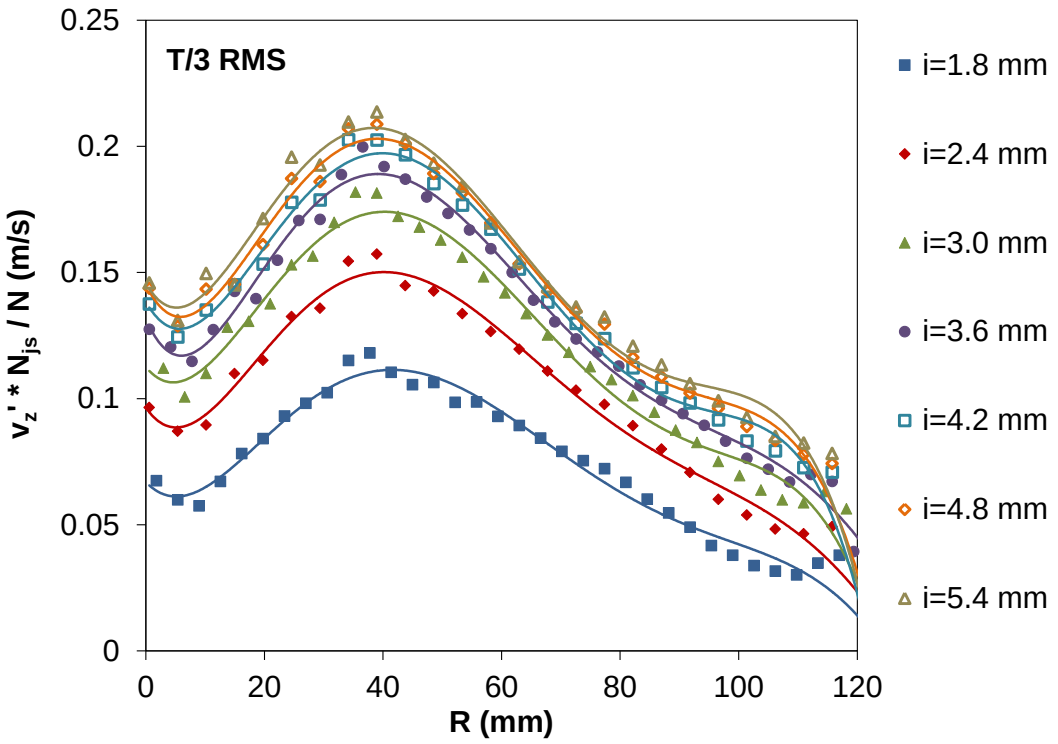

Figure 4-13b: The effect of the position of the measurement plane on axial rms velocities. Axial rms velocities were obtained with LES and scaled with N_{js} data for 1.5 wt% SG with the A310 T/3 at C/D = 0.75.

Figure 4-13b shows the scaled axial rms velocity profiles at a fixed off-bottom clearance, C/D=0.75, for a T/3 impeller. As the plane is pulled away from the bottom of the tank the trend of the profiles remains the same, but the magnitude of the velocities increases. Between the first plane, i=1.8 mm, and the second plane, i=2.4 mm, the magnitude of the velocities increases significantly, showing that the position of the measurement plane makes a significant difference in the velocities. Starting from 3.6 mm the profiles collapse onto each other, indicating that from 3.6 mm to 5.4 mm the axial rms velocities do not change significantly. This analysis shows that the velocities are not a strong function of the position of the measurement plane in the 3.5-4.5 mm range.

4.3.5. Comparison between the T/3 and the T/2 impellers

Solid-liquid mixing is a power intensive operation; therefore, the power consumption is an important criterion in choosing an impeller. The power consumption at just suspended conditions (P_{js}) can be calculated from:

$$P_{js} = \rho_{sl} N_p N_{js}^3 D^5 \qquad 4\text{-}18$$

Figure 4-14 shows the comparison of power consumption between the T/3 and the T/2 impellers for the SG and the LG slurries at 1.5 wt% and SG+B mixture at 27wt% at varying off-bottom clearances. For all slurries the power consumption with the T/3 impeller is significantly lower than the T/2 impeller. Referring back to Figure 4-3 we see that N_{js} is higher for the T/3 impeller than the T/2 impeller for both the SG and the LG slurries. From an operational point of view, the power consumption is a better criterion than N_{js} for choosing an impeller.

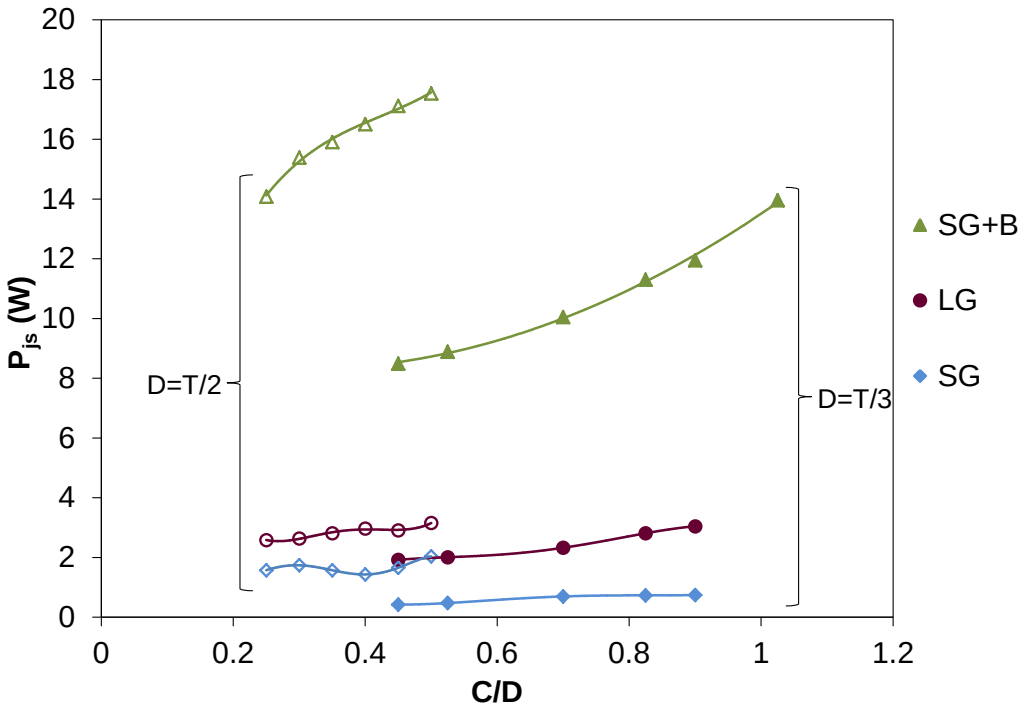

Figure 4-14: The comparison of power consumption between the A310 T/3 and the T/2. The power consumption was calculated for the SG and the LG slurries at 1.5 wt%, and for the mixture at 26 wt% SG with 1.3 wt% B. Solid and hollow symbols represent D=T/3 and D=T/2, respectively.

A comparison of the two impellers in terms of the solids suspension mechanisms shows two different trends. For the T/2 impeller some combination of the mean flow and turbulent eddies provides solids suspension, and neither of these mechanisms dominate. For the T/3 impeller a single mechanism, turbulence, dominates and the required level of turbulence with the small impeller is approximately one third the levels observed for the T/2 impeller. The T/3 impeller

is also less power intensive. It can be concluded that the T/3 impeller is more efficient because the convective flow is more efficient, which in turn minimizes the amount of turbulence energy dissipation required to suspend the solids.

4.4. Conclusions

The goal of this study was to investigate the mechanisms that drive solids suspension in stirred tanks. The analysis was based on the hypothesis that at complete off-bottom suspension a critical flow condition exists close to the bottom of the tank at every clearance for fixed solids, tank geometry, and constant circulation pattern. The flow condition might be dominated by either the mean flow in a convective mechanism, or the turbulence in an eddy-lifting mechanism.

Data was collected using visual observations of the tank bottom, PIV, and LES. The PIV measurements were collected at a single rotational speed. The data was analyzed using three separate methods. First the velocity profiles were scaled with N_{js} and plotted together to determine whether the profiles collapsed to a single critical flow condition at N_{js}. Second, the degree of collapse was quantified using the change in normalized standard deviation from the raw measured profiles to the scaled velocity profiles. Last, the size of the smallest eddies was estimated and compared with the size of the particles to determine the most likely type of particle-eddy interactions for each particle species. The results led to the following conclusions:

- Solids suspension occurs as a result of the combination of mean flow and turbulent eddies. Complete off-bottom suspension cannot be obtained in the absence of one of these mechanisms.
- When the impeller diameter is changed the dominant solids suspension mechanism, or the lack of a clear mechanism becomes evident.The solids deposition pattern changes when the off-bottom clearance is changed giving a visible demonstration of the dramatic effect of geometry.

    - For the T/3 impeller the hypothesis holds true. The critical flow condition is dominated by the level of turbulence and convection plays a secondary role.
    - For the T/2 impeller the hypothesis does not hold true. Both mechanisms play an active role, but neither mechanism dominates. The shape of the radial velocity profile is unfavourable for solids suspension so a larger impeller speed is needed to achieve the same amount of convective flow, and this results in a significant amount of additional and unnecessary turbulence and power consumption at the point of solids suspension.
- The solids suspension mechanism also depends on the type of the particle, because the particle-eddy interactions are different for each particle species.
    - The SG is submerged in the viscous sub-layer and it is significantly smaller than the most energetic eddies.
    - The LG lies in the middle of the spectrum with highly energetic particle-eddy interactions all along the tank bottom.
    - The B lies somewhere in between: it is larger than the viscous sub-layer and the smallest eddy sizes, but the particle-eddy interactions are not as strong as for LG. This suggests that the B is moved away from the tank bottom as a result of both turbulent eddies and near wall lift.
- The T/3 impeller is more efficient for solids suspension because less energy is lost to excess turbulent energy dissipation.

4.5. References

Armenante, P.M., Nagamine, E.U., Susanto, J., 1998. Determination of correlations to predict the minimum agitation speed complete solid suspension in agitated vessels. Can. J. of Chem. Eng., 76, 413-419.

Ayranci, I., Kresta, S.M., 2011. Design rules for suspending concentrated mixtures of solids in stirred tanks. Chem. Eng. Res. and Des., 89, 1961-1971.

Baldi, G., Conti, R., Alaria, E.,1978. Complete suspension of particles in mechanically agitated vessels. Chem. Eng. Sci., 33, 21-25.

Bittorf, K.J., Kresta, S.M., 2003. Prediction of cloud height for solid suspension in stirred tanks. Trans IChemE, 81(A), 568-577.

Davies, J.T., 1972, Turbulence Phenomena, An introduction to the eddy transfer of momentum, mass, and heat, particularly at interfaces, Chapter 3, Academic Press, New York.

Derksen, J., Van den Akker, H.E.A., 1999. Large eddy simulations on the flow driven by a Rushton turbine. AIChE Journal, 45, 209-221.

Garcia, M.H., 2008. Sedimentation engineering: processes, management, modeling, and practice. American Soc. of Civil Eng., 21-306.

Ghionzoli, A., Bujalski, W., Grenville, R.K., Nienow, A.W., Sharpe, R.W., Paglianti, A., 2007. The effect of bottom roughness on the minimum agitator speed required to just fully suspend particles in a stirred vessel. Trans. IChemE., 85 (A5), 685-690.

Grenville, R.K., Mak, A.T.C., Brown, D.A.R., 2010. An improved correlation to predict “just suspension” speed for solid-liquid mixtures with axial flow impellers in stirred tanks. North American Mixing Forum, Victoria, BC, Canada, June 20-June 25.

Kresta, S.M., Wood, P.E., 1993. The mean flow field produced by a 45º pitched blade turbine: changes in the circulation pattern due to off bottom clearance. Can. J. of Chem. Eng., 71, 42-53.

Madej, A.M., Babazadeh, H., Nobes, D.S., 2011. The effect of chamber length and Reynolds number on jet precession. Exp. in Fluids, 51(6), 1623-1643.

Molerus O., Latzel, W., 1987. Suspension of solid particles in agitated vessels. Part. Sci. and Tech., 5(3), 235-260.

Myers, K.J., Fasano, J.B., 1992. The influence of baffle off-bottom clearance on the solids suspension of pitched-blade and high-efficiency impellers. Can. J. of Chem. Eng., 70, 596-599.

Nienow, A.W., 1968. Suspension of solid particles in turbine agitated baffled vessels. Chem. Eng. Sci., 23, 1453-1459.

Nouri, J. M., Whitelaw, J. H., Yianneskis, M., 1987. The scaling of the flow field with impeller size and rotational speed in a stirred reactor. 2nd International Conference on Laser Anemometry-Advances and Applications, Strathclyde, UK.

Tatterson, G.B., Yuan, H.H.S., Brodkey, R.S., 1980. Steoroscopic visualization of the flows for pitched blade turbines. Chem. Eng. Sci., 35 (6), 1369-1375.

Thorpe, R.B., Stevenson, P., 2003. Suspension of particles from the bottom of pipes and stirred tanks by gassed and ungassed flows. Can. J. of Chem. Eng., 81, 351-359.

Vanoni, V.A., 2006. Chapter II: Sediment Transportation Mechanics, Sedimentation Engineering. ASCE Manuals and Reports on Engineering Practice, 2nd ed., vol. 54, 11-189.

Wilson, K.C., 2005. Slurry transport using centrifugal pumps. Springer, New York, pp. 123-151.

Wilson, K.C., Sanders, R.S., Gillies, R.G., Shook, C.A., 2010. Verification of the near-wall model for slurry flow. Pow. Tech., 197, 247-253.

Zhou, G., Kresta, S.M., 1996. Impact of tank geometry on the maximum turbulence energy dissipation rate for impellers. AIChE Journal, 42, 2476-2490.

Zwietering, Th.N., 1958. Suspending of solid particles in liquid by agitators. Chem. Eng. Sci., 8, 244-253.

Chapter 5 : Summary, Conclusions and Future Work

Three studies were conducted to develop an understanding of solids suspension mechanisms and the effect of geometry on the mechanisms, and to solve the industrial problem of the lack of a design model for mixed slurry suspension. The important conclusions from these studies, the contributions to the field of study, and suggested future work are given below.

5.1. Solids suspension of mixtures of solids at high solids loadings

The suspension behaviour of mixed slurries is more complicated than for unimodal slurries. The ratio of particle size and density of the solid phases can have an effect on the mixed slurry N_{js}. In this thesis complete off-bottom suspension behaviour of five binary mixtures was tested. The mixtures were chosen carefully to cover a range of particle size and density ratios. In all mixtures there was a dense and a less dense solid phase. The solids loading of the more dense particles was kept constant while the solids loading of the less dense particles was increased. When the less dense particles have a much smaller N_{js} than the dense particles, and when $Ar<40$ for the less dense particles, the addition of the less dense particles does not change mixture N_{js} significantly at low solids loadings. If the less dense particles have $Ar>>40$, then the mixture N_{js} increases significantly even at low solids loadings. At high solids loadings (>25 wt%) particle-particle interactions start to dominate. For one of the mixtures tested this was resulted in a significant drop in mixture N_{js}. A summary of the comparison of the N_{js} of the mixtures to the current design heuristic (the maximum N_{js} in the mixture) is given in Table 5-1. A comparison of the power consumption with the two test impellers, an A310 and a PBT, showed that the A310 impeller consumes much less energy at just suspended conditions.

Table 5-1: Comparison of mixture N_{js} to the current design heuristic

Mixtures	d_p relation	ρ relation	$N_{js} \stackrel{?}{=} N_{js,max}$
Small glass + Bronze	$d_1 < d_2$	$\rho_1 < \rho_2$	YES <12wt% NO >26wt%
Large glass + Bronze	$d_1 > d_2$	$\rho_1 < \rho_2$	NO
Resin + Bronze	$d_1 > d_2$	$\rho_1 < \rho_2$	NO
Small glass + Nickel	$d_1 \approx d_2$	$\rho_1 < \rho_2$	YES
Resin + Large glass	$d_1 \approx d_2$	$\rho_1 \approx \rho_2$	NO

5.2. Prediction of just suspended speed for mixed slurries

Previously it was seen that the mixed slurry N_{js} is quite complicated because of the different physical properties of each solid phase. The findings of Chapter 2 provided a baseline for Chapter 3. Additional data was taken and a deeper analysis was done to generate an empirical model to predict mixture N_{js}. We proposed and tested two new models to predict mixture N_{js}: the power model and the momentum model. The current design heuristic was also tested to provide a baseline.

The current design heuristic failed to capture the physics behind solids suspension; therefore, it should not be used to predict mixture N_{js}. This is seen clearly from Figure 5-1.

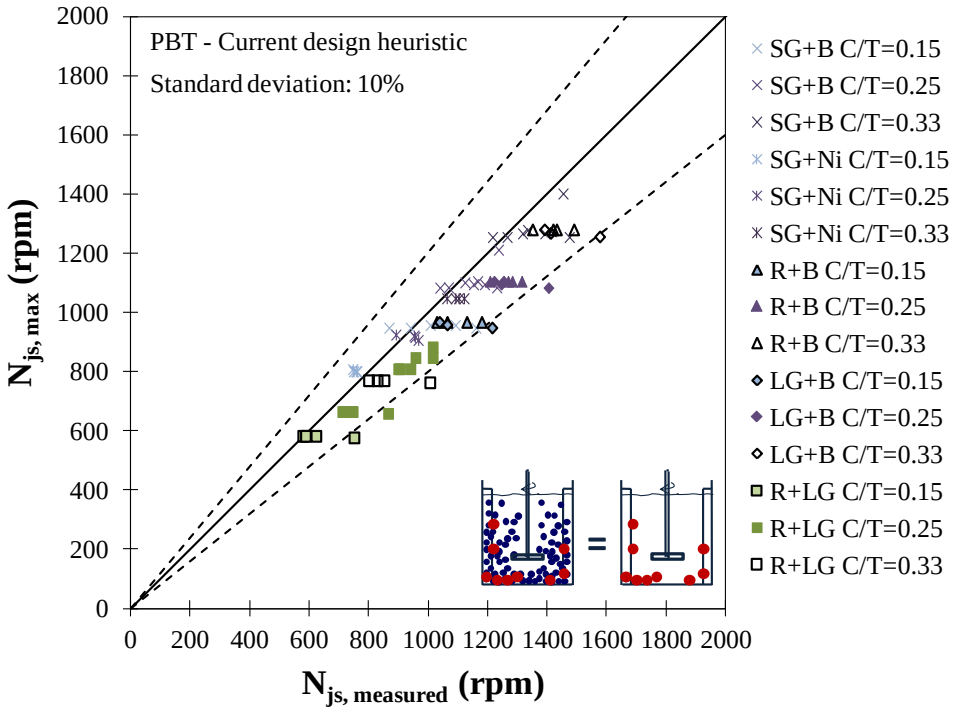

Figure 5-1: The parity plot between the current design heuristic and the experimental data with a PBT impeller. The current design heuristic uses the maximum N_{js} in the mixture, calculated using the Zwietering correlation.

The momentum model over-predicts mixture N_{js}, so this model is not applicable either. The power model on the other hand, successfully predicted mixture N_{js} up to 27 wt% solids at a range of off-bottom clearances for two impellers. The model is based on the summation of power consumption required to suspend each solid phase present in the slurry. The model is limited to the cases where there are no significant particle-particle interactions.

$$N_{js,mix} = \left(\frac{\rho_{sl,1} N_{js,1}{}^{3} + \rho_{sl,2} N_{js,2}{}^{3}}{\rho_{sl,mix}} \right)^{1/3} \qquad (5\text{-}1)$$

The power model requires the unimodal slurry N_{js} of each solid phase. This led to an analysis of the off-bottom clearance and solids loading on unimodal slurry N_{js}. The effect of off-bottom clearance cannot be quantified in a simple way because it is a function of many parameters: type of the particle, solids loading of the particle, type of the impeller. The effect of off-bottom clearance was lumped

in S in the Zwietering correlation. In this work this effect was isolated from the rest of the analysis by using S values that match the exact geometries used.

The effect of solids loading is also complicated. In the Zwietering correlation the exponent on solids loading is 0.13. The analysis on the particles used in this study up to high solids loadings showed that the reality is different. Three possible exponents were found: 0.18, 0.24, and 0.33. A group of particles followed 0.18, while the rest followed 0.33. The average exponent that represents the entire data set is 0.24, but it should be noted that the data is scattered with this exponent. We suggest that if possible, experimental unimodal slurry N_{js} should be used. If that is not possible, then one of the suggested exponents can be used.

The combination of these results with the results in section 5.1 shows an interesting portrait. The Zwietering correlation works well for solids loadings below 10 wt%. For higher loadings one of the new exponents on concentration should be used; however, it is not clear which one of these exponents should be used for particles with different properties then the test particles. For the mixtures the current design heuristic works perfectly only for one type of mixture. The power model works well up to 20 wt% for all mixtures. Above that limit particle-particle interactions start to play a role. An unexpected drop in mixture N_{js} was seen with one mixture, but it is not possible to predict this drop without actually conducting experiments. The power model works for the rest of the mixtures up to 27 wt% solids loadings, but some caution is necessary because of the possible particle-particle interactions.

5.3. Solids suspension mechanisms

In order to understand solids suspension in stirred tanks the flow field close to the bottom of the tank needs to be considered as seen in Figure 5-2.

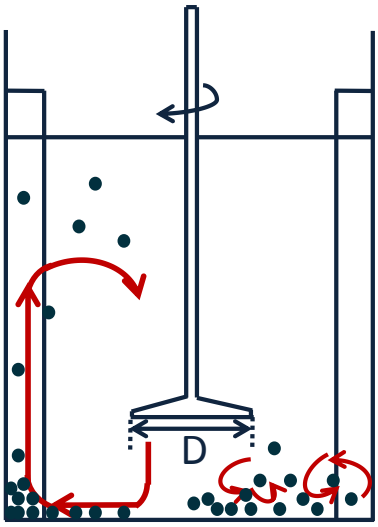

Figure 5-2: Flow close to the bottom of the tank. Both turbulent eddies and mean flow is effective.

The bulk of the tank, or flow around the impeller does not provide information about what happens at the bottom of the tank where the solids are suspended. Based on this thought we hypothesized that at the just suspended speed a critical flow condition occurs close to the bottom of the tank. This flow condition is the same for a fixed geometry, solids content, and it is dominated by mean flow or turbulence. The results showed that the solids suspension in stirred tanks occurs as a result of some combination of mean flow and turbulent eddies. The solids suspension mechanism changes when the impeller diameter is changed and the solids deposition pattern changes when the off-bottom clearance is changed. It was already known that the geometry had a significant effect on solids suspension. These results quantitatively prove that the effect is much deeper than previously anticipated. For the T/3 impeller the turbulence dominates the critical flow condition. The mean flow has a secondary effect. For the T/2 impeller however, neither of the mechanisms dominates. A larger impeller speed is needed to achieve the necessary mean flow, so a significant amount of additional turbulence is also generated. The hypothesis of a critical flow condition holds true for the T/3 impeller, but it falls apart with the T/2 impeller.

The solids suspension mechanism also depends on the type of the particle, because the particle-eddy interactions vary for each particle species. The particles that are submerged in the viscous sub-layer are significantly smaller than the most energetic eddies, so eddies are not helpful in suspending these particles. For particles that are significantly larger than the viscous sub-layer strong particle-eddy interactions are seen. Some particles lay in between these two cases, and for these particles some particle-eddy interactions are expected, but the mean flow can also show an effect.

The results led to a practical conclusion for design: for solids suspension applications a T/3 impeller is more efficient than a T/2 impeller. The T/2 impeller has an unfavourable radial profile shape, and a significant amount of energy is lost to excess turbulent energy. Solids suspension with the T/3 impeller on is dominated by the turbulent eddies, so it is more energy efficient.

5.4. Thesis Outcomes

This PhD study contributed to the field in the following ways:

1. Mixed slurry suspension was an area with no previous investigation; therefore, no experimental data and understanding was established. A wide data set was given with a general understanding of behaviour of particles in mixtures. The effective parameters were defined.
2. It was proved that the current design heuristic that is used in industry is inaccurate in both predicting mixture N_{js} and the physics behind solids suspension.
3. The power model – was developed to accurately predict mixture N_{js}. This is the first physical model proposed for this application; therefore, it is very useful for industrial design.
4. Two solids suspension mechanisms in stirred tanks were defined: turbulent eddies and mean flow. This will change the general thought that relates solids suspension to turbulence only.

5. The area of focus to understand solids suspension was defined as the flow close to the bottom of the tank. Until now, the region close to the impeller was the centre of attention because there is established knowledge about impeller related properties.
6. The effect of geometry on the solids suspension was shown to be deeper than anticipated. The solids suspension mechanism changes once the impeller diameter is changed. The solids deposition pattern is also affected by the geometry, because the pattern changes when the off-bottom clearance is changed.
7. The effect of solids properties was also shown to be far more complex than previously anticipated.

5.5. Future Work

Research on mixed solids suspension is only beginning to be developed. This Ph.D. thesis provides very useful contributions to the understanding of solids suspension and practical solutions to industrial problems. There is need for future research in the following points:

- Further improvement on the power model is required to include particle-particle interactions at high solids loadings. Continuing empirical developments seem to have a limited potential for global success. Multiscale modeling seems promising, but is very computationally demanding. The effect of tank geometry is clear. Some clever combination of strategies will likely be required.
- The power model was tested only for binary mixtures. The industrial slurries possibly include more solid phases. The model should be extended to mixtures with more than two solid phases.
- The rheology of the slurry may change with the presence of many small particles (<50μm). All the studies in this thesis were done for Newtonian fluids. The effect of rheology should be addressed.

- The two solid phases have different cloud heights. While the less dense particles can be distributed in the tank almost uniformly, the dense particles can only reach a certain height. The solids distribution, and the effect of concentration of one solid phase on the distribution of the other solid phase requires investigation.